NTNU – Trondheim
Norwegian University of
Science and Technology

Robust Adaptive Control of a Surface Vessel in Managed Ice Using Hybrid Position- and Force Control

Vegar Østhus

Master of Science in Cybernetics and Robotics
Submission date: June 2014
Supervisor: Lars Imsland, ITK

Norwegian University of Science and Technology
Department of Engineering Cybernetics

NTNU

Faculty of Information Technology, Mathematics and Electrical Engineering
Department of Engineering Cybernetics

PROJECT DESCRIPTION SHEET

Name of the candidate: Vegar Østhus

Thesis title (Norwegian):

Thesis title (English): Robust adaptive control of a surface vessel in managed ice using hybrid position- and force control

Background

As offshore oil- and gas production enters arctic seas, the presence of sea ice becomes a substantial challenge in station-keeping operations. In many cases, operations will take place in managed ice, an ice field of broken ice generated by ice breakers to make station keeping possible. Station keeping is performed by a DP system which should keep the vessel in place subject to significantly varying ice forces. This Master's Thesis should be based on the project work done in the fall of 2013. It should develop the Hybrid Impedance Controller to include concepts from adaptive control to make the controller adapt to a dynamic environment of managed ice and enhance its performance with respect to fuel efficiency. The system should be implemented and tested in the Numerical Ice Tank software. Results and findings should be discussed in a final report. Further, the thesis should include a brief literature study reviewing previous work in DP systems in ice and sea ice modelling.

Work description

1. Give a brief overview of ice management operations and the role of the DP system in this regard.
2. Describe briefly the ingredients of conventional DP control.
3. Give a brief literature review of previous work on sea ice modelling.
4. Give a brief overview of concepts used in adaptive control, and investigate how these concepts could be used in an ice management system.
5. Based on the project work, construct an adaptive control system with concepts from impedance/force control, and implement the system in a test set-up.
6. Make illustrative simulations, write a report and discuss findings.

Start date: 6. January, 2014 **Due date:** 10. June, 2014

Supervisor: Lars Imsland
Co-advisor(s): Øivind Kåre Kjerstad, IMT

Trondheim, __10. January 2014_____

Lars Imsland
Supervisor

Address Sem Sælandsvei 5 NO-7491 Trondheim
Org.no. 974 767 880 E-mail: postmottak@itk.ntnu.no http://www.itk.ntnu.no
Location O.S. Bragstads plass 2D NO-7034 Trondheim
Phone + 47 73 59 43 76
Fax + 47 73 59 45 99
Phone: + 47 47 23 19 49

NTNU

Abstract

Faculty of Information Technology, Mathematics and Electrical Engineering
Department of Engineering Cybernetics

Studies done in recent years have shown a significant decline in the coverage of arctic sea ice. This trend has made the Arctic more accessible and has resulted in expanded naval activity in this region. Furthermore, an increasing desire among international petroleum operators to extend their operations towards the Arctic have resulted in vast investments in the development of these areas.

The increasing development of the oil and gas industry in the Arctic region makes rise to several challenges concerning navigation and control of the vessels operating in these waters. Although the trend shows a decrease in the thick multi-year ice cape covering most of the Arctic, a proportional increase in thinner ice floes is observed. The technology for vessel stationkeeping used in open waters today, known as Dynamic Positioning (DP), has not shown to perform sufficiently well in areas where ice is present.

In this thesis two model reference adaptive control schemes are implemented as a mean to achieve automatic vessel control in an ever changing sea ice environment. The first scheme is an indirect MRAC scheme, which aims to regulate the vessel dynamics with respect to the environment in order to achieve convergence to desired positions.

The second scheme is an extended MRAC scheme, referred to as MRAHFC, which incorporates hybrid force control into the vessel DP control system. Force control aims to regulate the vessel-environment interaction force dynamics in order to reduce environmental influence.

The proposed control schemes are demonstrated and compared with a reference PD controller with acceleration feed-forward. The results suggest that the indirect MRAC performs better relative to the reference controller in regulating the vessel to a stationary setpoint. Moreover, energy consumption is reduced, as the vessel applies less force in the process. However, neglection of cross terms in the system models results in drift-offs and excessive thrust force due to sway-yaw interaction. The results for the MRAHFC scheme show that the force controller does operate as intended. However, in the form demonstrated, it does not reduce energy consumption any further. Nor does it result in a noteworthy reduction in environmental influence, compared to the classic MRAC.

The results from the case study furthermore indicate that adaptive control might constitute as an enhancement relative to conventional systems. Nevertheless, more work has to be done in order to enhance the MRAC performance, as it does not, in the implemented form, account for cross terms in the system models. Enhancing the MRAC performance thus implies developing an adaptive control system for multi-variable systems. Such a development is believed to pose as a possible improvement of force control in this regard as well, as precise force control would require knowledge of every term in the system models. Finally, further work should be done in order to optimize the proposed control schemes with respect to fuel consumption and choice-of-route through the ice.

NTNU

Sammendrag

Fakultet for Informasjonsteknologi, Matematikk og Elektroteknikk
Institutt for Teknisk Kybernetikk

Studier gjort de siste årene har vist en betydelig nedgang i dekningen av sjøis i arktiske strøk. Dette har gjort arktiske strøk mer tilgjengelig, og har ført til utvidet marin virksomhet i disse områdene. Videre har en økt interesse blant internasjonale petroleumsoperatører om å utvide sine virksomheter til Arktis ført til store investeringer i utviklingen av disse sektorene.

Den økte utviklingen av petroleumsindustrien i arktiske strøk fører til flere utfordringer vedrørende navigasjon og kontroll av fartøyene som skal operere i disse områdene. Selv om man har registrert en nedgang i den fleråriige iskappen som dekker store deler av Arktis, observeres en proporsjonal økning i tynnere isflak, isfjell og drivis. Teknologien for settpunktsregulering brukt i åpne farvann i dag, dynamisk posisjonering (DP), har vist seg å være utilstrekkelig i områder med sjøis.

I denne hovedoppgaven blir to adaptive kontrollsystemer for automatisk fartøykontroll i et varierende sjøismiljø konstruert. Det første kontrollsystemet, referert til som MRAC, tar sikte på å tilpasse fartøyets dynamiske egenskaper relativt omgivelsene, for dermed å oppnå konvergens til ønsket posisjon.

Det andre kontrollsystemet (MRAHFC) er et utvidet system relativt det første. MRAHFC inkorporerer hybrid kraftkontroll i DP-systemet, og tar sikte på å regulere fartøyets interaksjonskrefter med omgivelsene for å redusere påvirkningen fra disse.

De nevnte kontrollsystemene er demonstrert og sammenlignet med en PD-regulator med foroverkobling fra forstyrrelser. Resultatene fra sammenligningen tyder på at MRAC-systemet har bedre ytelse relativt PD-regulatoren med tanke på å regulere fartøyet til ønsket settpunk. Resultatene viser også et redusert energiforbruk som følge av mindre påtrykt kraft fra fartøyets framdriftssystem. Neglisjering av koblede kryssledd i systemmodellene fører imidlertid til uønsket avdrift fra referansevinkelen i yaw. Resultatene for MRAHFC-systemet viser at den hybride kraftregulatoren fungerer som tiltenkt, men at den, i demonstrert form, ikke reduserer energiforbruket ytterligere. Heller ikke påvirkningen fra omgivelsene blir nevneverdig redusert ved bruk av kraftregulering.

Resultatene indikerer at adaptiv regulering har noe for seg, og at det muligens kan stå for en forbedring av konvensjonelle systemer i arktiske strøk. Mer arbeid må uansett påberegnes for å utbedre de demonstrerte systemene da de i skrivende stund ikke tar hensyn til kryssledd i systemets modellmatriser. En forbedring av systemet impliserer dermed utvikling av adaptive regulatorer for multivariable systemer. Dette kan også vise seg å forbedre systemer for kraftkontroll siden presis kraftkontroll krever kunnskap av samtlige ledd i systemmodellene. Endelig må mer arbeid påberegnes for å optimalisere de demonstrerte systmene med tanke på drivstofforbruk og valg av rute gjennom isen.

Preface

The work of this thesis has been conducted during the spring semester of 2014 and makes the course TTK4900 Engineering Cybernetics, Master Thesis at NTNU. It counts for 30 credits and aims to apply the knowledge acquired during 5 years of university education to do research based on litterature studies, and combine the knowledge gained into a project report in collaboration with supervisors.

I would like to show my gratitude to my supervisor, Professor Lars Imsland, for good supervising and good advises regarding the final report, and for giving corrections and directions during the thesis process.

This thesis has been conducted in close collaboration with The Department of Marine Technology, and I would like to thank my co-supervisor Øivind Kåre Kjerstad for providing me with good ideas on the implementation of control systems, as well as advises on how the project could be conducted and software help.

Finally, I would like to thank my excellent classmates and friends through the study for a good class environment and good discussions, on- and off-topic.

Vegar Østhus
Trondheim, June 2014

Contents

List of figures

List of tables

List of Symbols

N North position.

E East position.

θ Pitch angle.

ϕ Roll angle.

ψ Yaw angle.

u Surge velocity.

v Sway velocity.

r Yaw rate.

ω Resonant frequency.

ζ Damping ratio.

m Mass.

I Inertia.

d Damping.

$Z(s)$ Mechanical impedance, system transfer function numerator polynomial.

$R(s)$ System characteristic polynomial.

k System high frequency gain.

$\Lambda(s)$ Filter polynomial.

δ Constant gain parameter for dynamic normalization.

α Scaling factor.

$\boldsymbol{M}$ System inertia matrix.

$\boldsymbol{D}$ System linear damping matrix.

$\boldsymbol{d}$ System non-linear damping matrix.

$\boldsymbol{C}$ Matrix of non-linear Coriolis- and centripetal forces.

$\boldsymbol{R}$ General rotation matrix.

$\boldsymbol{\Gamma}$ Adaption gain matrix.

$\boldsymbol{K}_p$ Proportional gain matrix for PID control.

$\boldsymbol{K}_i$ Integral gain matrix for PID control.

$\boldsymbol{K}_d$ Derivative gain matrix for PID control.

$*$ Superscript denoting actual parameter.

n Superscript denoting nth polynomial order.

(n) Superscript denoting nth derivative.

n Subscript denoting model of nth order.

RB Subscript denoting general rigid body.

v Subscript denoting vessel parameter.

c, C Subscript denoting environment parameter.

m Subscript denoting reference model.

d Subscript denoting desired value.

r Subscript denoting reference value.

p Subscript denoting general plant, VP coordinates.

N Subscript denoting North.

E Subscript denoting East.

x Subscript denoting surge.

y Subscript denoting sway.

ψ Subscript denoting yaw.

zz Subscript denoting inertia about z axis.

$\boldsymbol{\eta}$ Vessel position in NED coordinates.

$\boldsymbol{\nu}$ Vessel velocity in BODY coordinates.

$\boldsymbol{F}_T$ Vector of thrust forces and moments.

$\boldsymbol{F}_C$ Vector of environmental forces and moments.

$\boldsymbol{\tau}$ Vector of vessel generalized forces and moments.

$\boldsymbol{\tau}_e$ Vector of environment generalized forces and moments.

$\boldsymbol{\theta}$ Vector of parameters.

$\boldsymbol{\mu}$ Regressor, vector of filtered input signals for adaptive law.

$\boldsymbol{\omega}$ Vector of filtered input signals for MRAC control law.

$\boldsymbol{\alpha}(s)$ Vector of derivatives.

List of Acronyms

AFF Acceleration Feed-Forward.

CG Center of Gravity.

CO Center of Origin.

DOF Degree of Freedom.

DP Dynamic Positioning.

DYPIC Dynamic Positioning in Ice.

EOM Equation of Motion.

HSVA Hamburgische Schiffbau-Versuchsanstalt (Hamburg Ship Model Basin).

IMO International Maritime Organization.

MIMO Multiple Inputs, Multiple Outputs.

MRAC Model Reference Adaptive Control.

MRAHFC Model Reference Adaptive Hybrid Force Control.

NIT Numerical Ice Tank.

NTNU Norges Teknisk-Naturvitenskapelige Universitet
(Norwegian University of Science and Technology).

PE Persistence of Excitation.

SISO Single Input, Single Output.

SSE Sum of Square Error.

Chapter 1

Introduction

1.1 Background and motivation

Surface and satellite-based observations have shown a noticeable decline in Arctic sea ice extent during the last 50 years (Stroeve et al., 2007; Eisenman et al., 2011). The reduction of the multi-year Arctic ice cape has made the Arctic more accessible for marine operations, and has resulted in an expanded naval activity in the area. Furthermore, an increased desire among international petroleum operators to extend their operations towards the Arctic, has led to vast investments in the development of these areas. In a 2008 study performed by the United States Geological Survey, a potential of 90 billion barrels of oil and 44 billion barrels of natural gas was estimated for the areas north of the arctic circle (Robertson and Pierce, 2008).

Even though studies show a decrease in the multi-year ice cape covering most of the Arctic, a proportional increase in thinner, seasonal ice and ice floes are observed (Eisenman et al., 2011). Such areas poses a challenge for marine activity as the sea ice represents a significant hazard to equipment applied in the operations. Some attempts on decreasing the vulnerability and increasing the performance of ice going vessels has been made, including research done on vessel hull design and power requirements (Juva and Riska, 2002; Riska, 2011). However, systems for vessel guidance and control in the case of ice interference are not well developed (Jenssen et al., 2009).

Vessels equipped with dynamic positioning (DP) systems operating in ice covered marine areas are usually situated in a type of environment known as managed ice. Managed ice refers to the type of scenario where one or more ice breakers, operating upstream from the DP vessel, breaks solid ice into scattered ice floes drifting down an ice channel (Kjerstad et al., 2014; Metrikin et al., 2013). This approach has given good results in full scale experiments involving automatic vessel control (Jenssen et al., 2012).

1.1.1 Dynamic positioning in Arctic areas

According to the IMO Resolution MSC/Circ. 645 (IMO, 1994) a DP vessel is defined as a vessel that automatically maintains its position (be it a static setpoint or a possibly time varying trajectory) exclusively by the means of thruster force. Set-point regulation in the DP context is used extensively in many marine operations, such as drilling, hydrocarbon extraction and cargo loading.

In operations situated at deep ocean sites, Dynamic Positioning (DP) is the only way to keep a surface vessel at a predefined position. In these situations vessel guidance is conducted purely by the means of the ship thrusters, which attempts to counteract for environmental disturbances such as wind, waves and ocean currents.

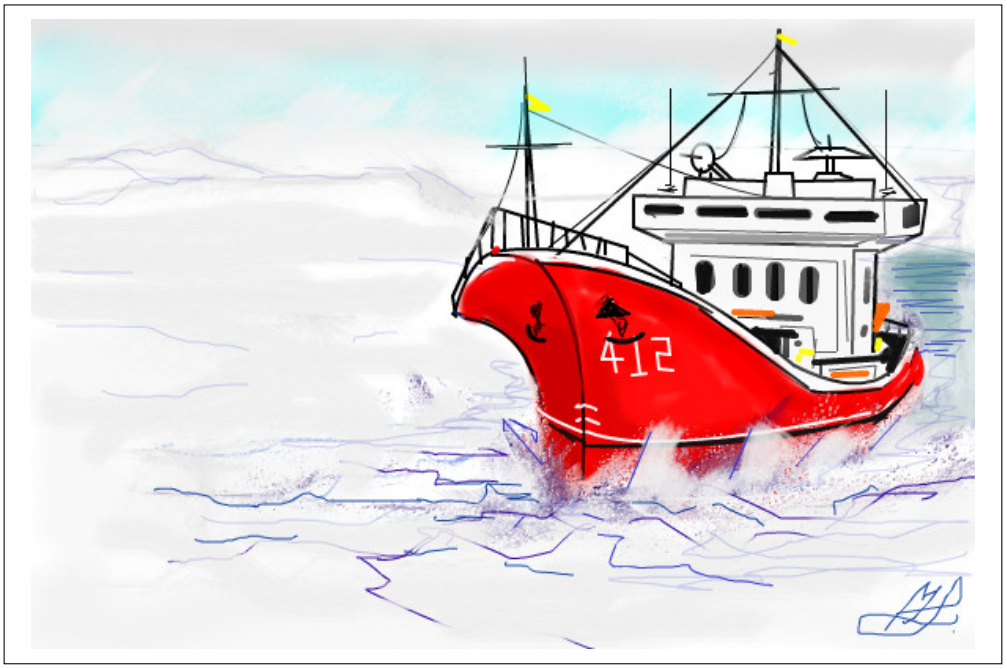

FIGURE 1.1: Vessel operating in a sea ice environment. Courtesy of marky

Figure 1.1 shows an ice going vessel in a typical Arctic environment. In recent years, several studies have investigated the effect of sea ice interference on vessels operating in Arctic areas. The studies have shown that vessel control systems shown to be successful in open waters have proven ineffective in environments where sea ice is present. One of the reasons for this is that the ice loads represents a rather large, quickly varying disturbance force(Jenssen et al., 2012). In addition, the ice forces acts on the vessel in a seemingly non-deterministic manner. Thus, models proposed to date, describing sea ice behavior, has yet to prove adequate in a practical setting. Classic control techniques, including pole placement and feed-forward of environmental force predictions, are therefore difficult to conduct.

An additional reason for the difficulties associated with vessel control during sea ice interaction, is that the sea ice is believed to change the dynamics of the vessel. In the process of withstanding the ice loads, the vessel thrusters have to overcome the additive inertia, friction and adhesive properties of the ice. The sea ice interference thus represents a vessel-ice *system coupling*. This entails that the vessel model coefficient matrices might become time-varying and heavily dependent on the conditions in the environment at any time. A static model of a sea ice environment may therefore be deficient in order to describe the disturbances induced by the ice loads (Wold, 2013).

1.1.2 Adaptive control

Control schemes for static environments, including PID control with static gain matrices has proven effective in situations where changes of the system can be assumed small enough to be neglected, or the changes in the environmental forces are sufficiently slow. However, in cases where a quickly changing environment has non-desirable effects on a system, such control schemes might be left ineffective. Furthermore, the schemes may even become unstable when the design variables no longer meet the demands set by the environment (Ioannou and Sun, 1996).

Adaptive control schemes aim to make a control system adapt to changes in the operating environment, or even changes in the system itself. These changes could be due to weather hazards or aging on equipment involved in the control system.

If an ice going vessel could be made to adapt to the ever-changing dynamics of the sea ice, positioning performance might be increased. Moreover, thruster usage might be decreased, as such a controller would calculate the control signal more precisely relative to controllers applied by open water systems.

1.1.3 Impedance control

Impedance control is a technique used to manipulate the mechanical impedance of a system to better comply with the interacting forces of the environment. Impedance control has been used extensively in robotics for several years. The technique allows a system to interact with and manipulate the environment in a controlled manner (Anderson and Spong, 1988; Liu and Goldenberg, 1991).

In light of the studies conducted with regards to sea ice interference on surface vessels, a pure setpoint regulating control system might not be the best option in terms of energy consumption and wear and tear on vessel machinery. With the conventional open water control systems in use today, a vessel encountering large, rigid ice loads would attempt to drive its thrusters to their operational limit, even though the setpoint cannot be reached due to excessive ice forces. If a control system could be implemented, which

better handles large interacting forces exerted by the ice, this might result in decreased energy consumption, as well as reduced wear on mechanical equipment.

The concept of impedance control can be extended to incorporate *force control*. Force control allows a system to control the *environmental* forces in a given direction by adjusting its own perceived mechanical impedance (Singh and Popa, 1995).

For DP operations in ice, a control system which takes into account the interaction between vessel and ice is assumed to be be advantageous with regards to precision, robustness and energy consume, as well as to wear and tear on the vessel hull and thruster propellers.

1.2 Scope of work

The main motivation for this thesis is to investigate the feasibility of adaptive control designs and force control for DP systems in managed sea ice. Conventional systems tested in these areas to date have shown a vast potential of improvement in this field of research.

Figure 1.2 shows the outline of a general DP system. The focus of this thesis will be the highlighted box representing the motion control part of the system.

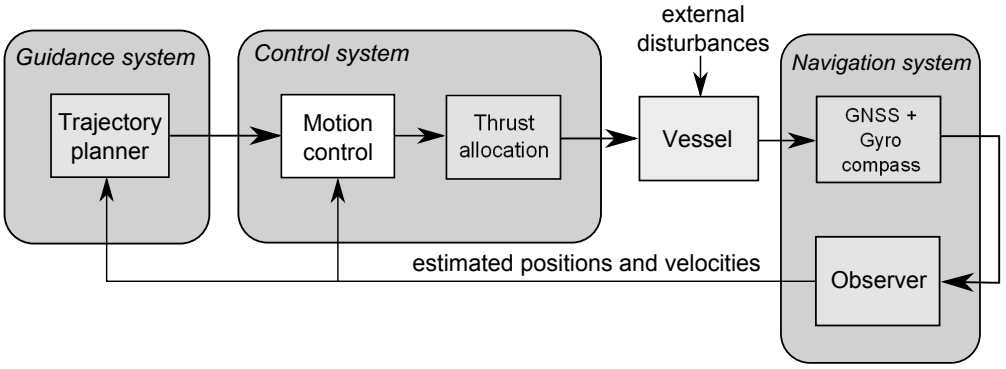

FIGURE 1.2: Modules of the DP system

The thesis will investigate two hypotheses in particular.

Hypothesis 1. An adaptive control system, which adjusts its actuating signal based on key parameters of the vessel and the environment, is better suited for operations where varying, non-predictable operating conditions are affecting the vessel in a non-desirable manner.

Hypothesis 2. Incorporating concepts from explicit force control will alleviate the environmental forces acting on the vessel, resulting in decreased energy consume by the vessel thrusters, as well as reducing mechanical damage and wear and tear on vessel equipment.

A robust indirect model reference adaptive controller (MRAC) is implemented to cope with the disturbances induced mainly by drifting sea ice in a managed ice channel. The MRAC scheme utilizes a reference model, which applies concepts of impedance control by inhabiting desirable dynamic properties. Moreover, a control law is determined based on the properties of the reference model, as well as the coupled dynamics of the vessel and the environment, such that the vessel is controlled to track the output furnished by the reference model. The reference model is allowed to switch between providing a position trajectory or a force trajectory. This is achieved by dividing the control domain into *subspaces* based on whether position control or force control is desirable in a given situation.

Throughout the thesis, it will be assumed that a proper measurement of the environmental forces in three degrees of freedom is available. Such a signal can be acquired through acceleration measurements as described in (Kjerstad et al., 2011; Kjerstad and Skjetne, 2012).

1.2.1 Implementation and execution of tests

The proposed MRAC scheme was implemented using Simulink® and MATLAB. Furthermore, a novel high-fidelity tool developed at NTNU was employed to simulate a DP vessel moving through a managed ice field (Metrikin et al., 2013). The proposed MRAC scheme was tested in the simulator and compared to a PD controller with feed-forward of the environmental forces. The latter has shown good results in tests performed at the large ice tank of the Hamburgische Schiffbau-Versuchsanstalt (Hamburg Ship Model Basin) (HSVA) in 2012 within the European R&D project DYPIC (Jenssen et al., 2012).

1.3 Thesis outline

Figure 1.3 shows the outline of the thesis. Chapter 2-4 will cover the relevant theory applied in this work. As this thesis is a continuation of the project work conducted during the fall of 2013, Chapters 2 and 3 will to a great extent be based on the sections on the respective topics in Østhus (2013). These topics are included to produce a coherent and stand-alone dissertation.

Chapter 5 will present the implementation of the proposed control schemes, and the case study investigating the performance of these is carried out in Chapter 6. In Chapter 7 the results from the case study is presented, while Chapter 8 discusses the results. In Chapter 9 conclusions are drawn.

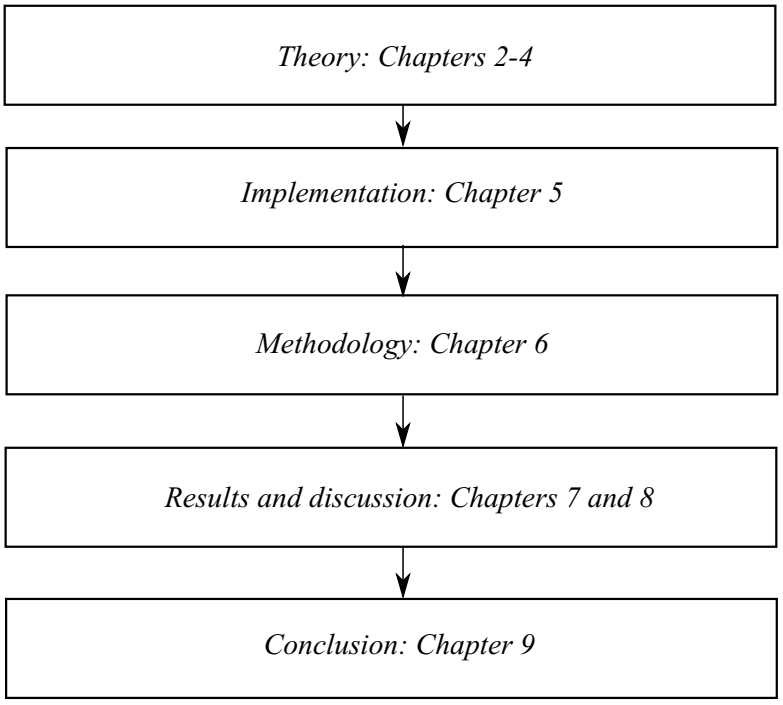

FIGURE 1.3: Thesis outline

Chapter 2

Mathematical modelling of marine craft

The knowledge of the characteristic dynamics of a marine craft is essential in order to develop control designs for any purpose. Allthough a qualitative behavior of a vessel can be observed in ship model tank experiments, knowledge of the interaction between control forces and environment in the different degrees of freedom (DOF) is crucial in order to get good results.

In this chapter, a linear model of a floating vessel in 3 DOF, as it appears in Fossen (2011), is derived. The chapter will begin by presenting the different frames of reference commonly used in vessel control. Next, the mathematical modeling of a surface vessel in the general case is addressed. Furthermore, the model is simplified and linearized for the case of low-speed purposes. Thereafter, the modeling of environmental forces acting on the vessel is examined. The last part of the chapter unveils issues related to sea ice interference in the case of DP operations in Arctic areas.

2.1 Reference frames

The analysis of marine craft motion usually includes two Earth-centered and a number of geographical reference frames. Nevertheless, in this thesis it is assumed that the craft resides in a relatively small area of operation. Moreover, the velocity of the craft is assumed to be relatively small. Thus, effects caused by the rotation of the Earth is neglected. Fuinally, all movements are assumed to occur in an area defined by a tangential reference frame fixed to some position on the surface of the Earth. The following reference frames are employed (Fossen, 2011).

ECEF The Earth Centered Earth-fixed coordinate system denoted $\{e\} = \{x_e, y_e, z_e\}$ rotates with the Earth. This is the reference frame in which global location coordinates

are given as a position vector $\Theta_{en} = [l \ \mu]^T$, where l and μ denotes longitude and latitude respectively. In this report the ECEF frame is used to specify the location of the inertial reference frame.

NED When the area of operation is constrained to a small area, and the velocity is close to zero, the NED frame may be referred to as the inertial frame denoted $\{n\} = (x_n, y_n, z_n)$. Its origin o_n is then fixed at a specified location Θ_{en} on the surface of the Earth. This is referred to as flat Earth navigation. Defined on a plane tangential to a local reference surface, its x-axis points towards true *north*, its y-axis points towards *east* and its z-axis points *downwards* normal to the plane.

BODY The BODY reference frame $\{b\} = (x_b, y_b, z_b)$ moves and rotates with the vessel. Its x-axis points along the vessel's longitudinal axis (aft to fore), the y-axis points starboard and the z-axis completes the coordinate system pointing downwards normal to the plane defined by the x and y axis.

VP The vessel parallel (VP) coordinate frame denoted $\{p\} = \{x_p, y_p, z_p\}$ is obtained by rotating the NED frame an angle ψ clockwise. Thus, the x_p axis is parallel to the vessel heading, while its origin o_p coincides with the origin o_n of the NED frame.

Figure 2.1 shows the different reference frame used in this work as described in Fossen (2011).

2.1.1 Rotation matrices

A rotation matrix relates a vector represented in one coordinate frame to a corresponding vector in some other coordinate system. Introducing the notion of *Euler angles* a coordinate frame can be expressed in terms of some other coordinate system and the rotation matrix that relates the two. Euler angles is based on Euler's theorem for rotation of rigid bodies in Euclidean space. The theorem states that every rotation can be decomposed into three simple rotations about each of the orthogonal axes (Euler, 1776). The magnitude of each of these rotations is denoted by the angles roll (ϕ), pitch (θ) and yaw (ψ) for rotations about the x-axis, y-axis and z-axis respectively. The rotation matrices for each of these simple rotations are given by

$$\mathbf{R}_{x,\phi} = \begin{pmatrix} 1 & 0 & 0 \\ 0 & c(\phi) & -s(\phi) \\ 0 & s(\phi) & c(\phi) \end{pmatrix}, \quad \mathbf{R}_{y,\theta} = \begin{pmatrix} c(\theta) & 0 & s(\theta) \\ 0 & 1 & 0 \\ -s(\theta) & 0 & c(\theta) \end{pmatrix}, \quad \mathbf{R}_{z,\psi} = \begin{pmatrix} c(\psi) & -s(\psi) & 0 \\ s(\psi) & c(\psi) & 0 \\ 0 & 0 & 1 \end{pmatrix} \tag{2.1}$$

By composing these matrices one can represent every rotation in three dimensional Euclidean space. The transformation of a vector defined in $\{b\}$ to the corresponding vector defined in $\{n\}$ is given by

$$\nu_n = \mathbf{R}_b^n \nu_b \tag{2.2}$$

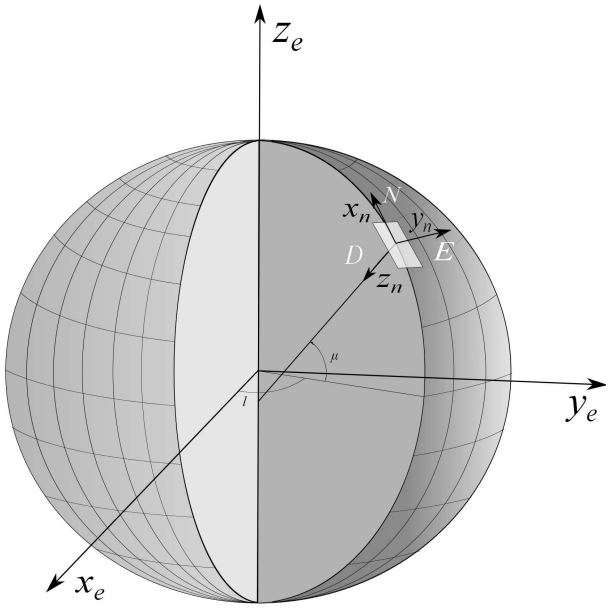

(A) Definition of longitude l, latitude μ and the NED coordinate frame

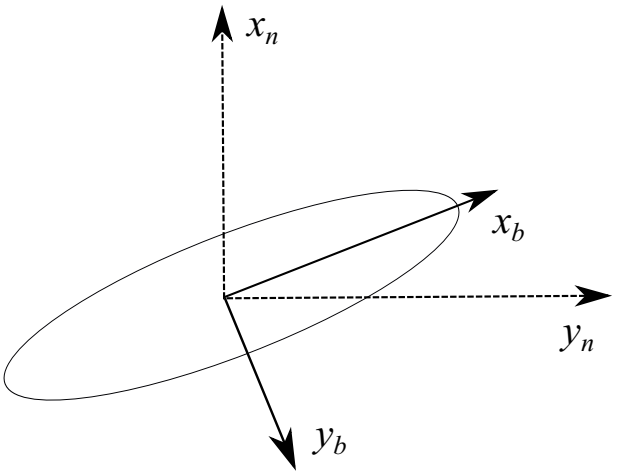

(B) Depiction of the BODY frame relative to the NED. The VP coordinate frame in this case coincides with the BODY frame.

FIGURE 2.1: Definitions of the coordinate frames

where ν_n is a vector expressed in $\{n\}$, ν_b is a vector defined in $\{b\}$, and $\mathbf{R}_b^n$ is defined as

$$\mathbf{R}_b^n := \mathbf{R}_{z,\psi}\mathbf{R}_{y,\theta}\mathbf{R}_{x,\phi} \tag{2.3}$$

where ψ, θ, ϕ are the angles of rotation about x_b, y_b, z_b relative to the corresponding axes in $\{n\}$ respectively.

In order to derive the equations of motion (EOM) for a surface vessel, some knowledge of rigid body kinetics is required. This is covered in the following section.

2.2 Mathematical modelling of marine crafts

When deriving the equations of motion for a marine vessel it is common to define two points of reference, namely

CO The Center of Origin

CG The Center of Gravity

The CG is dependent on the design of the vessel as well as the load conditions. The CO is usually specified by the control engineer and is the reference point used in guidance and control systems. Moreover, the CO is the origin of the BODY reference frame $\{b\}$ (Fossen, 2011).

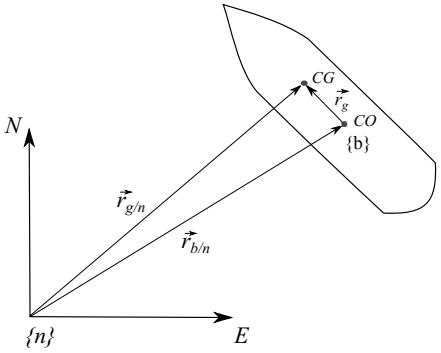

FIGURE 2.2: Definitions of position vectors related to CG and CO

As stated in Section 2.1, in this thesis the NED frame is used as the inertial reference frame. Accordingly, $\vec{r}_{g/n}$ is the coordinate free position vector of CG relative to o_n, $\vec{r}_{b/n}$ is the coordinate free position vector of CO relative to o_n and $\vec{r}_g$ is the coordinate free position vector of CG relative to CO, as shown in Figure 2.2.

2.2.1 Modelling of rigid-body kinetics in 6 DOF

The following will present the EOM of a rigid body moving in an inertial coordinate frame. The terms included in the equations are described in a fundamental manner.

The EOM of a rigid body in 6 DOF is derived from the Newton-Euler formulation which states that the motion of the point CG about CO defined in a moving reference frame can be described by (Fossen, 2011)

$$m\left[\dot{\boldsymbol{\nu}}^b_{b/n} + \boldsymbol{S}(\dot{\boldsymbol{\omega}}^b_{b/n})\boldsymbol{r}^b_g + \boldsymbol{S}(\boldsymbol{\omega}^b_{b/n})\boldsymbol{\nu}^b_{b/n} + \boldsymbol{S}^2(\boldsymbol{\omega}^b_{b/n})\boldsymbol{r}^b_g\right] = \boldsymbol{f}^b_b \tag{2.4}$$

$$\boldsymbol{I}_b\dot{\boldsymbol{\omega}}^b_{b/n} + \boldsymbol{S}(\boldsymbol{\omega}^b_{b/n})\boldsymbol{I}_b\boldsymbol{\omega}^b_{b/n}\boldsymbol{\omega}^b_{b/n} + m\boldsymbol{S}(\boldsymbol{r}^b_g)\dot{\boldsymbol{\nu}}^b_{b/n} + m\boldsymbol{S}(\boldsymbol{r}^b_g)\boldsymbol{S}(\boldsymbol{\omega}^b_{b/n})\boldsymbol{\nu}^b_{b/n} = \boldsymbol{m}^b_b \tag{2.5}$$

In Equations (2.4), (2.5), m is the mass of the body, $\boldsymbol{\nu}^b_{b/n}$ and $\boldsymbol{\omega}^b_{b/n}$ is the translational and angular velocity respectively of the point CG relative to CO expressed in $\{b\}$. $\boldsymbol{f}^b_b$ and $\boldsymbol{m}^b_b$ are the forces and moments acting on CG respectively. $\boldsymbol{I}_b$ is given by

$$\boldsymbol{I}_b = \boldsymbol{I}_g - m\boldsymbol{S}^2(\boldsymbol{r}^b_g) \tag{2.6}$$

where $\boldsymbol{r}^b_g = [x_g, y_g, z_g]^\top$ is the coordinate position vector of CG expressed in $\{b\}$. $\boldsymbol{I}_g \in \mathbb{R}^{3\times3}$ is known as the inertia matrix about the point CG in a moving reference frame, defined as

$$\boldsymbol{I}_g \triangleq \begin{bmatrix} I_x & -I_{xy} & -I_{xz} \\ -I_{yx} & I_y & -I_{yz} \\ -I_{zx} & -I_{zy} & I_z \end{bmatrix}, \qquad \boldsymbol{I}_g = \boldsymbol{I}_g^\top > 0 \tag{2.7}$$

Equation (2.6) is known as the parallel-axes theorem. The parallel-axes theorem transforms the inertia matrix (2.7) to yield for the motion of CG about any point on the rigid body.

The last three terms on the left of Equations (2.4), (2.5) are cross product terms, written in matrix form, that relates the motion of CG expressed in $\{b\}$ to the motion of o_b about $\{n\}$.

The equations (2.4), (2.5) can be written in matrix form (Fossen, 2011)

$$\boldsymbol{M}_{RB}\dot{\boldsymbol{\nu}} + \boldsymbol{C}_{RB}(\boldsymbol{\nu})\boldsymbol{\nu} = \boldsymbol{\tau} \tag{2.8}$$

where $\boldsymbol{\nu} = [u, v, w, p, q, r]$ is a generalized vector of velocities expressed in $\{b\}$, and $\boldsymbol{\tau} = [X, Y, Z, K, M, N]$ is a generalized vector of forces and moments expressed in $\{b\}$. $\boldsymbol{M}_{RB}$ can be written as

$$\boldsymbol{M}_{RB} = \begin{bmatrix} m\boldsymbol{I}_{3\times3} & m\boldsymbol{S}(r^b_g) \\ m\boldsymbol{S}(r^b_g) & \boldsymbol{I}_b \end{bmatrix} \tag{2.9}$$

The matrix $\boldsymbol{C}_{RB}$ consists of non-linear Coriolis- and centripetal force terms found from $\boldsymbol{M}_{RB}$ by Theorem 3.2 in Fossen (2011),

$$\boldsymbol{C}_{RB} = \begin{bmatrix} \boldsymbol{0}_{3\times3} & -\boldsymbol{S}(\boldsymbol{M}_{RB_{11}}\boldsymbol{\nu}_1 + \boldsymbol{M}_{RB_{12}}\boldsymbol{\nu}_2) \\ -\boldsymbol{S}(\boldsymbol{M}_{RB_{11}}\boldsymbol{\nu}_1 + \boldsymbol{M}_{RB_{12}}\boldsymbol{\nu}_2) & -\boldsymbol{S}(\boldsymbol{M}_{RB_{21}}\boldsymbol{\nu}_1 + \boldsymbol{M}_{RB_{22}}\boldsymbol{\nu}_2) \end{bmatrix} \tag{2.10}$$

In Equation (2.10), $\boldsymbol{M}_{RB_{ij}}$ corresponds to the term at index ij in $\boldsymbol{M}_{RB}$, and $\boldsymbol{\nu}_1$ and $\boldsymbol{\nu}_2$ are the translational and the rotational part of the velocity vector expressed in $\{b\}$ respectively.

An important thing to note from this is that if CO coincides with CG, $r_g = [0, 0, 0]$ and the cross products of $\boldsymbol{M}_{RB}$ cancels out. If, in addition, the body axes (x_b, y_b, z_b) coincides with the principal axes of rotation, this results in a diagonal rigid-body mass

matrix

$$\boldsymbol{M}_{RB} = \begin{bmatrix} m\boldsymbol{I}_{3\times3} & \boldsymbol{0}_{3\times3} \\ \boldsymbol{0}_{3\times3} & \boldsymbol{I}_g \end{bmatrix} \tag{2.11}$$

where $\boldsymbol{I}_g = diag\{I_x^{cg}, I_y^{cg}, I_z^{cg}\}$ and $I_i^{cg}, i \in \{x, y, z\}$ is the moment of inertia about the corresponding axes of rotation according to Definition 3.1 in Fossen (2011). This ideal property will be exploited and applied as a simplification to the system investigated in this thesis.

2.2.2 Simplifications for low-speed maneuvering

When stationkeeping operations for surface vessels are considered, it is convenient to simplify the EOM to a 3 DOF dynamic positioning (DP) model. The DP model includes the EOM for surge, sway and yaw. The equations for heave, roll and pitch are neglected as the motions and corresponding motion rates for these DOFs are considered small. The 3 DOF DP model is valid for low-speed operations up to approximately 2 m/s, and can be written (Fossen, 2011)

$$\boldsymbol{M}_{RB}^{3\times3}\dot{\boldsymbol{\nu}} + \boldsymbol{C}_{RB}^{3\times3}(\boldsymbol{\nu})\boldsymbol{\nu} = \boldsymbol{\tau} \tag{2.12}$$

where

$$\boldsymbol{M}_{RB}^{3\times3} = \begin{bmatrix} m & 0 & 0 \\ 0 & m & mx_g \\ 0 & mx_g & I_z^{cg} \end{bmatrix}, \quad \boldsymbol{C}_{RB}^{3\times3} = \begin{bmatrix} 0 & 0 & -m(x_g r + v) \\ 0 & 0 & mu \\ m(x_g r + v) & -mu & 0 \end{bmatrix}$$

and $\boldsymbol{\nu}, \boldsymbol{\tau} \in \mathcal{R}^3$ are the corresponding generalized vectors of velocity and force and moments respectively.

In the remainder of this thesis only the EOM in 3 DOF will be considered. Thus, the superscript 3×3 denoting matrix dimensions is implied and will be omitted in the following sections.

2.2.3 Modeling of environmental forces

When environmental forces are included in the DP model, the rigid-body kinetic model may be described as (Fossen, 2011)

$$\boldsymbol{M}_{RB}\dot{\boldsymbol{\nu}} + \boldsymbol{C}_{RB}(\boldsymbol{\nu})\boldsymbol{\nu} = \boldsymbol{\tau} + \boldsymbol{\tau}_{env} \tag{2.13}$$

where the term $\boldsymbol{\tau}_{env}$ denotes environmental (hydrodynamic) forces and disturbances. For open water purposes $\boldsymbol{\tau}_{env}$ can be modelled as

$$\boldsymbol{\tau}_{env} = -\boldsymbol{M}_c\dot{\boldsymbol{\nu}} - \boldsymbol{C}_c(\boldsymbol{\nu}_r)\boldsymbol{\nu}_r - \boldsymbol{D}_c\boldsymbol{\nu}_r - \boldsymbol{d}_c(V_{rc}, \gamma_{rc}) \tag{2.14}$$

where $\boldsymbol{\nu}_r$ is the velocity of the ship relative to the surrounding fluid, This gives

$$\underbrace{(\boldsymbol{M}_{RB}+\boldsymbol{M}_c)}_{\boldsymbol{M}}\dot{\boldsymbol{\nu}}+\underbrace{(\boldsymbol{C}_{RB}(\boldsymbol{\nu})\boldsymbol{\nu}+\boldsymbol{C}_c(\boldsymbol{\nu}_r)\boldsymbol{\nu}_r)}_{\boldsymbol{C}}+\boldsymbol{D}_c\boldsymbol{\nu}_r+\boldsymbol{d}_c(V_{rc},\gamma_{rc})=\boldsymbol{\tau} \tag{2.15}$$

It can be seen from (2.15) that the dynamics of the system are changed due to the environmental forces. The matrices $\mathbf{M_c}$ and $\mathbf{C_c}$, which are called added mass matrices, arises from the fact that as the vessel maneuver through the surrounding fluid, the fluid moves aside and thus obtains a certain kinetic energy. The energy T_c is given by

$$T_c=\frac{1}{2}\boldsymbol{\nu}^\top\boldsymbol{M}_c\boldsymbol{\nu} \tag{2.16}$$

where $\boldsymbol{M}_c$ is the inertia matrix of the fluid itself given by

$$\boldsymbol{M}_c=\boldsymbol{M}_c^\top=\begin{bmatrix}-X_{\dot{u}} & 0 & 0\\ 0 & -Y_{\dot{v}} & -Y_{\dot{r}}\\ 0 & -Y_{\dot{r}} & -N_{\dot{r}}\end{bmatrix} \tag{2.17}$$

This leads to a corresponding additive matrix of Coriolis terms

$$\boldsymbol{C}_c(\boldsymbol{\nu}_r)=-\boldsymbol{C}_c^\top(\boldsymbol{\nu}_r)=\begin{bmatrix}0 & 0 & Y_{\dot{v}}v_r+Y_{\dot{r}}r\\ 0 & 0 & -X_{\dot{u}}u_r\\ -Y_{\dot{v}}v_r-Y_{\dot{r}}r & X_{\dot{u}}u_r & 0\end{bmatrix} \tag{2.18}$$

The matrix $\boldsymbol{D}_c$ is called the linear damping matrix and consists of linear damping terms due to dampening effects of the fluid acting on the vessel.

$$\boldsymbol{D}_c=\begin{bmatrix}-X_u & 0 & 0\\ 0 & -Y_v & -Y_r\\ 0 & -N_v & -N_r\end{bmatrix} \tag{2.19}$$

The terms in (2.17)-(2.19) represents forces and moments due to hydrodynamic accelerations and velocities. They are written in the notation of SNAME (1950). For example, the hydrodynamic added mass force Y along the y axis due to an acceleration $\dot{r}$ about the z axis is written

$$Y=-Y_{\dot{r}}\dot{r},\qquad Y_{\dot{r}}\triangleq\frac{\partial Y}{\partial\dot{r}} \tag{2.20}$$

While the linear matrix $\boldsymbol{D}_c$ defined above is an important term for low-speed maneuvers and stationkeeping, the term $\boldsymbol{d}_c(V_{rc},\gamma_{rc})$ dominates at higher speeds. $\boldsymbol{d}_c(V_{rc},\gamma_{rc})$ is a vector consisting of the nonlinear current forces acting on the vessel, given by (Fossen,

2011)

$$\boldsymbol{d}_c(V_{rc}, \gamma_{rc}) = \begin{bmatrix} -\frac{1}{2}\rho A_{F_c} C_X(\gamma_{rc}) V_{rc}^2 \\ -\frac{1}{2}\rho A_{L_c} C_Y(\gamma_{rc}) V_{rc}^2 \\ -\frac{1}{2}\rho A_{L_c} L_{oa} C_N(\gamma_{rc}) V_{rc}^2 - N_{|r|r}|r|r \end{bmatrix} \tag{2.21}$$

where ρ denotes the density of the fluid, A_{F_c} and A_{L_c} are the frontal and lateral projected current areas of the vessel, L_{oa} is the length of the waterline (length overall), and $N_{|r|r} > 0$ is a damping term used to counteract for destabilizing terms in yaw. The constants C_X, C_Y and C_N are the so-called *current coefficients*, which can be found empirically by the use of scale models in wind tunnels. V_{rc} and γ_{rc} are the relative current speed and angle of attack with respect to $\{b\}$ defined by

$$V_{rc} = \sqrt{u_{rc}^2 + v_{rc}^2} = \sqrt{(u - u_c)^2 + (v - v_c)^2} \tag{2.22}$$

$$\gamma_{rc} = -\text{atan2}(v_{rc}, u_{rc}) \tag{2.23}$$

$$u_c = V_c \cos(\beta_c - \psi) \tag{2.24}$$

$$v_c = V_c \sin(\beta_c - \psi) \tag{2.25}$$

where V_c is the current speed and β_c is the current direction with respect to $\{n\}$. The dynamics can now be combined into a final equation, given by

$$\boldsymbol{M}\dot{\boldsymbol{\nu}} + \boldsymbol{C}(\boldsymbol{\nu})\boldsymbol{\nu} + \boldsymbol{D}_c\boldsymbol{\nu} + \boldsymbol{d}_c(V_{rc}, \gamma_{rc}) = \boldsymbol{\tau} \tag{2.26}$$

where

$$\boldsymbol{M} = \begin{bmatrix} m - X_{\dot{u}} & 0 & 0 \\ 0 & m - Y_{\dot{v}} & mx_g - Y_{\dot{r}} \\ 0 & mx_g - Y_{\dot{r}} & I_z - N_{\dot{r}} \end{bmatrix}$$

$$\boldsymbol{C} = \begin{bmatrix} 0 & 0 & -m(x_g r + v) + Y_{\dot{v}} v_r + Y_{\dot{r}} r \\ 0 & 0 & mu - X_{\dot{u}} u_r \\ m(x_g r + v) - Y_{\dot{v}} v_r - Y_{\dot{r}} r & -mu + X_{\dot{u}} u_r & 0 \end{bmatrix}$$

The general DP model can now be described from (2.26) (Fossen, 2011)

$$\dot{\boldsymbol{\eta}} = \boldsymbol{R}_\Theta(\boldsymbol{\eta})\boldsymbol{\nu} \tag{2.27a}$$

$$\boldsymbol{M}\dot{\boldsymbol{\nu}} + \boldsymbol{C}(\boldsymbol{\nu})\boldsymbol{\nu} + \boldsymbol{D}_c\boldsymbol{\nu} + \boldsymbol{d}_c(V_{rc}, \gamma_{rc}) = \boldsymbol{\tau} \tag{2.27b}$$

where $\boldsymbol{\eta}$ is the state vector in $\{n\}$ and $\boldsymbol{R}_\Theta(\boldsymbol{\eta})$ is the rotation matrix relating a velocity vector expressed in the $\{b\}$ frame to the corresponding vector in the $\{n\}$ frame.

2.2.4 Linearizing the DP model

For stationkeeping operations, where $u, v \leq 2$ m/s, the Coriolis term $\boldsymbol{C}(\boldsymbol{\nu})$ and the non-linear damping term $\boldsymbol{d}_c(V_{rc}, \gamma_{rc})$ can be considered small. Thus, for such low-speed operations, it is convenient to simplify the model (2.27) by neglecting these terms and include only the added mass term $\boldsymbol{M}_c$ and linear damping $\boldsymbol{D}_c$ when considering environmental forces (Fossen, 2011). Furthermore, by rotating the position vector $\boldsymbol{\eta}$ in (2.27) an angle ψ about the z axis, positions can be expressed in the vessel parallel (VP) coordinates introduced in Section 2.1. The VP position vector is given by

$$\boldsymbol{\eta}_p = \boldsymbol{R}_\Theta^\top(\psi)\boldsymbol{\eta} \tag{2.28}$$

Differentiating (2.28) with respect to time gives

$$\dot{\boldsymbol{\eta}}_p = r\boldsymbol{S}\boldsymbol{\eta}_p + \boldsymbol{\nu} \tag{2.29}$$

where $r = \dot{\psi}$ and

$$\boldsymbol{S} = \begin{bmatrix} 0 & 1 & 0 \\ -1 & 0 & 0 \\ 0 & 0 & 0 \end{bmatrix} \tag{2.30}$$

As stationkeeping is considered, r may be assumed to be small. Thus, the cross terms in (2.29) may be neglected and

$$\dot{\boldsymbol{\eta}}_p \approx \boldsymbol{\nu} \tag{2.31}$$

This gives the *linearized* DP model

$$\dot{\boldsymbol{\eta}}_p = \boldsymbol{\nu} \tag{2.32a}$$

$$\boldsymbol{M}\dot{\boldsymbol{\nu}} + \boldsymbol{D}_c\boldsymbol{\nu} = \boldsymbol{\tau} \tag{2.32b}$$

2.3 Motion control in Arctic conditions

The system matrices $\boldsymbol{M}$, $\boldsymbol{D}_c$ in (2.32) as well as the Coriolis matrix $\boldsymbol{C}(\boldsymbol{\nu})$ and the vector of nonlinear current forces $\boldsymbol{d}_c(V_{rc}, \gamma_{rc})$ in (2.27) may be modeled relatively easy in open-water settings by the theory in Section 2.2.3. Thus, they can be compensated for by introducing compliant terms in the model. For instance, consider the PID control law

$$\boldsymbol{\tau} = -\boldsymbol{R}_\Theta^\top(\boldsymbol{\eta})\boldsymbol{K}_p\tilde{\boldsymbol{\eta}} - \boldsymbol{R}_\Theta^\top(\boldsymbol{\eta})\boldsymbol{K}_d\dot{\boldsymbol{\eta}} - \boldsymbol{R}_\Theta^\top(\boldsymbol{\eta})\boldsymbol{K}_i\int_0^t \tilde{\boldsymbol{\eta}}\,d\tau \tag{2.33}$$

where

$$\tilde{\boldsymbol{\eta}} = \boldsymbol{\eta}_r - \boldsymbol{\eta} \tag{2.34}$$

The gain parameters $\boldsymbol{K}_p$, $\boldsymbol{K}_d$ and $\boldsymbol{K}_i$ in (2.33) may now be determined by well known techniques as for example pole placement, as the dynamics of the system are known (Fossen, 2011).

However, if forces due to sea ice interference are included in $\boldsymbol{\tau}_{env}$ this will complicate matters as there are few, if any, good models of sea ice dynamics available (Eik, 2010). Furthermore, it is believed that sea ice interference represents a severe, varying change in the vessel dynamics (2.26). In such a situation, if the variations are excessive, conventional open-water DP schemes might become inadequate (Wold, 2013).

By introducing force feedback in Equation (2.27), the *apparent impedance* of the system may be changed in a desirable manner. This concept will be exploited in the proposed control scheme of this thesis, and may be illustrated by a simple example taken from Spong et al. (2006).

Example 2.1. *Consider the one-dimensional system in Figure 2.3 consisting of a mass M on a frictionless surface subject to an environmental force F and control input u. The equation of motion of the system is*

$$M\ddot{x} = u - F$$

With $u = 0$, the object "appears to the environment" as a pure inertia with mass M.

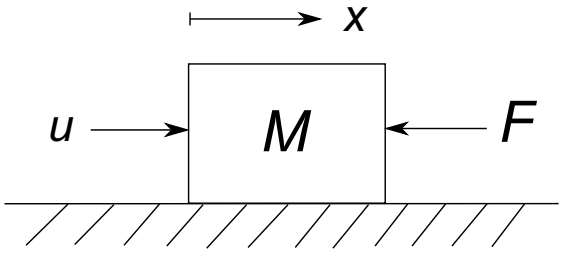

FIGURE 2.3: One-dimensional system

Suppose the control input u is chosen as a force feedback term $u = -mF$. Then the closed-loop system is

$$M\ddot{x} = -(1+m)F \Rightarrow \frac{M}{1+m}\ddot{x} = -F$$

*The object now appears to the environment as an inertia with mass $\frac{M}{1+m}$. Thus, the force feedback has the effect of changing the **apparent inertia** of the system.* △

Example 2.1 shows that by designing an appropriate control law u, the dynamics of the system may be changed with respect to the environment it operates within. In the following chapters such a technique will be investigated with regards to vessel control in a managed ice environment.

Chapter 3

Mechanical impedance

In order to describe the mechanical systems considered in this thesis in a kinematic sense, it is convenient to introduce the notion of *mechanical impedance*.

Mechanical impedance captures the relation between force and motion. Put simply, it can be viewed as to what extent a system (e.g. some manipulator, for example a vessel) resists a force put upon it by an external system (e.g. some environment) (Šabanović and Ohnishi, 2011).

3.1 Network models

The concept of mechanical impedance can be clarified by representing a system as a *one port network models*. Any system can be modeled as a one port network with an input and an output as illustrated in Figure 3.1. The dynamics of the system determine the *port variables* F and V, which, to generalize the concept, is referred to as *effort* and *flow* respectively. Using an analogy from electrical systems, effort corresponds to the voltage across the input terminals, while flow corresponds to the current flowing through the system. For mechanical systems, effort corresponds to the force exerted on the system, while flow corresponds to the resulting system velocity.

The port variables furthermore define the *mechanical impedance* of the system. The mechanical impedance $Z(s)$ of a system is defined as the ratio of the Laplace transform $F(s)$ of the effort and the Laplace transform $V(s)$ of the flow (Spong et al., 2006).

$$Z(s) = \frac{F(s)}{V(s)} \tag{3.1}$$

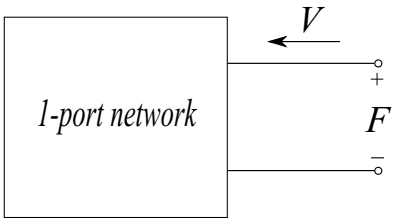

FIGURE 3.1: One-port network model

Two one port networks can be coupled together to represent the interaction between systems. In Figure 3.2 two network models share the common port variables F and V. The port variables now define the mechanical impedance of the coupled system.

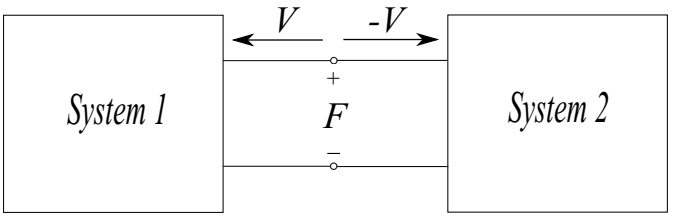

FIGURE 3.2: System interaction

A mechanical system may be classified into three general categories. The system is said to be of type

Inertial if $|Z(0)|=0$

Resistive if $|Z(0)| = B$ for some constant $0 < B < \infty$

Capacative if $|Z(0)| = \infty$

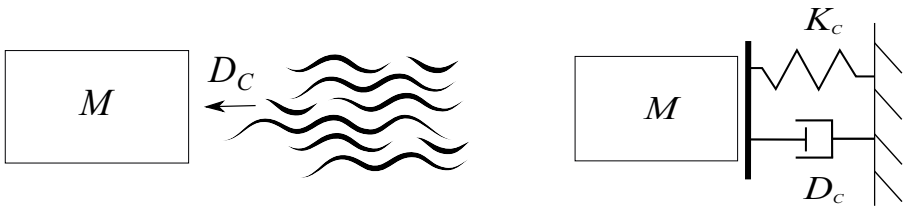

(A) Inertial system (B) Capacative system

FIGURE 3.3: System types

It is common to illustrate a system's type by modeling the system using a mass, some dissipative element and/or a spring. For an inertial system, which might resemble a floating vessel, a system model could be a mass M situated in a fluid representing a resistive force, as shown in Figure 3.3a. A capacitive system, on the other hand, can be viewed as a mass acting upon a spring, representing a capacitive force, in parallel with

a dashpot, representing a damping force. Figure 3.3b shows a depiction of a capacitive system.

The concept of system type can be further illustrated using a simple example taken from Spong et al. (2006).

Example 3.1. *Suppose a mass-spring-damper system is described by the differential equation*

$$M\ddot{x} + D\dot{x} + Kx = F$$

Taking the Laplace transform of both sides (and assuming zero initial conditions) it follows that the system impedance is given by

$$Z(s) = \frac{F(s)}{V(s)} = Ms + B + \frac{K}{s}$$

This impedance represents a capacitive system as the last term will grow unbounded as $s \to 0$. △

3.2 Impedance control

It can be shown that for an inertial system, the *compliant* system is capacitive, and vice versa. Furthermore, in order to interact with the environment in a controllable manner, a vessel needs to appear as the compliant of the environment in which it operates. This is known as the *duality principle*. The duality principle implies that a manipulator operating in a capacitive environment cannot be position controlled, whereas a manipulator operating in an inertial environment cannot be force controlled (Anderson and Spong, 1988).

As a consequence of the duality principle, when dealing with system interaction, force and motion cannot be controlled independently at the same time (Hogan, 1985). The reason for this is that if the vessel experiences a limiting physical constraint in its operating environment, the motions of the vessel will depend on the forces the constraint puts upon it. Moreover, when the vessel is free to move, force cannot be controlled as there is no constraining object for the vessel to oppose a force upon.

In order to be position controlled, a manipulator needs to be situated in an inertial environment, as well as inhabiting capacitive dynamics. Furthermore, a vessel inhabiting inertial dynamics in a capacitive environment will allow for effective force control against the environmental disturbances (Anderson and Spong, 1988).

All though the motion of the vessel and its contact forces with the environment cannot be controlled simultaneously, the mechanical impedance of the vessel can be manipulated to regulate the vessel in a changing environment. Manipulating the dynamics of a system in this manner is referred to as *impedance control*. A properly designed impedance controller

compencates for a system's natural dynamics and provides a desired disturbance response to externally applied forces (Love and Book, 1995). That is, the impedance of the system is manipulated to comply with its environment.

3.2.1 Relation to robotics

Impedance control, and specifically (hybrid) force control, to be discussed in Section 3.3, has been used extensively in the design of robot manipulators for several years. Industrial robots, such as welders and packaging robots utilizes the technology as it allows for controlled interaction with physical objects in the robot environment. If the robot *end effector* comes in contact with a physical object, the controller adjusts the impedance of the robot, regulating the contact forces the robot exerts on the object. This enables the robot to manipulate objects in a precise manner.

When deriving an impedance controller for some robot manipulator, it is convenient to operate in the task space of the manipulator rather than in joint space. In robot terminology, the *Jacobian* matrix relates the manipulator joint space to the task space as it describes the relationship between the individual joint velocities $\dot{\boldsymbol{q}}(t)$ to the translational and angular velocities of the end effector $\boldsymbol{v}_n^0(t)$ and $\boldsymbol{\omega}_n^0(t)$. The velocities of the end effector can be included in the vector $\boldsymbol{\xi}(t) = \begin{bmatrix}\boldsymbol{v}_n^0(t) & \boldsymbol{\omega}_n^0(t)\end{bmatrix}^\top$ in order to obtain the relationship (Spong et al., 2006)

$$\boldsymbol{\xi} = \boldsymbol{J}\dot{\boldsymbol{q}} \tag{3.2}$$

The Jacobian $\boldsymbol{J}$ corresponds to the rotation matrix $\boldsymbol{R}_\Theta(\boldsymbol{\eta})$ in Equation (2.27) as the joint space of the robot manipulator corresponds to the BODY coordinate frame of a marine vessel. Furthermore, the task space of the robot manipulator corresponds to the NED coordinate frame (Fossen, 2011). Thus, the concept of impedance control for robot manipulators may be transferred to vessel control.

3.2.2 Network models and system coupling

When working with impedance control and the coupling of different systems it is convenient to analyze the systems by using the network models introduced in Section 3.1. For linear systems, the network models may be concretized as *Norton* and *Thévenin* equivalents, where a Norton equivalent is used to represent a capacitive system, and a Thévenin equivalent is used to represent an inertial system. The network equivalents are depicted in Figure 3.4, where 3.4a resembles a flow source v with a shunted impedance Z, and 3.4b shows the same impedance in series with an effort source F.

The network equivalents in Figure 3.4 have the property of being each other's *dual*. Furthermore, they may be connected to represent the relationship between a system and its environment. Figure 3.5a shows the representation of a system coupling between a

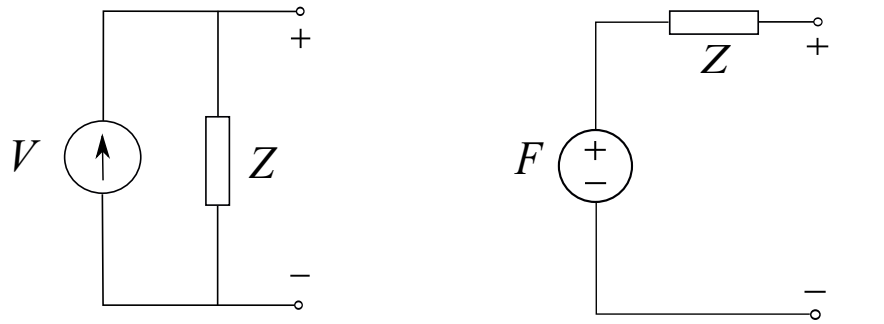

(A) Capacative system representation by a Norton equivalent

(B) Inertial system representation by a Thévenin equivalent

FIGURE 3.4: Network model representations

vessel inhabiting capacitive dynamics and an inertial environment. Figure 3.5b shows the vice versa case with an inertial vessel and a capacitive environment.

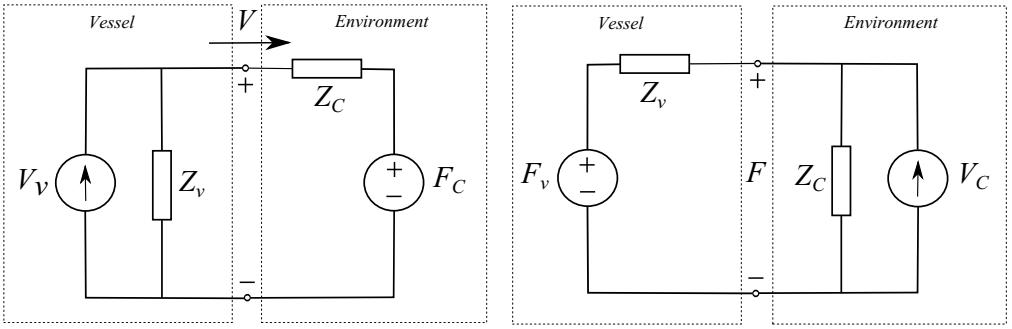

(A) System coupling with inertial environment

(B) System coupling with capacative environment

FIGURE 3.5: System couplings

It can be shown that a coupled system inhabiting the duality condition guarantees zero steady-state error. Too see this, first consider Figure 3.5a with an inertial environment, that is $Z_e(0) = 0$. Since the duality principle allows for motion control in this case, the resulting velocity V can be found from a simple current division

$$\frac{V}{V_\nu} = \frac{Z_\nu(s)}{Z_\nu(s) + Z_c(s)} \tag{3.3}$$

The steady state error to a step input $1/s$ can be found from the final value theorem as

$$\begin{aligned} e_{ssv} = \lim_{t\to\infty}(V - V_\nu) &= \lim_{t\to\infty} \frac{Z_\nu(s)}{Z_\nu(s) + Z_c(s)} V_\nu - V_\nu \\ &= \lim_{t\to\infty} \frac{Z_\nu(s)}{Z_\nu(s) + Z_c(s)} V_\nu - \frac{Z_\nu(s) + Z_c(s)}{Z_\nu(s) + Z_c(s)} V_\nu \\ &= \lim_{t\to\infty} \frac{-Z_c(s)}{Z_\nu(s) + Z_c(s)} V_\nu \\ &= \frac{-Z_c(0)}{Z_\nu(0) + Z_c(0)} V_\nu = 0 \end{aligned} \tag{3.4}$$

as long as the vessel impedance is non-inertial. For the case of the capacitive environment represented by the network in Figure 3.5b, the resulting force F can be found from voltage division

$$\frac{F}{F_\nu} = \frac{Z_c(s)}{Z_\nu(s) + Z_c(s)} \tag{3.5}$$

Furthermore, it can be shown that the steady state error in this case becomes

$$e_{ssf} = \lim_{t\to\infty}(F - F_v) = \frac{-Z_v(0)}{Z_v(0) + Z_c(0)}F_v = 0 \tag{3.6}$$

as long as the vessel impedance is non-capacitive.

3.3 Hybrid force control

The notion of hybrid force control (HFC) describes how one can control the force of a system in one direction, while simultaneously controlling some other control variable, for example its position or velocity, in another direction (Spong et al., 2006).

Before further clarification of the concept of HFC, the notion of *subspace division* is introduced. In the case of 3 DOF vessel control, a subspace is the set of directions which inhabits some property. For instance, one subspace could be the set of directions in which the vessel is free to move, while another subspace could be the set of directions in which the vessel experiences a limiting physical constraint, shown as the dashed line in Figure 3.6.

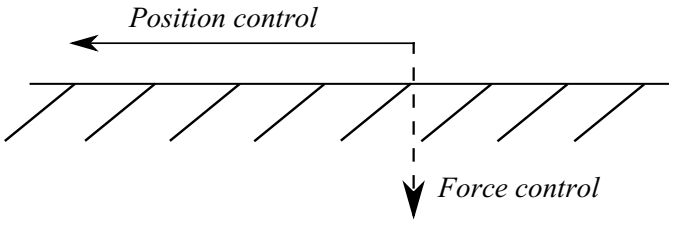

FIGURE 3.6: Subspace division based on feasible motions

Suppose now, that it is desirable to force control the vessel only in the directions in which a constraint is detected. If, for example, the vessel experiences excessive ice forces in sway, it might be desirable to "back up" and pause the position control in that specific direction until the ice loads has dissolved. That is, if the reference position is not conveniently reachable at some time t, it may be possible to reach it at a later time $t + T$, with less effort. This might reduce the total energy consumption associated with position tracking in managed ice environments. To realize such a controller, one could imagine dividing the impedance controller discussed in Section 3.2 into different subspaces. In this manner the vessel could be manipulated to inhabit capacitive dynamics in the directions where

motion control is possible, while inhabiting inertial dynamics where the vessel is required to be force controlled.

The hybrid force controller incorporates these ideas by using a conditional term to determine in which DOFs the vessel is to be position controlled, and in which DOFs the vessel is to be force controlled. In this thesis, it will be assumed that the DP model is decoupled into linear single DOFs equations of motion, so that linear circuit theory like the network models in Figure 3.4 can be applied.

In order to manipulate the vessel's apparent impedance to comply with the impedance of the environment, a proper model of the combined dynamics of the interacting systems is required. If a good kinematic model may be found, it might be possible to design a controller that compensates for the sea ice dynamics. This might lead to decreased energy consumption by the vessel thrusters.

In order to obtain a good model of the system dynamics this thesis will apply concepts from adaptive control taken from the excellent book on the topic Ioannou and Sun (1996). This is done in the next chapter.

Chapter 4

Adaptive control

Techniques applied in vessel control today, including pole placement and feed-forward of the environmental forces described by (2.14), has proven successful in operations situated in open waters. However, as stated in Section 2.3, when forces due to sea ice interference have to be accounted for, matters are complicated considerably. The reason for this is that good models of sea ice behavior are non-existent due to the difficulty associated with modeling the seemingly random properties of the ice (Metrikin et al., 2013).

Several experiments, conducted both in ship model basins and in the real world, have shown that to maintain position in a managed ice environment, a vessel equipped with conventional control systems must generate excessive counteracting forces to withstand the immense forces exerted by the ice (Kerkeni et al., 2013).

This thesis will investigate the possibilities for using impedance control to cope with sea ice interference. As sea ice interference are believed to affect the coefficient matrices of the vessel model, both environmental dynamics and the dynamics of the vessel itself will be considered unknown. Concepts from adaptive control will be applied to estimate the dynamics of both systems and, furthermore, combine these in the calculation of an appropriate control law.

Adaptive control has been an extensive area of research since the early 1950s where it was motivated by the need for autopilot designs applied in the aircraft industry. It has become one of the main approaches taken to solve a control problem in which one or more of the system parameters may be considered unknown (Ioannou and Sun, 1996).

Adaptive control usually involves three steps: in the first step, an appropriate parameterization of the plant model is selected. This is done in order to collect the parameters to be estimated in an unknown parameter vector, and the corresponding input signals in a regressor.

The second step involves the selection of an *adaptive law*. The adaptive law is usually a differential equation based on the difference between the observed system response and

the parameterized model. Moreover, the adaptive law is used to generate an updated value of the parameters at any time t..

The third step of adaptive control is to determine a control law that utilizes the parameters obtained in the second step to generate an appropriate control signal that regulates the actual plant to some setpoint or pre-defined trajectory.

The following subsections will encompass the three steps mentioned above to derive an adaptive control scheme referred to as *model reference adaptive control* (MRAC). An MRAC scheme utilizes a reference model which possesses some desired dynamics that the actual plant is intended to follow. This can be interpreted as the system attempting to obtain certain dynamic properties dictated by the reference model. Thus, in some sense, the concepts investigated in this chapter can be used to incorporate an implicit form of impedance control.

Remark 4.1. In this thesis it is chosen to estimate both the parameters of the environment *and* the parameters of vessel. In the general case the vessel parameters might be known. In such a case a model reference control (MRC) scheme would accomplish the task of guiding the vessel to the desired reference point. In an MRC scheme, the system characteristics are known. Therefore, the scheme does not utilize a system identification algorithm to generate estimates of system parameters. The system parameters are thus applied directly to generate an appropriate control law. In this work, however, it is chosen to consider the vessel parameters unknown, as the parameters might vary with different load conditions, etc. Moreover, it is desirable to observe if the sea ice has any effect on the vessel parameters. This might, for instance, be due to some of the ice mass adhering to the vessel hull as the vessel maneuvers through the ice.

The following sections deals with the concepts in a general manner. This is done in order to obtain results that can be applied in a general setting. Chapter 5 will incorporate the results obtained in Chapters 2 and 3 with the results obtained in the current chapter.

Remark 4.2. It is important to note that pure adaptive control is based on the assumptions that the plant model is free of disturbances, noise and unmodelled dynamics. In order to make some adaptive control scheme applicable to a system where these assumptions do not hold (i.e. any system under the influence of some disturbance), some modifications have to be made. This is referred to as *robust adaptive control* and is dealt with in Section 4.4.

4.1 Linear parameterization

The first step when deriving an adaptive control scheme, includes obtaining an appropriate parameterization of the system to be controlled (hereby referred to as the *plant*). Plant parameterization is performed to define the unknown parameters to be estimated

and to collect these in an unknown parameter vector $\boldsymbol{\theta}$. The signals corresponding to the unknown parameters are filtered in a signal vector denoted $\boldsymbol{\mu}$, known as the regressor.

In this thesis one of the simplest and most intuitive parametric model will be utilized, namely, the *linear parametric model*. The linear parametric model is straightforward to obtain for linear plants, including the linear DP model considered in this thesis.

The following derivation of the linear parametric model is taken from Ioannou and Sun (1996). Consider a plant expressed as the transfer function

$$y = G(s)u = \frac{Z(s)}{R(s)}u \tag{4.1}$$

where

$$Z(s) = b_m s^m + b_{m-1}s^{m-1} + \cdots + b_1 s + b_0 \tag{4.2}$$
$$R(s) = s^n + a_{n-1}s^{n-1} + \cdots + a_1 s + a_0 \tag{4.3}$$

where $m < n$ such that the transfer function $G(s)$ is strictly proper. This corresponds to the nth-order differential equation

$$y^{(n)} + a_{n-1}y^{(n-1)} + \cdots + a_0 y = b_m u^{(m)} + b_{m-1}u^{(m-1)} + \cdots + b_0 u \tag{4.4}$$

where the superscript (n) denotes the nth derivative.

Collecting the parameters in differential equation (4.4) in the parameter vector

$$\boldsymbol{\theta}^* = [b_m, b_{m-1}, \ldots, b_0, a_{n-1}, a_{n-2}, \ldots, a_0]^\top \tag{4.5}$$

and collecting the corresponding I/O signals and their derivatives in the signal vector.

$$\boldsymbol{\xi} = \left[u^{(m)}, u^{(m-1)}, \ldots, u, -y^{(n-1)}, -y^{(n-2)}, \ldots, -y\right]^\top \tag{4.6}$$

gives the linear model

$$y^{(n)} = \boldsymbol{\theta}^{*\top}\boldsymbol{\xi} \tag{4.7}$$

In most applications the signal derivatives $u^i, i = 1, 2, \ldots, m$, $y^j, j = 1, 2, \ldots, n$ are not available. Thus, the use of these in the model is not desirable. The next step in developing the parametric model is therefore to filter each side of (4.7) with an nth-order stable filter $H(s) = \frac{1}{\Lambda(s)}$ where $\Lambda(s)$ is a monic nth-order polynomial. This gives

$$\frac{1}{\Lambda(s)}y^{(n)} = \frac{1}{\Lambda(s)}\boldsymbol{\theta}^{*\top}\boldsymbol{\xi} \tag{4.8}$$

This can be written as

$$z = \boldsymbol{\theta}^{*\top}\boldsymbol{\mu} \tag{4.9}$$

where

$$z \triangleq \frac{1}{\Lambda(s)} y^{(n)} = \frac{s^n}{\Lambda(s)} y, \qquad \boldsymbol{\mu} \triangleq \left[\frac{\boldsymbol{\alpha}_m^\top}{\Lambda(s)} u, -\frac{\boldsymbol{\alpha}_{n-1}^\top}{\Lambda(s)} y \right]$$

$$\boldsymbol{\alpha}_i(s) \triangleq \left[s^i, s^{i-1}, \ldots, s, 1 \right]^\top$$

and

$$\Lambda(s) = s^n + \lambda_{n-1} s^{n-1} + \cdots + \lambda_0$$

where λ_j, $j = 0, \ldots, n-1$ are positive real numbers.

Equation (4.9) is the linear parametric model applied to estimate the system parameters in this thesis.

4.2 Online parameter estimation

The parametric model derived in Section 4.1 may be applied to represent several types of dynamic systems. A system behavior is determined by the parameters involved in the model. However, if these parameters are unknown the system behavior may be difficult to establish. This is where the techniques of system identification and parameter estimation might be applicable.

If the system is known to be constant, linear and stable, the system parameters may be easy to deduce using time or frequency domain system identification techniques. Such techniques are described for instance in Ljung (1999). Other times it might be possible to calculate the parameters using the laws of physics, symmetry and the properties of materials. In many cases, however, the plant parameters are believed to change over time. This can be due to changes in operating conditions, wear and tear, or aging of equipment. In these cases such *off-line* estimation techniques are often left ineffective. The best approach in the case of time-varying plant parameters might be to apply techniques that provide frequent, real-time parameter estimates. Such techniques are often referred to as *on-line* estimation methods (Ioannou and Sun, 1996).

This section will introduce and describe a well known on-line parameter estimation method, known as the *gradient method*. The gradient method is an intuitive method which is easy to implement in various forms, and for different plants.

4.2.1 The gradient method

The linear parametric model (4.9) can be used to generate several adaptive laws for estimating the unknown parameter vector $\boldsymbol{\theta}^*$. In this thesis the well known gradient method is utilized in order to obtain estimates for the dynamics of both the vessel and the sea ice disturbances.

The idea behind the gradient method in terms of system identification is to minimize some convex cost function $J(\boldsymbol{\theta})$ in order to arrive at an optimal estimate of some parameter vector $\boldsymbol{\theta}^*$. Since $J(\boldsymbol{\theta})$ is designed to be convex, this optimum can be found by finding the minimum of $J(\boldsymbol{\theta})$. This is done by calculating the gradient $\nabla J(\boldsymbol{\theta})$ and utilize this in a continuous-time differential equation describing the rate of change of the parameter $\boldsymbol{\theta}$ (Ioannou and Sun, 1996)

$$\dot{\boldsymbol{\theta}} = -\boldsymbol{\Gamma}\boldsymbol{\nabla}_{\boldsymbol{\theta}} J(\boldsymbol{\theta}(t)), \quad \boldsymbol{\theta}(t_0) = \boldsymbol{\theta}_0 \tag{4.10}$$

where $\boldsymbol{\Gamma} = \boldsymbol{\Gamma}^\top > 0$ is a scaling matrix used to increase or decrease the rate of change of the parameter estimate.

The differential equation (4.10) is known from optimization theory as the *steepest descent method* (Nocedal and Wright, 2006). The solution of the steepest descent method is the steepest descent path in the time domain along the surface described by $J(\boldsymbol{\theta})$ starting from $t = t_0$. The value of $\boldsymbol{\theta}$ at which (4.10) meet some optimization criteria is considered the best estimate of $\boldsymbol{\theta}$.

As an example, consider the linear parametric model (4.9) and choose the cost function

$$J(\boldsymbol{\theta}) = \frac{\epsilon^2 m^2}{2} = \frac{(z - \boldsymbol{\theta}^\top \boldsymbol{\mu})^2}{2m^2} \tag{4.11}$$

where the *estimation error* ϵ is given by

$$\epsilon = \frac{z - \hat{z}}{m^2} = \frac{z - \boldsymbol{\theta}^\top \boldsymbol{\mu}}{m^2} \tag{4.12}$$

$z = \boldsymbol{\theta}^* \boldsymbol{\mu}$ and $m^2 = 1 + n_s^2 = 1 + \boldsymbol{\mu}^\top \boldsymbol{\mu}$. Suppose that it would be desireable to minimize the estimation error represented by the convex function (4.11) with respect to the parameter vector $\boldsymbol{\theta}$. This is equivalent to finding the parameter $\boldsymbol{\theta}$ that makes the parametric model resemble the actual plant in an optimal sense.

In order to find the optimal estimate of $\boldsymbol{\theta}^*$ the gradient method can be applied. By finding the gradient of (4.11) with respect to $\boldsymbol{\theta}$

$$\boldsymbol{\nabla}_{\boldsymbol{\theta}} J = -\frac{\boldsymbol{\mu}(z - \boldsymbol{\theta}^\top \boldsymbol{\mu})}{m^2} = -\epsilon \boldsymbol{\mu} \tag{4.13}$$

and applying the steepest descent method (4.10) the update law for the parameter estimate is obtained as

$$\dot{\boldsymbol{\theta}} = \boldsymbol{\Gamma} \epsilon \boldsymbol{\mu} \tag{4.14}$$

In system identification theory the update law (4.14) is referred to as the *gradient method* (Ioannou and Sun, 1996).

Remark 4.3. The divisor m in Equation 4.12 is a *normalization* term chosen so that

$$\frac{\boldsymbol{\mu}}{m}, \frac{z}{m} \in \mathcal{L}_\infty \tag{4.15}$$

This is done so that boundedness can be guaranteed for all input signals. Bounded input signals are an important property for a system as it will allow for the design of adaptive control systems that is stable in the $\mathcal{L}_p$ sense. For unstable plants boundedness of the estimator input signals $z, \boldsymbol{\mu}$ cannot always be guaranteed, and thus $\mathcal{L}_p$ stability of the closed loop adaptive system cannot be proved. In such cases a normalization term is crucial both for the system performance and analysis (Ioannou and Sun, 1996). The notion of $\mathcal{L}_p$ stability is defined in Appendix B.

4.2.2 Parameter convergence and persistence of excitation

Before the convergence properties of the gradient method are presented, an important property of the signals involved in the estimation scheme needs to be introduced. This property, known as persistence of excitation, is a key property whenever parameter convergence is of major importance.

Definition 4.4 (Persistence of excitation (PE)). (Ioannou and Sun, 1996) A piecewise continous signal vector $\boldsymbol{\mu} : \mathcal{R}^+ \to \mathcal{R}^n$ is PE in $\mathcal{R}^n$ with a level of excitation $\alpha_0 > 0$ if there exists constants $\alpha_1, T_0 > 0$ such that

$$\alpha_1 \boldsymbol{I} \geq \frac{1}{T_0} \int_t^{t+T_0} \boldsymbol{\mu}(\tau)\boldsymbol{\mu}^\top(\tau) d\tau \geq \alpha_0 \boldsymbol{I}, \ \forall t \geq 0 \tag{4.16}$$

where $\boldsymbol{I}$ is the identity matrix. The convergence properties of the gradient method can now be summarized by the following theorem.

Theorem 4.5. *(Ioannou and Sun, 1996) The adaptive law 4.14 guarantees that*

(i) $\epsilon, \epsilon n_s, \boldsymbol{\theta}, \dot{\boldsymbol{\theta}} \in \mathcal{L}_\infty$

(ii) $\epsilon, \epsilon n_s, \dot{\boldsymbol{\theta}} \in \mathcal{L}_2$

independent of the boundedness of the signal vector $\boldsymbol{\mu}$ *and*

(iii) if $n_s, \boldsymbol{\mu} \in \mathcal{L}_\infty$ *and* $\boldsymbol{\mu}$ *is PE, then* $\boldsymbol{\theta}(t)$ *converges exponentially to* $\boldsymbol{\theta}^*$

The proof for this theorem can be found in Appendix C.

4.3 Model reference adaptive control

As stated in Section 2.3, the system matrices $\boldsymbol{M}$ and $\boldsymbol{D}_c$ changes in a non-deterministic manner in situations where the vessel is under the influence of sea ice. Since good models of sea ice dynamics are non-existent, strategies as compliant model terms and feed-forward cancellation of environmental forces is difficult to conduct. If, however, one assumes that the system matrices of the DP model (2.27) are time-varying due to the influence of the environment, one could attempt to estimate these matrices at given points in time. Moreover, if an appropriate control law can be found based on these estimates, such an estimation scheme might make a precise mathematical model of disturbance terms superfluous.

By estimating the dynamics of the environment adjacent to the craft in a similar manner, one could incorporate this idea with the concept of impedance control. By deciding how the vessel should behave in some given environment situation, the energy consumption associated with motion control in managed ice might be decreased.

In this thesis a certain control scheme referred to as *model reference adaptive control* (MRAC) is utilized to achieve vessel control. Simultaneously, the scheme will carry out an attempt to manipulate the vessel dynamics to comply with the environment in which the vessel resides.

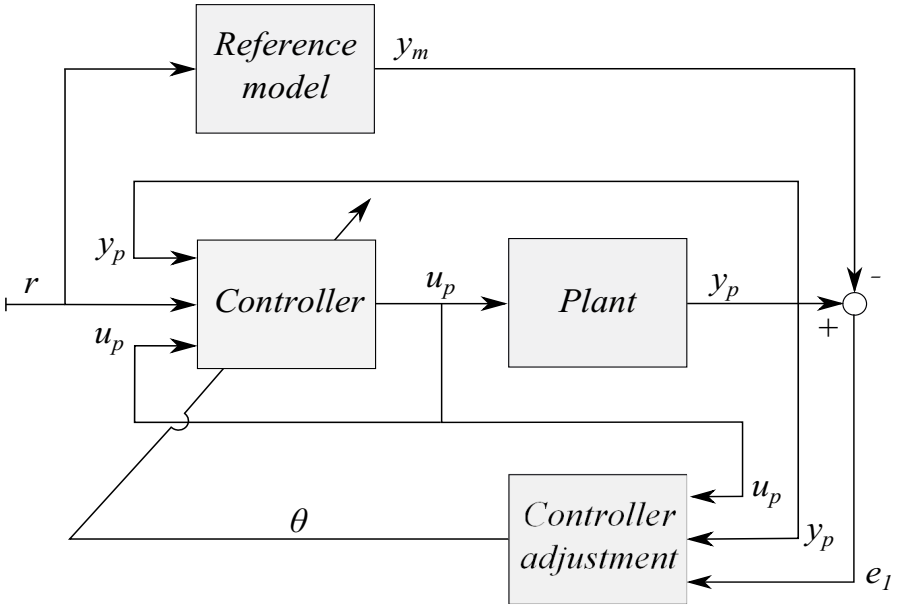

FIGURE 4.1: Structure of classic MRAC scheme

Model reference adaptive control is one of the main approaches to adaptive control (Ioannou and Sun, 1996). It involves the design of a reference model that generates a certain desirable output trajectory y_m. The plant output y_p is then controlled to follow this trajectory. A general outline of a classical MRAC scheme is shown in Figure 4.1.

The adjustment mechanism in Figure 4.1 updates the controller continuously based on its input signals. This can be done in two different manners achieving similar results. These are referred to as *direct* MRAC and *indirect* MRAC. In the direct MRAC scheme the controller parameters are estimated directly from the plant parameterization without involving the system parameters. The indirect MRAC scheme, on the other hand, calculates the controller parameters based on estimates of the plant parameters. This is done via intermediate equations relating the two. The control scheme implemented in this thesis employs the indirect approach. This will allow for monitoring the estimated vessel parameters over time, which might be beneficial for analysis and discussion.

The following section deals with the control law used in this work and the derivation of the equations relating the plant and the control law parameters.

4.3.1 Control law

In order to arrive at the MRAC control scheme, the control objective in question has to be stated. Consider again the plant (4.1) rewritten as

$$y_p = G_p(s)u_p = k_p \frac{Z_p(s)}{R_p(s)} u_p \tag{4.17}$$

where G_p is the plant transfer function, Z_p is a monic Hurwitz polynomial of degree m_p, R_p is a monic polynomial of degree n and k_p is referred to as the high frequency gain of the system. The relative degree $n^* = n - m_p$ of the plant is assumed to be known.

The control objective is now to regulate the output y_p of (4.17) to follow a reference trajectory represented by the output y_m of a reference model

$$y_m = W_m(s)r = k_m \frac{Z_m(s)}{R_m(s)} r \tag{4.18}$$

where $Z_m(s)$, $R_m(s)$ is monic Hurwitz polynomials of degree q_m, p_m respectively, where $p_m \leq n$. This implies that W_m is stable and minimum phase. Moreover, the relative degree $n_m^* = p_m - q_m$ of $W(s)$ is assumed to be the same as that of $G_p(s)$

It is chosen to apply a control law on the form

$$u_p = \boldsymbol{\theta}_1^{*\top} \frac{\boldsymbol{\alpha}(s)}{\Lambda(s)} u_p + \boldsymbol{\theta}_2^{*\top} \frac{\boldsymbol{\alpha}(s)}{\Lambda(s)} y_p + \theta_3^* y_p + c_0^* r \tag{4.19}$$

where

$$\begin{aligned} \boldsymbol{\alpha}(s) &\triangleq \boldsymbol{\alpha}_{n-2}(s) = [s^{n-2}, s^{n-3}, \ldots, s, 1]^\top \quad \text{for } n \geq 2 \\ \boldsymbol{\alpha}(s) &\triangleq 0 \qquad\qquad\qquad\qquad\qquad\qquad\quad \text{for } n = 1 \end{aligned}$$

and $\boldsymbol{\theta}_1^*$, $\boldsymbol{\theta}_2^* \in \mathcal{R}^{n-1}$, c_0^*, $\theta_3^* \in \mathcal{R}^1$ are the control parameters to be calculated, $\Lambda(s)$ is a monic Hurwitz polynomial of degree $n-1$ that contains $Z_m(s)$ as a factor, that is

$$\Lambda(s) = \Lambda_0(s) Z_m(s) \tag{4.20}$$

The control law (4.19) can be realized by the following state-space representation (Ioannou and Sun, 1996)

$$\begin{aligned} \dot{\boldsymbol{\omega}}_1 &= \boldsymbol{F}\omega_1 + \boldsymbol{g}u_p, \qquad & \boldsymbol{\omega}_1(0) &= 0 \\ \dot{\boldsymbol{\omega}}_2 &= \boldsymbol{F}\omega_2 + \boldsymbol{g}y_p, \qquad & \boldsymbol{\omega}_2(0) &= 0 \\ u_p &= \boldsymbol{\theta}_a^{*\top}\boldsymbol{\omega} \end{aligned} \tag{4.21}$$

where $\boldsymbol{\omega}_1 = \frac{\boldsymbol{\alpha}(s)}{\Lambda(s)}u_p$, $\boldsymbol{\omega}_2 = \frac{\boldsymbol{\alpha}(s)}{\Lambda(s)}y_p \in \mathcal{R}^{n-1}$,

$$\boldsymbol{\theta}_a^* = [\boldsymbol{\theta}_1^{*\top}, \boldsymbol{\theta}_2^{*\top}, \theta_3^*, c_0^*]^\top, \qquad \boldsymbol{\omega} = [\boldsymbol{\omega}_1^\top, \boldsymbol{\omega}_2^\top, y_p, r]^\top \tag{4.22}$$

$$\boldsymbol{F} = \begin{bmatrix} -\lambda_{n-2} & -\lambda_{n-3} & \lambda_{n-4} & \cdots & -\lambda_0 \\ 1 & 0 & 0 & \cdots & 0 \\ 0 & 1 & 0 & \cdots & 0 \\ \vdots & \vdots & \ddots & \ddots & \vdots \\ 0 & 0 & \cdots & 1 & 0 \end{bmatrix}, \quad \boldsymbol{g} = \begin{bmatrix} 1 \\ 0 \\ 0 \\ \vdots \\ 0 \end{bmatrix} \tag{4.23}$$

λ_i are the coefficients of

$$\Lambda(s) = s^{n-1} + \lambda_{n-2}s^{n-2} + \cdots + \lambda_1 s + \lambda_0 = \det(s\boldsymbol{I} - \boldsymbol{F})$$

and $\boldsymbol{F}$, $\boldsymbol{g}$ is the state-space representation of $\frac{\boldsymbol{\alpha}(s)}{\Lambda(s)}$. Applying the control law (4.19) to the plant (4.17) gives

$$\begin{aligned} y_p &= G_p u_p \\ &= k_p \frac{Z_p}{R_p} \boldsymbol{\theta}_a^{*\top} \omega \\ &= k_p \frac{Z_p}{R_p} \left(\boldsymbol{\theta}_1^{*\top} \frac{\boldsymbol{\alpha}(s)}{\Lambda(s)} u_p + \boldsymbol{\theta}_2^{*\top} \frac{\boldsymbol{\alpha}(s)}{\Lambda(s)} y_p + \theta_3^* y_p + c_0^* r \right) \\ &= \boldsymbol{\theta}_1^{*\top} \frac{\boldsymbol{\alpha}(s)}{\Lambda(s)} y_p + k_p \frac{Z_p}{R_p} \left(\boldsymbol{\theta}_2^{*\top} \frac{\boldsymbol{\alpha}(s)}{\Lambda(s)} y_p + \theta_3^* y_p + c_0^* r \right) \end{aligned}$$

Re-arranging terms gives

$$y_p \left(1 - \boldsymbol{\theta}_1^{*\top} \frac{\boldsymbol{\alpha}(s)}{\Lambda(s)} - k_p \frac{Z_p}{R_p} \frac{\boldsymbol{\alpha}(s)}{\Lambda(s)} \boldsymbol{\theta}_2^{*\top} - k_p \frac{Z_p}{R_p} \theta_3^* \right) = k_p \frac{Z_p}{R_p} c_0^* r$$

which leads to the transfer function $\frac{y_p}{r} = G_r(s)$, that is

$$y_p = \frac{c_0^* k_p Z_p \Lambda(s)^2}{\Lambda(s)\left[\left(\Lambda(s) - \boldsymbol{\theta}_1^{*\top}\boldsymbol{\alpha}(s)\right) R_p - k_p Z_p \left(\boldsymbol{\theta}_2^{*\top}\boldsymbol{\alpha}(s) + \theta_3^*\Lambda(s)\right)\right]} r \tag{4.24}$$

The closed loop system (4.24) may be represented in the state-space form

$$\begin{aligned} \dot{\boldsymbol{Y}} &= \boldsymbol{A}_r \boldsymbol{Y} + \boldsymbol{B}_r c_0^* \boldsymbol{r}, \qquad \boldsymbol{Y}(0) = \boldsymbol{Y}_0 \\ y_p &= \boldsymbol{C}_r^\top \boldsymbol{Y} \end{aligned} \tag{4.25}$$

where $\boldsymbol{Y} = [x_p^\top, \boldsymbol{\omega}_1^\top, \boldsymbol{\omega}_2^\top]$ is an augmented state vector consisting of the system states and the controller filter states $\boldsymbol{\omega}_1, \boldsymbol{\omega}_2$, and the triple $(\boldsymbol{A}_r, \boldsymbol{B}_r c_0^*, \boldsymbol{C}_r)$ is the state space representation of G_r. That is,

$$\boldsymbol{C}_r^\top (s\boldsymbol{I} - \boldsymbol{A}_r)^{-1} \boldsymbol{B}_r c_0^* = \frac{c_0^* k_p Z_p \Lambda(s)^2}{\Lambda(s)\left[\left(\Lambda(s) - \boldsymbol{\theta}_1^{*\top}\boldsymbol{\alpha}(s)\right) R_p - k_p Z_p \left(\boldsymbol{\theta}_2^{*\top}\boldsymbol{\alpha}(s) + \theta_3^*\Lambda(s)\right)\right]}$$

Further, Equation (4.24) implies

$$W_m(s) = \frac{c_0^* k_p Z_p \Lambda(s)^2}{\Lambda(s)\left[\left(\Lambda(s) - \boldsymbol{\theta}_1^{*\top}\boldsymbol{\alpha}(s)\right) R_p - k_p Z_p \left(\boldsymbol{\theta}_2^{*\top}\boldsymbol{\alpha}(s) + \theta_3^*\Lambda(s)\right)\right]} \tag{4.26}$$

The closed loop system (4.24) with the implication (4.26) is the MRAC objective. That is, the MRAC scheme aims to match the transfer function of the actual plant to that of the reference model. The control objective furthermore implies

$$\boldsymbol{C}_r^\top (s\boldsymbol{I} - \boldsymbol{A}_r)^{-1} \boldsymbol{B}_r c_0^* = W_m(s)$$

and so, by replacing $\boldsymbol{Y}$ with the corresponding state vector of the reference model $\boldsymbol{Y}_m$, the reference model may be represented by the state-space system (4.25), that is

$$\begin{aligned} \dot{\boldsymbol{Y}}_m &= \boldsymbol{A}_r \boldsymbol{Y}_m + \boldsymbol{B}_r c_0^* \boldsymbol{r} \qquad \boldsymbol{Y}_m(0) = \boldsymbol{Y}_{m0} \\ y_m &= \boldsymbol{C}_r^\top \boldsymbol{Y}_m \end{aligned} \tag{4.27}$$

Now, by letting $e = \boldsymbol{Y} - \boldsymbol{Y}_m$ and $e_1 = y_p - y_m$ be the state and output of the tracking error respectively, representing the difference between the reference model and plant for all t, one could write

$$\begin{aligned} \dot{e} &= \boldsymbol{A}_r e \\ e_1 &= \boldsymbol{C}_r^\top e \end{aligned} \tag{4.28}$$

This shows that since $\boldsymbol{A}_r$ is a stable matrix (as W_m is stable) the output error $e_1(t)$ converges exponentially to zero if the controller parameters $\boldsymbol{\theta}_1^{*\top}, \boldsymbol{\theta}_2^{*\top}, \theta_3^*, c_0^*$ could be chosen so that the closed-loop poles of G_r were stable and $G_r = W_m$.

By choosing $c_0^* = \frac{k_m}{k_p}$ and $\Lambda(s) = \Lambda_0(s)Z_m$ the matching equation (4.26) can be written.

$$\left(\Lambda - \boldsymbol{\theta}_1^{*\top}\boldsymbol{\alpha}\right) R_p - k_p Z_p \left(\boldsymbol{\theta}_2^{*\top}\boldsymbol{\alpha} + \theta_3^*\Lambda\right) = Z_p\Lambda_0 R_p \tag{4.29}$$

Moreover, (4.29) can be divided by $R_p(s)$ to obtain

$$\Lambda - \boldsymbol{\theta}_1^{*\top}\boldsymbol{\alpha} - k_p\frac{Z_p}{R_p}(\boldsymbol{\theta}_2^{*\top}\boldsymbol{\alpha} + \theta_3^*\Lambda) = Z_p\left(Q + k_p\frac{\Delta^*}{R_p}\right) \tag{4.30}$$

where $Q(s)$ is the quotient and $k_p\Delta^*$ is the remainder of $\frac{\Lambda_0 R_m}{R_p}$. By matching factors, this gives three equations relating the controller parameters $c_0^*, \boldsymbol{\theta}_i^*$, $i = 1, 2, 3$ to the plant polynomials.

$$c_0^* = \frac{k_m}{k_p} \tag{4.31a}$$

$$\boldsymbol{\theta}_1^{*\top}\boldsymbol{\alpha}(s) = \Lambda(s) - Z_p(s)Q(s) \tag{4.31b}$$

$$\boldsymbol{\theta}_2^{*\top}\boldsymbol{\alpha}(s) + \theta_3^*\Lambda(s) = \frac{1}{k_p}\left[Q(s)R_p(s) - \Lambda_0(s)R_m(s)\right] \tag{4.31c}$$

When the plant polynomials are known, the controller parameters may be found by solving the equations (4.31). However, when the plant parameters are unknown $\boldsymbol{\theta}^*$ cannot be calculated. In this case a reasonable approach would be to replace k_p, Z_p and R_p with their estimates $\hat{k}_p$, $\hat{Z}_p$ and $\hat{R}_p$, and then calculate the estimate $\boldsymbol{\theta}$ of $\boldsymbol{\theta}^*$ using these estimates. This gives the following state-space representation of the control law:

$$\begin{aligned} \dot{\boldsymbol{\omega}}_1 &= \boldsymbol{F}\boldsymbol{\omega}_1 + \boldsymbol{g}u_p, & \boldsymbol{\omega}_1(0) &= 0 \\ \dot{\boldsymbol{\omega}}_2 &= \boldsymbol{F}\boldsymbol{\omega}_2 + \boldsymbol{g}y_p, & \boldsymbol{\omega}_2(0) &= 0 \\ u_p &= \boldsymbol{\theta}^\top\boldsymbol{\omega} \end{aligned} \tag{4.32}$$

where ω, F and g is defined as in (4.22), (4.23), and $\boldsymbol{\theta}(t)$ is the estimate of $\boldsymbol{\theta}^*$. The control law (4.32) is the control law used in this thesis. The adaptive law used to estimate the vessel parameters is derived in the following section.

4.3.2 Adaptive law

In order to derive an adaptive law that meets the MRAC objective (4.24) and (4.26) it is convenient to start with the plant (4.17), which can be expressed in the form

$$y_p = \frac{b_m s^m + b_{m-1}s^{m-1} + \cdots + b_0}{s^n + a_{n-1}s^{n-1} + \cdots + a_0}u_p \tag{4.33}$$

The linear parametrization of the plant becomes

$$z = \boldsymbol{\theta}_p^*\boldsymbol{\mu} \tag{4.34}$$

where

$$z = \frac{1}{\Lambda_p(s)} y_p \qquad \boldsymbol{\mu} = \left[\frac{\boldsymbol{\alpha}_{n-1}^\top(s)}{\Lambda_p(s)} u_p, -\frac{\boldsymbol{\alpha}_{n-1}^\top(s)}{\Lambda_p(s)} y_p \right]^\top$$

$$\boldsymbol{\theta}_p^* = [b_m, \ldots, b_0, a_{n-1}, \ldots, a_0]^\top$$

and $\Lambda_p(s) = s^n + \lambda_p^\top \boldsymbol{\alpha}_{n-1}(s)$ is Hurwitz.

Choosing the cost function

$$J(\boldsymbol{\theta}_p) = \frac{\epsilon^2 m^2}{2} \tag{4.35}$$

and using the gradient method from Section 4.2.1 this gives the following update law of the plant parameter vector estimate

$$\dot{\hat{\boldsymbol{\theta}}}_p = \boldsymbol{\Gamma} \epsilon \boldsymbol{\mu} \tag{4.36}$$

where

$$\hat{\boldsymbol{\theta}}_p = [\hat{b}_m, \ldots, \hat{b}_0, \hat{a}_{n-1}, \ldots, \hat{a}_0]^\top$$

The plant polynomials can now be evaluated as

$$\hat{R}_p(s) = s^n + \hat{a}_{n-1} s^{n-1} + \cdots + \hat{a}_0 \tag{4.37}$$

$$\hat{Z}_p(s) = s^n + \hat{b}_m s^m + \hat{b}_{m-1} s^{m-1} + \cdots + \hat{b}_0 \tag{4.38}$$

$$\hat{k}_p = \hat{b}_m \tag{4.39}$$

and the controller parameters $\boldsymbol{\theta}_1^\top, \boldsymbol{\theta}_2^\top, \theta_3, c_0$ can be calculated using equations (4.31).

4.4 Robust adaptive control

The adaptive control law presented in the previous sections are developed for plants which are assumed to be perfectly modeled and free of disturbances. When applying these control laws on real plants, these assumptions may no longer hold. The modeling uncertainties may arise from the fact that the physical plant is extremely complex and simply too difficult to model. Discrepancies evolved over time due to wear and tear, and aging on equipment may also be the cause of differences between a model and a real world plant. Moreover, external disturbances due to weather hazards and physical obstacles (such as ice floes for instance) in the environment in which the plant are intended to operate motivates the development of an adaptive control law that are *robust* in the sense that it is applicable under changing operating conditions.

Ioannou and Sun (1996) suggests many modifications to the adaptive law developed in section 4.3.2. In this thesis it is chosen to utilize two modification techniques to the adaptive law (4.36) known as *leakage* and *dynamic normalization*. These techniques are discussed in the following sections.

4.4.1 Leakage

Consider the parameterized plant (4.34) with an added unknown disturbance σ which will be considered bounded

$$z = \boldsymbol{\theta}_p^* \boldsymbol{\mu} + \sigma \tag{4.40}$$

The unknown parameter vector $\boldsymbol{\theta}_p^*$ will be estimated using the adaptive law

$$\dot{\boldsymbol{\theta}}_p = \boldsymbol{\Gamma} \epsilon \boldsymbol{\mu}, \qquad \epsilon = z - \boldsymbol{\theta}_p \boldsymbol{\mu} \tag{4.41}$$

By treating $\boldsymbol{\theta}_p^*$ as a constant and inserting for z and ϵ, the adaptive law can be written in terms of the parameter error as follows

$$\dot{\tilde{\boldsymbol{\theta}}}_p = \boldsymbol{\Gamma} \epsilon \boldsymbol{\mu}, \qquad \epsilon = -\tilde{\boldsymbol{\theta}}_p \boldsymbol{\mu} + \sigma \tag{4.42}$$

where $\tilde{\boldsymbol{\theta}}_p = \boldsymbol{\theta}_p - \boldsymbol{\theta}_p^*$ is the parameter error. The stability properties of the adaptive law (4.42) can be analyzed by the use of Luyapunov theory. Consider the Lyapunov function candidate

$$V(\tilde{\boldsymbol{\theta}}_p) = \frac{\tilde{\boldsymbol{\theta}}_p^\top \boldsymbol{\Gamma}^{-1} \tilde{\boldsymbol{\theta}}_p}{2} \tag{4.43}$$

Differentiating (4.43) along the trajectories of the solution of (4.42) gives

$$\dot{V} = \tilde{\boldsymbol{\theta}}_p \epsilon \boldsymbol{\mu} = -\epsilon^2 + \epsilon\sigma \leq -|\epsilon|(|\epsilon| - d_0) \tag{4.44}$$

where d_0 is an upper bound on the distubance σ. If $\sigma = 0$ (4.44) would be negative for all inputs $\boldsymbol{\mu} \in \mathcal{L}_\infty$. However, when $\sigma \neq 0$ $\dot{V}$ will be positive whenever $d_0 \geq |\epsilon|$, and thus no conclusion can be made on the boundedness of $\tilde{\boldsymbol{\theta}}_p$. One method to avoid this situation is to add a *leakage* term to the original adaptive law (4.41)

$$\dot{\boldsymbol{\theta}}_p = \boldsymbol{\Gamma} \epsilon \boldsymbol{\mu} - \boldsymbol{\Gamma} w \boldsymbol{\theta}_p \tag{4.45}$$

where

$$w = \begin{cases} 0, & \text{if } |\boldsymbol{\theta}_p(t)| < M_0 \\ w_0 \left(\frac{|\boldsymbol{\theta}_p(t)|}{M_0} - 1 \right), & \text{if } M_0 \leq |\boldsymbol{\theta}_p(t)| < 2M_0 \\ w_0, & \text{if } |\boldsymbol{\theta}_p(t)| \geq 2M_0 \end{cases} \tag{4.46}$$

and $w_0 > 0$. The adaptive law (4.45) is the adaptive law used in the implementation of the control schemes proposed in this thesis.

The idea behind the leakage term (4.46) is to modify the adaptive law when the parameter estimates exceeds certain bounds, so the derivative of the Lyapunov function used to analyze the adaptive scheme becomes negative (Ioannou and Sun, 1996). It requires some knowledge of the parameter vector $\boldsymbol{\theta}_p^*$, so that the upper bound M_0 can be chosen to be $M_0 > |\boldsymbol{\theta}_p^*|$. The analysis of the adaptive law (4.45) is similar to (4.41), and can be found in Appendix C.

4.4.2 Dynamic normalization

In the previous section the disturbance term σ was considered bounded. When dealing with adaptive control, disturbances and uncertainties are often dependent on the signals involved in the adaptive scheme. Suppose now, that the signal vector $\boldsymbol{\mu}$ is not necessarily bounded, and that the disturbance term σ in the linear model (4.40) is either bounded, or bounded from above by the signal vector $\boldsymbol{\mu}$. Then the normalizing signal m discussed in Section 4.2 can be used to guarantee that the signals involved in the scheme are bounded. If, however, the disturbance σ is not necessarily bounded by $|\boldsymbol{\mu}|$, but related to $\boldsymbol{\mu}$ through some transfer function, as in the plant equation

$$z = \boldsymbol{\theta}_p^* \boldsymbol{\mu} + \sigma, \quad \sigma = \boldsymbol{\theta}_p^* \Delta_m(s) \boldsymbol{\mu} + d \tag{4.47}$$

where $\Delta_m(s)$ denotes a so called multiplicative perturbation that is strictly proper and stable, and d is an unknown bounded disturbance. Then the static properties of m is not enough to ensure boundedness of all signals in the scheme (Ioannou and Sun, 1996).

If an expression for some upper bound of the disturbance σ in the case of (4.47) can be found, this would motivate a new choice of m that will guarantee boundedness for all signals in the adaptive scheme in a robust sense. An expression for the upper bound on σ can be found by assuming that $\Delta_m(s)$ is strictly proper and analytic in Re[s] $\geq -\frac{\delta_0}{2}$ for some $\delta_0 > 0$, and using the properties of the $\mathcal{L}_{2\delta}$ norm defined in Appendix B and Lemma B.6 to obtain

$$\begin{aligned} |\sigma(t)| &\leq |\boldsymbol{\theta}_p^*| ||\Delta_m(s)||_{2\delta} ||\boldsymbol{\mu}_t||_{2\delta} + |d(t)| \\ &\leq \boldsymbol{\mu}_0 ||\boldsymbol{\mu}_t||_{2\delta} + d_0 \end{aligned} \tag{4.48}$$

where $\boldsymbol{\mu}_0 = |\boldsymbol{\theta}^*| ||\Delta_m(s)||_{2\delta}$ is constant and d_0 is an upper bound on $d(t)$. A normalizing term that bounds both $\boldsymbol{\mu}$ and σ is given by (Ioannou and Sun, 1996)

$$m^2 = 1 + \boldsymbol{\mu}^\top \boldsymbol{\mu} + n_s^2 \tag{4.49}$$

where

$$\begin{aligned} n_s^2 &= m_s \\ \dot{m}_s &= -\delta_0 m_s + \boldsymbol{\mu}^\top \boldsymbol{\mu}, \quad m_s(0) = 0 \end{aligned} \tag{4.50}$$

Applying (4.49) to the modified adaptive law (4.45) gives the adaptive law used in this work

$$\dot{\boldsymbol{\theta}}_p = \boldsymbol{\Gamma} \bar{\epsilon} \boldsymbol{\mu} - \boldsymbol{\Gamma} w \boldsymbol{\theta}_p \tag{4.51}$$

where

$$\bar{\epsilon} = \frac{z - \boldsymbol{\theta}_p \boldsymbol{\mu}}{m^2}$$

and where w is defined as in (4.46). The analysis of the adaptive law (4.51) can be found in Appendix C.

This concludes the relevant theory used in this report. In the next chapter, the concepts presented in Chapters 2-4 will be incorporated into the implementaton of two MRAC schemes. These control schemes includes a modified MRAC scheme that utilizes a hybrid force control scheme to cope with ice loads acting on the vessel.

Chapter 5

Implementation

This chapter will incorporate the concepts discussed in Chapter 2-4, and address the implementation of a MRAC/HFC control scheme for the purpose of vessel control in Arctic areas.

The first part of the chapter will give an overview of the proposed MRAC scheme. Moreover, it will look at the different parts of the system, and present the system equations implemented in each module. These equations include the system control laws, and the update laws for estimating both the vessel parameters and the parameters of the environment.

5.1 Modified MRAC and control system design

Figure 5.1 shows the conceptual structure of the modified MRAC scheme, used in this work. Note that for the modified MRAC, as opposed to the MRAC scheme presented in Section 4.3, both the reference model and the controller is updated continuously based on the environment in which the vessel is situated. In addition, the diagram shows that the vessel and the environment influences each other with a force of interaction F, making robustness adjustments to the MRAC scheme crucial for stability and parameter convergence.

The following sections will consider each of the blocks of Figure 5.1 and present the implementation of each part of the modified MRAC scheme.

5.1.1 System dynamics and reference model

The control signal in Figure 5.1 is driven by the difference between the vessel state, and the output of a reference model. The reference model is designed to inhabit certain dynamic properties, which the vessel is controlled to follow.

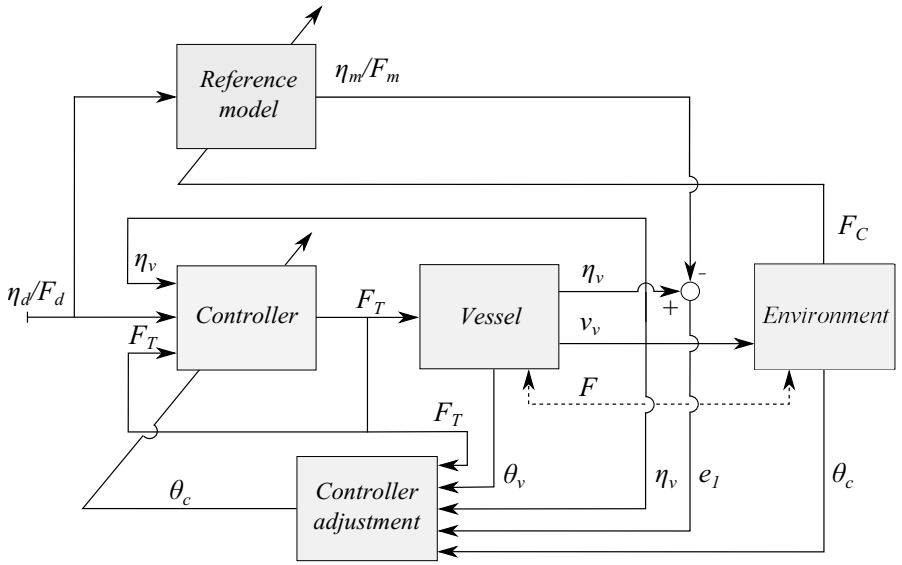

FIGURE 5.1: Structure of the modified MRAC

The reference model depends on the measured force $\boldsymbol{F}_C$, exerted by the environment in which the vessel is situated. In the subspace where the environmental forces are considered sufficiently small (i.e. motion control is considered possible), the reference model provides a position trajectory for the vessel to track. On the other hand, if forces due to the environment exceeds a given threshold, the reference model switches to provide a force trajectory. The vessel will then be controlled to *interact with the environment* in accordance to the force trajectory rather than tracking the reference position.

Figure 5.2 shows three plots describing the intended behavior of the vessel controlled by a hybrid force control scheme. The topmost plot shows the vessel position η for a stationkeeping scenario. It is seen that when the environmental force f_C, shown in the middle plot, exceeds the threshold f_{tol}, the desired interaction force f_m in this case starts to track f_C in order to make the vessel follow the motion of the ice loads. The thrust force f_T, shown in the bottommost plot, then goes to zero, while the vessel position starts to drift away from the desired position η_d. At the time f_C decreases below the threshold, position control is re-activated, and η re-converges to the desired position.

As a consequence of the subspace division introduced in Section 3.3, the reference model is divided to function in two distinct subspaces.

5.1.1.1 Position controlled subspace

In the subspace where forces due to environmental interaction are considered small, henceforth referred to as the position controlled subspace, it is desirable to let the vessel track a position trajectory provided by the reference model. The linear DP model is used

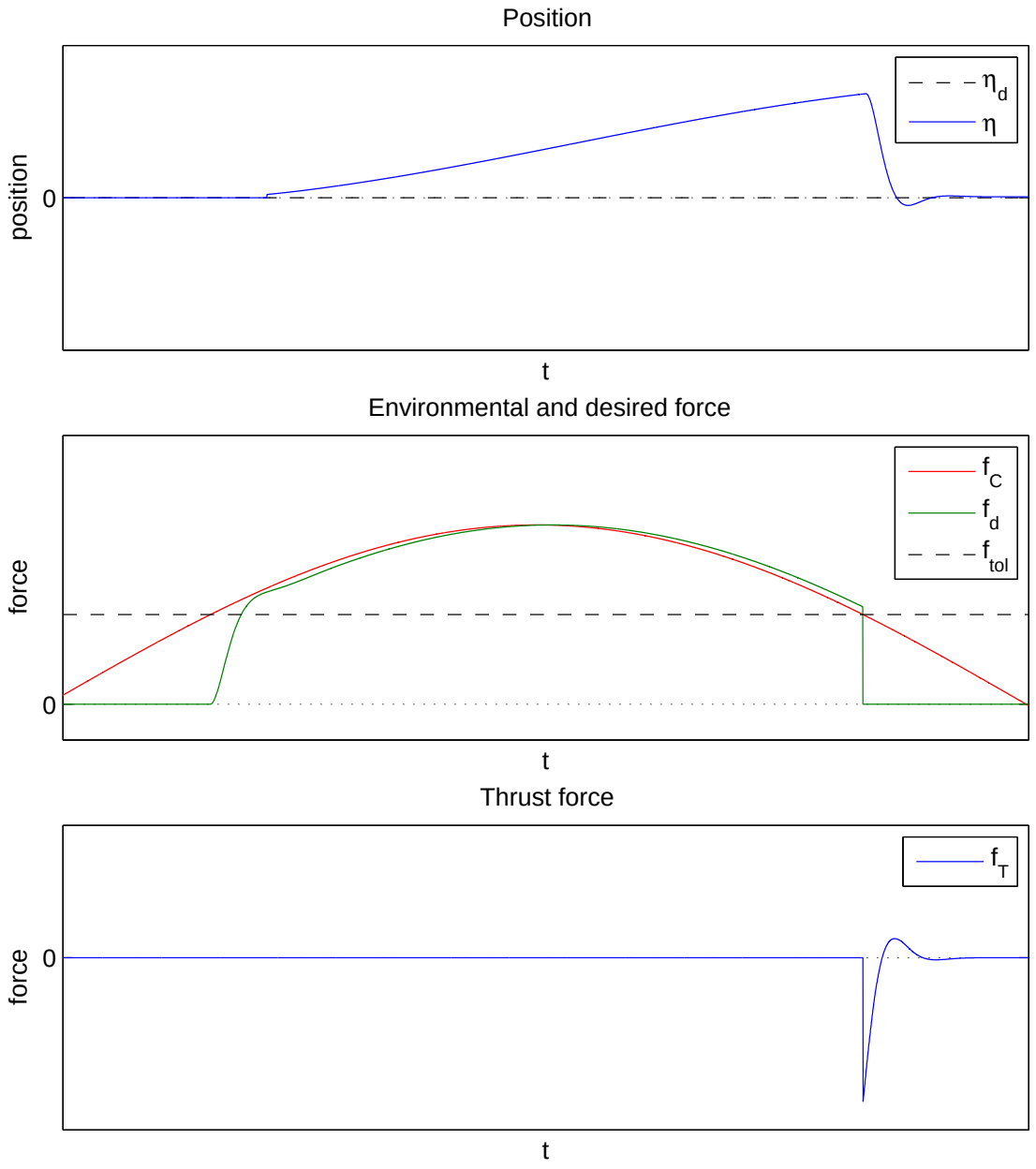

FIGURE 5.2: Conceptual visualization of MRAC with incorporated force control.

to describe the vessel dynamics

$$\dot{\boldsymbol{\eta}}_p = \boldsymbol{\nu} \tag{5.1a}$$

$$\boldsymbol{M}_{RB}\dot{\boldsymbol{\nu}} + \boldsymbol{D}\boldsymbol{\nu} = \boldsymbol{F}_T + \boldsymbol{F}_C \tag{5.1b}$$

In the model (5.1), $\boldsymbol{\eta}_p$ is the vessel position in VP coordinates, and $\boldsymbol{\nu}$ is the vessel velocity in BODY coordinates, defined as in Chapter 2. $\boldsymbol{F}_T$ are the thruster forces, $\boldsymbol{M}_{RB}$ is the vessel inertia matrix and $\boldsymbol{D}$ is the vessel drag vector (Metrikin et al., 2013). The drag vector $\boldsymbol{D}$ depends on the angle of attack of the ice forces, and both $\boldsymbol{D}$ and $\boldsymbol{M}_{RB}$ will be considered to be unknown and possibly varying. Note here, that the dynamics of the

environment are yet to be estimated, but that the environmental forces $\boldsymbol{F}_C$ are available for measurement.

The forces induced by ice loads in the position controlled subspace are believed to inhabit inertial dynamics. Moreover, it is assumed that they can be modeled as

$$\boldsymbol{M}_C\dot{\boldsymbol{\nu}}_c + \boldsymbol{D}_C\boldsymbol{\nu}_c = \boldsymbol{F}_C \tag{5.2}$$

where $\boldsymbol{M}_C, \boldsymbol{D}_C$ are the mass and damping matrices of the ice loads. The sea ice is assumed to possess a velocity $\boldsymbol{\nu}_c$ relative to the vessel given by

$$\boldsymbol{\nu}_c = -\boldsymbol{\nu} + \boldsymbol{\nu}_{drift} \tag{5.3}$$

where $\boldsymbol{\nu}_{drift}$ is the drift speed of the ice field.

Inserting (5.2) into (5.1b) gives the coupled system dynamics in the position controlled subspace

Coupled system dynamics, position controlled subspace

$$\dot{\boldsymbol{\eta}}_p = \boldsymbol{\nu} \tag{5.4a}$$

$$(\boldsymbol{M}_{RB} + \boldsymbol{M}_C)\dot{\boldsymbol{\nu}} + (\boldsymbol{D} + \boldsymbol{D}_C)\boldsymbol{\nu} = \boldsymbol{F}_T - \boldsymbol{D}_C\boldsymbol{\nu}_{drift} \tag{5.4b}$$

The last term on the right side of the equal sign represent a damping force on the vessel caused by the ice field drift.

In Section 3.2.2 it was shown that independent motion control was feasible in the case of a capacitive vessel dynamics in an inertial environment. Position control is thus possible in subspaces where moderate environmental forces affects the vessel. Therefore, in the position controlled subspace, the reference model will provide a position trajectory according to

Reference model, position controlled subspace

$$\dot{\boldsymbol{\eta}}_m = \boldsymbol{\nu}_m \tag{5.5a}$$

$$\dot{\boldsymbol{\nu}}_m + 2\zeta\omega_0\boldsymbol{\nu}_m + \omega_0^2\boldsymbol{\eta}_m = \omega_0^2\boldsymbol{\eta}_d \tag{5.5b}$$

where ζ, ω_0 are the desired damping ratio and natural resonant frequency of the system, $\boldsymbol{\eta}_d$ is the desired position, and $\boldsymbol{\eta}_m$ is the output trajectory.

By choosing reasonable values for ζ, ω_0, the model (5.5) and the output $\boldsymbol{\eta}_m$ represents a desired trajectory that converges to the desired position $\boldsymbol{\eta}_d$.

5.1.1.2 Force controlled subspace

Excessive ice forces, or *event loads*, can occur in all areas in the proximity of a vessel in a managed ice channel. Such event loads can be due to unfortunate geometrical configurations of ice floes acting on the vessel as one body, temporarily increasing the load level on the vessel to massive levels before dissolving. In addition, large ice floes that the ice breakers up stream have failed to break, or clogging of ice between the vessel and the ice channel ridge can result in similar effects (Kjerstad et al., 2014).

In the occurrence of such event loads, the vessel will be controlled to exert a desired force on the environment rather than being regulated to a reference position. This is referred to as force control. It is believed that this will alleviate the forces acting on the vessel hull, leading to less wear and tear, and resulting in decreased costs in terms of expenses associated with maintenance and repairs. In addition, a reduction in total environmental force acting on the vessel might reduce energy consumption over time.

It will be assumed that excessive environmental forces caused by event loads can be described by a single stiffness term

$$-\boldsymbol{K}_C(\boldsymbol{\eta}_p - \boldsymbol{\eta}_c) = \boldsymbol{F}_C \tag{5.6}$$

where $\boldsymbol{K}_C$ is the stiffness coefficient and $\boldsymbol{\eta}_c$ is some constant reference location for the capacitive force. Differentiating twice with respect to time and inserting into the vessel dynamics (5.1), the following relationship between the thruster force and the environmental force is obtained

Coupled system dynamics, force controlled subspace

$$\boldsymbol{M}\ddot{\boldsymbol{F}}_C + \boldsymbol{D}\dot{\boldsymbol{F}}_C + \boldsymbol{K}_C\boldsymbol{F}_C = -\boldsymbol{K}_C\boldsymbol{F}_T \tag{5.7}$$

The reference model will in this case be designed to output a desired force trajectory for the vessel to follow.

Using the same notation as in the position controlled case, the reference model in the force controlled subspace becomes

Reference model, force controlled subspace

$$\ddot{\boldsymbol{F}}_m + 2\zeta\omega_0\dot{\boldsymbol{F}}_m + \omega_0^2\boldsymbol{F}_m = \omega_0^2\boldsymbol{F}_d \tag{5.8}$$

where $\boldsymbol{F}_m$ is the reference model output, and $\boldsymbol{F}_d$ is the desired force of interaction with the environment.

Note here, that as the reference model (5.8) provides a force trajectory, the *vessel* will still behave as an inertial system. This is in accordance with the theory in Section 3.2. The exerted *force* is controlled to act as a capacitive system to achieve convergence to the desired force of interaction.

The outline of the reference model may now be illustrated by the pseudocode in Algorithm 1.

for *each DOF* i **do**
  if $f_{ci} \leq f_{ithreshold}$ **then**
    output position trajectory:

$$\begin{aligned} \dot{\eta}_{mi} &= \nu_{mi} \\ \dot{\nu}_{mi} + 2\zeta\omega_0\nu_{mi} + \omega_0^2\eta_{mi} &= \omega_0^2\eta_{di} \end{aligned}$$

  else
    output force trajectory:

$$\ddot{f}_{mi} + 2\zeta\omega_0\dot{f}_{mi} + \omega_0^2 f_{mi} = \omega_0^2 f_{di}$$

  end
end

Algorithm 1: Conditional reference model.

5.1.2 Control law calculation

Having established both the coupled systems dynamics and a suitable reference model, the MRAC control law can be determined. Consider the control law (4.19) given below for reference

$$u_p = \theta_1^\top \frac{\alpha(s)}{\Lambda(s)} u_p + \theta_2^\top \frac{\alpha(s)}{\Lambda(s)} y_p + \theta_3 y_p + c_0 r \tag{5.9}$$

The objective now is to calculate the parameters c_0, θ_i, $i = 1, 2, 3$ based on the coupled system models (5.4) (5.7), and the reference models (5.5), (5.8).

The control objective depends on the operating conditions. If the environmental forces are sufficiently low, it is desirable to control the vessel to a reference position. On the other hand, if the environmental forces are large, it might be beneficial to control the contact force with the environment to reduce equipment wear and tear.

For this reason the controller is divided into two parts. One part regulates vessel position in the subspace where position control is desired. The other part regulates the environment contact force in the subspace where the ice forces are considered too large.

5.1.2.1 Position controlled subspace

In the position controlled subspace, the control law (5.9) in the ith direction takes the following form

Position control law

$$f_{Ti} = \theta_{1pi}^{\top} \frac{\alpha(s)}{\Lambda(s)} (f_{Ti} + 2d_{ci}\nu_{idrift}) + \theta_{2pi}^{\top} \frac{\alpha(s)}{\Lambda(s)} \eta_{pi} + \theta_{3pi}\eta_{pi} + c_{0pi}\eta_{di} \tag{5.10}$$

where the product $2d_{ci}\nu_{idrift}$ is a term counteracting for the ice field drift. From (5.10) it can be seen that in the position controlled subspaces, the controller aims to regulate the vessel position η_{pi} to a desired position η_{di}.

5.1.2.2 Force controlled subspace

In the force controlled subspace, the control law takes the form

Force control law

$$f_{Ti} = \theta_{1fi}^{\top} \frac{\alpha(s)}{\Lambda(s)} f_{Ti} + \theta_{2fi}^{\top} \frac{\alpha(s)}{\Lambda(s)} f_{ci} + \theta_{3fi} f_{ci} + c_{0fi} f_{di} \tag{5.11}$$

From (5.11) it can be seen that in the force controlled subspace, the controller aims to regulate the interaction force f_{ci} with the ice to a desired contact force f_{di}.

5.1.2.3 Calculation of control law parameters

The calculation of the parameters $\theta_j, j = 1, 2, 3$ in the control laws for both control objectives, requires the definition of the respective system equations. Recalling the general plant transfer model presented in Section (4.19) rewritten for the above systems in the ith direction

$$y_i = \hat{k}_i \frac{\hat{Z}_i(s)}{\hat{R}_i(s)} f_{Ti} \tag{5.12}$$

where y_i is position or force in direction i, $\hat{k}_i$ is the high frequency gain of the system, $\hat{Z}_i(s) = 1$, and $\hat{R}_i(s)$ is the coupled system characteristic polynomial in the ith direction, given by

$$\hat{R}_i(s) = s^2 + a_1 s + a_0 \tag{5.13}$$

where $a_j, j = 0, 1$ are the coupled system coefficients corresponding to the coefficients in Equations (5.4b), (5.7). For example, in the position controlled subspace, the parameters $\hat{k}_i$, $\hat{Z}_i$ and $a_j, j = 0, 1$ becomes as follows

$$\hat{k}_i = \frac{1}{m_i + m_{ci}}, \ , \hat{Z}_i = 1, \ a_1 = \frac{d_i + d_{ci}}{m_i + m_{ci}}, \ a_0 = 0$$

Similarly, the reference model is represented by the transfer function

$$y_{mi} = k_{mi} \frac{Z_{mi}(s)}{R_{mi}(s)} r_i \tag{5.14}$$

where y_{mi} is the reference position or force output in the ith direction, $k_{mi} = \omega_0^2$ is the desired high frequency gain of the system, $Z_i(s) = 1$, r_i is the desired position or force, and $R_i(s)$ is the characteristic polynomial of the reference model given by

$$R_{mi}(s) = s^2 + 2\zeta\omega_0^2 s + \omega_0^2 \tag{5.15}$$

Using the mapping equations derived in Section 4.3.1, together with the filter polynomial $\Lambda_0 = (s + 1)$, the control law parameters $\theta_j, j = 1, 2, 3$ in the ith direction can now be found by solving the polynomial equations

Mapping equations for control law parameters

$$c_{0*i} = \frac{k_{mi}}{\hat{k}_i} \tag{5.16a}$$

$$\theta_{1*i} = (s + 1) - \hat{k}_i \hat{Q}_i(s) \tag{5.16b}$$

$$\theta_{2*i} + \theta_{3*i}(s + 1) = \frac{1}{\hat{k}_i} \left(\hat{Q}_i(s) \hat{R}_i(s) - (s + 1) R_{mi}(s) \right) \tag{5.16c}$$

where $*$ in the parameter subscripts denotes position or force control.

5.2 Estimation of system dynamics

In order to obtain the desired control law parameters, the MRAC scheme relies on the estimates $\hat{k}_i, \hat{Z}_i(s), \hat{R}_i(s)$. These polynomials define the estimated system dynamics.

For the case of simplicity, the linearized vessel model (5.1) will be assumed to be completely decoupled in the BODY frame. That is, the coefficient matrices $\boldsymbol{M}_{RB}$ and $\boldsymbol{D}$ in (5.1) are assumed to be diagonal. As a result, the motion in each DOF can be considered as a linear SISO system. Therefore, the estimation techniques discussed in Chapter 4 can be applied.

5.2.1 Vessel parametric model and adaptive law

Parameterizing the vessel model (5.1), gives the following parametric model of the vessel

Vessel linear parametric model

$$\boldsymbol{z}_v = \boldsymbol{\theta}_v^\top \boldsymbol{\mu}_v \tag{5.17}$$

where

$$\boldsymbol{z}_v = \frac{1}{\Lambda(s)}\boldsymbol{F}_T, \quad \boldsymbol{\theta}_v = [\boldsymbol{M}_{RB} \quad \boldsymbol{D}]^\top$$

$$\boldsymbol{\mu}_v = \left[\frac{s}{\Lambda(s)}\boldsymbol{\nu}, \quad \frac{1}{\Lambda(s)}\boldsymbol{\nu}\right]^\top, \quad \Lambda(s) = (s+1)^2$$

Applying the gradient method to (5.17) gives the following update law for the parameter vector $\boldsymbol{\theta}_v$.

Update law for vessel parameters

$$\dot{\boldsymbol{\theta}}_v = \boldsymbol{\Gamma}_v \boldsymbol{\epsilon}_v \boldsymbol{\mu}_v - \boldsymbol{\Gamma}_v \boldsymbol{w}_v \boldsymbol{\theta}_v \tag{5.18}$$

where

$$\boldsymbol{\epsilon}_v = \frac{\boldsymbol{z}_v - \hat{\boldsymbol{z}_v}}{m_v^2} = \frac{\boldsymbol{z}_v - \boldsymbol{\theta}_v^\top \boldsymbol{\mu}_v}{m_v^2}, \qquad \boldsymbol{\Gamma}_v = \boldsymbol{\Gamma}_v^\top > 0$$

and an element in the leakage term $\boldsymbol{w}_v$ in one DOF i is given by

$$w_{vi} = \begin{cases} 0, & \text{if } |\theta_{vi}(t)| < M_{0i} \\ \left(\frac{|\theta_{vi}(t)|}{M_{0i}} - 1\right), & \text{if } M_{0i} \leq |\theta_{vi}(t)| < 2M_{0i} \\ w_{0i}, & \text{if } |\theta_{vi}(t)| \geq 2M_{0i} \end{cases} \tag{5.19}$$

The dynamic normalization term m_v is given by

$$m_v^2 = 1 + \boldsymbol{\mu}_v^\top \boldsymbol{\mu}_v + m_{vs}, \tag{5.20}$$

$$\dot{m}_{vs} = -\delta m_{vs} + \boldsymbol{F}_T^\top \boldsymbol{F}_T + \boldsymbol{\nu}^\top \boldsymbol{\nu}, \qquad m_{vs}(0) = 0 \tag{5.21}$$

5.2.2 Environment parametric model and adaptive law

In order to update the reference model based on knowledge of the environment, the environment dynamics have to be estimated. This can be done in the same manner as for the estimation of the vessel dynamics in Section 5.2.

5.2.2.1 Low sea ice interference

When the forces due to the sea ice are low, it is assumed that the ice load inhabits inertial dynamics, given by the environmental model (5.2). Parameterizing (5.2) gives the linear parametric model for the environment

Environment linear parametric model

$$\boldsymbol{z}_c = \boldsymbol{\theta}_c^\top \boldsymbol{\mu}_c \tag{5.22}$$

where

$$\boldsymbol{z}_c = \frac{1}{\Lambda(s)} \boldsymbol{F}_C, \quad \boldsymbol{\theta}_c = [\boldsymbol{M}_C \quad \boldsymbol{D}_C]^\top$$

$$\boldsymbol{\mu}_c = \begin{bmatrix} \frac{s}{\Lambda(s)} \boldsymbol{\nu}_c & \frac{1}{\Lambda(s)} \boldsymbol{\nu}_c \end{bmatrix}^\top$$

Applying the gradient method to (5.22), the update law for the environment parameter vector becomes

Update law for environment parameters

$$\dot{\boldsymbol{\theta}}_c = \boldsymbol{\Gamma}_c \boldsymbol{\epsilon}_c \boldsymbol{\mu}_c - \boldsymbol{\Gamma}_c \boldsymbol{w}_c \boldsymbol{\theta}_c \tag{5.23}$$

where

$$\boldsymbol{\epsilon}_c = \frac{\boldsymbol{z}_c - \hat{\boldsymbol{z}}_c}{m_c^2} = \frac{\boldsymbol{z}_c - \boldsymbol{\theta}_c^\top \boldsymbol{\mu}_c}{m_c^2}, \qquad \boldsymbol{\Gamma}_c = \boldsymbol{\Gamma}_c^\top > 0$$

and where an element in the leakage term $\boldsymbol{w}_c$ in one DOF i is given by

$$w_{ci} = \begin{cases} 0, & \text{if } |\theta_{ci}(t)| < M_{0i} \\ \left(\frac{|\theta_{ci}(t)|}{M_{0i}} - 1 \right), & \text{if } M_{0i} \leq |\theta_{ci}(t)| < 2M_{0i} \\ w_{0i}, & \text{if } |\theta_{ci}(t)| \geq 2M_{0i} \end{cases} \tag{5.24}$$

The dynamic normalization term m_v is given by

$$m_c^2 = 1 + \boldsymbol{\mu}_c^\top \boldsymbol{\mu}_c + m_{cs}, \tag{5.25}$$

$$\dot{m}_{cs} = -\delta_c m_{cs} + \boldsymbol{\mu}_c^\top \boldsymbol{\mu}_c, \qquad m_{cs}(0) = 0 \tag{5.26}$$

5.2.2.2 High sea ice interference

When the ice forces are large, the ice loads are assumed to inhabit capacative dynamics, given by

$$-\boldsymbol{K}_C(\boldsymbol{\eta}_p - \boldsymbol{\eta}_c) = \boldsymbol{F}_C \tag{5.27}$$

Modeling the environment in the case of capacitive dynamics are more difficult than in the inertial case. The difficulty arises from the fact that to estimate the parameter $\boldsymbol{K}_C$, some reference point $\boldsymbol{\eta}_c$ of the event load causing the capacitive forces has to be known. In this thesis it is argued that this reference point is the location of the ice channel ridge in the direction from which the forces act. The capacitive force acting on the vessel in the case of vessel-ridge ice clogging could then be thought of as a spring force being proportional to the distance between the ridge and the vessel. The stiffness coefficient k_{ci} in direction i can then be found from

Calculation of environmental stiffness parameter

$$k_{ci} = \frac{f_{ci}}{\eta_{pi} - \eta_{ci}} \tag{5.28}$$

as long as $\eta_{pi} \neq \eta_{ci}$. However, while the location of the ice ridge might be known in this case, the location of such a reference position vector in the general case is difficult to establish. Therefore, some reservations has to be made when analyzing the results for the force controlled vessel, when the environment is modelled in this manner.

5.3 Realization

The MRAC scheme depicted in Figure 5.1, and presented in the preceding sections, was implemented in MATLAB/Simulink® and converted to C++ code using the `Simulink Coder` toolbox. The C++ project was then imported into Microsoft Visual Studio, where it was compiled as a static library to be used by the simulator software.

In the implementation, most of the scheme was written in MATLAB code run by `MATLAB Fnc` blocks in Simulink®. However, some kinematic tools, such as `Rotation`

`matrix in yaw`, were taken from the `Marine Systems Simulator` toolbox (Fossen and Perez, 2004) an put directly into the block diagram.

The different modules of the implemented MRAC scheme were finally composed to resemble the depiction in Figure 5.1.

The MATLAB functions and Simulink® diagrams used in the implementation can be found on the CD included in the back of this report.

Chapter 6

Case study

This chapter presents the case study carried out to investigate and demonstrate the control system presented in Chapter 5. The chapter will begin with presenting the numerical model employed to simulate the vessel and ice dynamics. Thereafter, the specific case scenario is outlined.

6.1 The NTNU Numerical Ice Tank

In order to carry out a satisfactory test of the control system, it is chosen to utilize The Numerical Ice Tank (NIT), a numerical model of an ice covered towing tank, developed at NTNU, Trondheim. The NIT is employed to simulate a vessel and the ice loads by which the vessel is influenced. Moreover, the software provides a graphical interface, resembling a virtual ship model towing tank which can be covered with an ice field of chosen ice concentration, thickness, density and floe size.

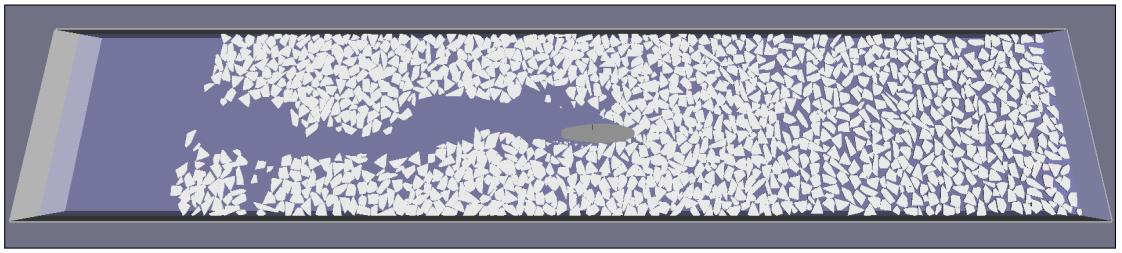

FIGURE 6.1: Screenshot of the NTNU Numerical Ice Tank midway through a simulation.

In order to carry out the analysis of an ice going vessel, the NIT simulates a ship model towing tank experiment. The experiment is carried out by simulating a vessel model tracking a predefined trajectory through the ice field. Equipped with virtual azimuth thrusters, the vessel model is actuated in surge, sway and yaw. Automatic vessel control

is achieved by employing a control system to be tested. Figure 6.1 shows a screen shot of the tool during a test run. In the figure, positive surge direction points towards the right, positive sway direction points downwards, and positive yaw direction turns clockwise.

The control system employed by the simulated vessel model is implemented in MATLAB/ Simulink® and transformed into C++ code before it is imported into Visual Studio. In Visual Studio the controller is compiled as a static library to be utilized by the simulator software. Thenceforth, the experiment is carried out using a time-stepping simulator based on non-smooth, rigid, multi-body dynamics, estimating the contact forces and friction between the ship model and the ice, as well as between each individual ice floe (Scibilia et al., 2014).

In order to provide the user with data from the simulations, the software outputs the vessel position in NED coordinates. This implies that the position vector $\boldsymbol{\eta}$ is required to be transformed to the VP coordinate position vector $\boldsymbol{\eta}_p$ prior to usage in the MRAC control law.

The software furthermore outputs vessel velocity relative to the ice in BODY coordinates, and environmental forces and thruster forces acting on the vessel CO, both given in BODY coordinates. In addition, the software is set to output estimates of vessel and environment parameters as the experiments are conducted. The data are then exported to MATLAB for further analysis.

The NIT allows for deciding the length of the simulation and the size of the ship model tank in which the tests are conducted. The ice tank measurements used in the case study are presented in Table 6.1. It is important to note here that all the parameters are given in model scale. This means that every parameter has to be multiplied by the scaling factor $\alpha = 33$ to be comparable to a full scale setting. The reader is referred to Appendix A for more information on model scaling.

Table 6.1: Ice Tank Measurements

Dimension	Value [m]
Length	100.0
Width	15.0
Depth	2.5

In addition to allowing for the choice of model tank measurement, in order to simulate different operating conditions, the NIT allows for choosing various ice parameters, including ice thickness and density, as well as the size of each individual ice floe.

The desired ice concentration may be chosen as well. However, the size and shape of each individual ice floe puts constraints upon the software's ability to obtain the desired coverage. Thus, the desired value may not always be achieved.

Table 6.2 summarizes the ice field parameters used in the case study.

TABLE 6.2: Physical Ice Parameters

Parameter	Unit	Value
Ice coverage (desired)	[%]	90
Ice density	[kg/m^3]	900.0
Ice thickness	[m]	0.1
Ice floe size	[m^2]	$\in [0.16, 0.81]$
Ice drift speed	[m/s]	$[-0.1\ 0\ 0]^\top$

6.2 Case study outline

The case study carried out in the following addresses the hypotheses given in Chapter 1. The hypotheses stated that, in harsh operating conditions such as sea ice environments, a control scheme with adaptive control parameters will perform better than a control system with static parameters in terms of automatic vessel control. In addition, an adaptive control system will result in decreased energy consume. This is because it will generate counteracting thrust forces with respect to disturbances in a more precise manner. Furthermore, the incorporation of force control, will reduce energy consume even more, as well as alleviate the environmental forces acting on the vessel.

To test the hypotheses, and to cover possible scenarios for the control systems, the case study includes two main cases:

Stationkeeping (SK)

The first case considers the scenario where a vessel is to remain at a predefined position solely by the use of thruster force. This is one plausible situation for a DP vessel in a managed ice setting. Potential scenarios includes drilling operations, and installation and maintenance of subsea equipment.

Waypoint tracking (WT)

The second case considers a situation where the vessel is to track a position trajectory. The test is conducted by letting the vessel stop at predefined, stationary waypoints while holding a constant heading angle at 0 degrees. This is done in order to resemble an intervention scenario, where a possible intention could be to gather sonar data of the seabed in different parts of the managed ice channel.

The latter case is conducted partly for analysis reasons with regards to the parameter estimates. In order to provide the estimation algorithms in the control scheme with

adequately excited input signals, satisfying the persistent excitation condition (4.16), some degree of motion in the estimated systems is required. Therefore, results and analysis concerning the parameter estimates in the MRAC scheme will only be carried out in the case of waypoint tracking.

6.2.1 The indirect MRAC and MRAHFC scheme

Two implementations of the MRAC scheme described in Chapter 5 are tested in the simulator.

Adaptive position control (MRAC)

The first implementation is an indirect MRAC scheme, in which the system parameters (i.e. the coefficient matrices in (5.4)) are estimated in order to calculate the parameters in the control law (5.10). This control scheme does not have the ability to force control the vessel. The indirect MRAC will henceforth be referred to simply as the MRAC.

Hybrid force control (MRAHFC)

The second implementation is an extension of the indirect MRAC scheme. The extended scheme will henceforth be referred to as MRAHFC. In this implementation, the controller has the ability to switch to force control in a given DOF whenever the environmental forces exceeds a certain threshold.

The force- and position tolerances for the MRAHFC scheme are carried out in the following section.

6.2.1.1 Force and position tolerances

In order to avoid large drift-offs from the reference position, the MRACHFC will only be allowed to force control the vessel within some margins off the reference position in sway and yaw. This is done to keep the vessel in close proximity of the reference point, while at the same time allowing some drift-off during force control.

In addition to the tolerance limits with regards to position, to ensure that position control is prioritized whenever the ice loads are small, the MRACHFC is implemented with force thresholds in sway and yaw. Furthermore, the tolerance limits are divided into upper and lower thresholds. When the environmental force exceeds the upper threshold with a positive slope, force control is activated. On the other hand, when the environmental force go below the lower threshold with a negative slope, force control is deactivated, and the controller re-activates position control. This is done in order to implement some degree of hysteresis, and to ensure that the environmental forces are sufficiently decreased

when position control is reactivated. Thus undesired shattering due to frequent changes in control domain is avoided.

Finally, force control is omitted in surge as it is assumed that the ice masses encountered in this direction will be well managed by the ice breaking capabilities of the vessel.

Table 6.3 summarizes the tolerance boundaries for the demonstrated MRAHFC scheme.

TABLE 6.3: Force, moment and position tolerance limits for MRAHFC

			Values	
Parameter	Unit	Description	SK	WT
F_{uYtol}	[N]	Upper force tolerance sway	3	3
$F_{u\psi tol}$	[Nm]	Upper moment tolerance yaw	3	3
F_{lYtol}	[N]	Lower force tolerance sway	1	1
$F_{l\psi tol}$	[Nm]	Lower moment tolerance yaw	1	1
e_{Ytol}	[m]	Position tolerance sway	± 0.3	± 0.5
$e_{\psi tol}$	[rad]	Heading tolerance	± 0.02	± 0.03

The values for force and moment tolerances are set rather low. The reason for this is that it is desirable to activate force control before the environmental forces build up to high levels. At the same time, the position tolerances are set to low values to avoid excessive drift-offs from the reference. Force control can only be activated within the boundaries listed.

6.2.1.2 MRAC reference model and lowpass filtering

The MRAC reference model is designed in order to make to vessel behave in accordance to some reasonable performance specifications. The choice of values of the damping ratio ζ and the resonant frequency ω_0, has an impact of the transient response of the system to a step in desired position. A high resonant frequency will result in a high initial convergence rate. On the other hand, a large damping ratio will influence the last part of the transient, decreasing the convergence rate as the vessel approaches the desired position.

In the case study, it is chosen to apply different values for the damping ratio ζ and the resonant frequency ω_0 for the MRAC system and the MRAHFC respectively. The reason for this, is that, for the MRAC, high accuracy with respect to positioning is desired. Thus, for the MRAC, it is chosen to use a reference model with high values for the damping ratio and the resonant frequency.

On the other hand, for the MRACHFC, the aim is to lower the energy consumption, offering less thought to positioning performance. The reference model for the MRACHFC is therefore modeled with a lower resonant frequency and higher damping ratio *when position control is re-activated from force control*. This will result in a slower convergence rate when the vessel is to recover to the desired position after a drift-off.

In the simulations, the reference model needs to account for the dynamic properties of the vessel thrusters. In a real world situation, vessel thrusters are normally geared in three stages from 0 to 100 [%] thrust force. These stages vary in length and distribution, but may for instance be divided in the intervals $[0, 60\rangle$, $[60, 90\rangle$ and $[90, 100\rangle$ [%] (Wold, 2013). In the NIT, this thrust rate limitation is approximated by a lowpass filter. As a consequence, in order to generate an achievable reference trajectory, a similar lowpass filter is applied to the desired position signal $\boldsymbol{\eta}_d$ by the reference generator. The LP filter can be modeled as

$$H_{LP}(s) = \frac{1}{Ts + 1} \tag{6.1}$$

The time constant T in the filter (6.1) is tuned to correspond to the time constant of the vessel thrusters. In real life, this time constant will be minimum 20 to 30 [s] for diesel-mechanical propulsion, and about 10 to 15 [s] for diesel-electric propulsion. These are approximate minimum values of the time constants, found from conversations with Ph.d candidate Aleksander Veksler at NTNU, and Mr. Helge Asle Lundeberg from Scana Mar-El, cited in Wold (2013). However, the vessel simulated in the NIT has a time constant of about 60 [s] in real world scale. Thus, applying a scaling factor of $\alpha = 33$, a time constant of

$$T = \frac{60}{\sqrt{33}} \approx 10.5 \text{ [s]}$$

was used for the model scale experiments. Figure 6.2, shows the lowpass filter in series with the MRAC.

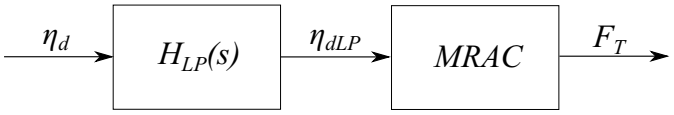

FIGURE 6.2: Series connection of LP filter and MRAC.

Table 6.4 summarizes the parameters of the MRAC reference model. Keep in mind that the value for ω_0 given for MRAHFC, only applies for the cases where accuracy in terms of position has low priority (i.e. when position control is re-activated from force control). Otherwise, the parameters are the same as for the MRAC scheme. The parameters given in Table 6.4 results in a reference model resembling an open loop system, with pole locations according to Figure 6.3. The reference model parameters, along with the time constant of the LP filter, results in the step responses shown in Figure 6.4.

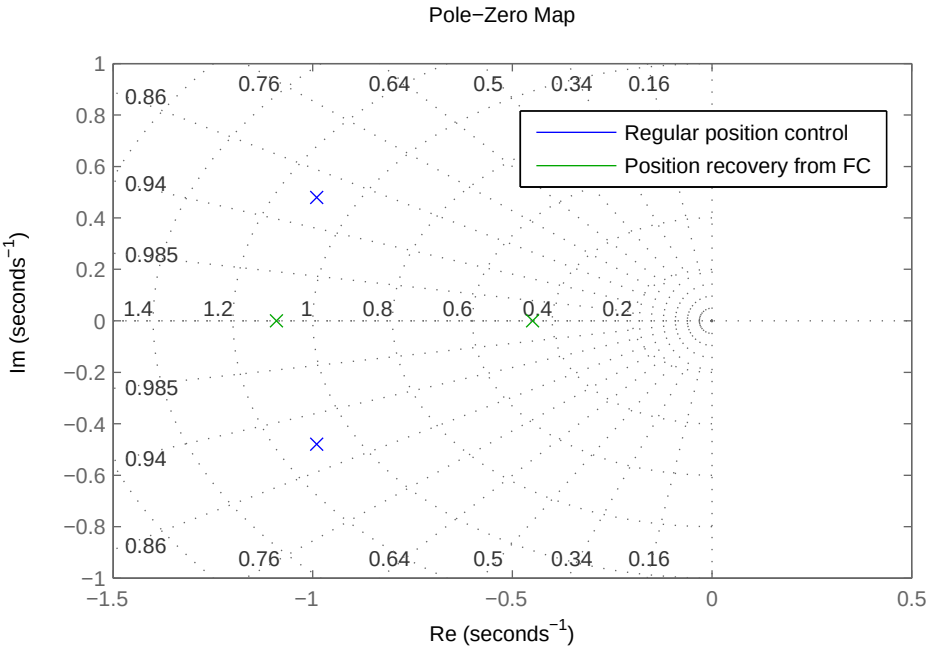

FIGURE 6.3: MRAC reference model pole locations.

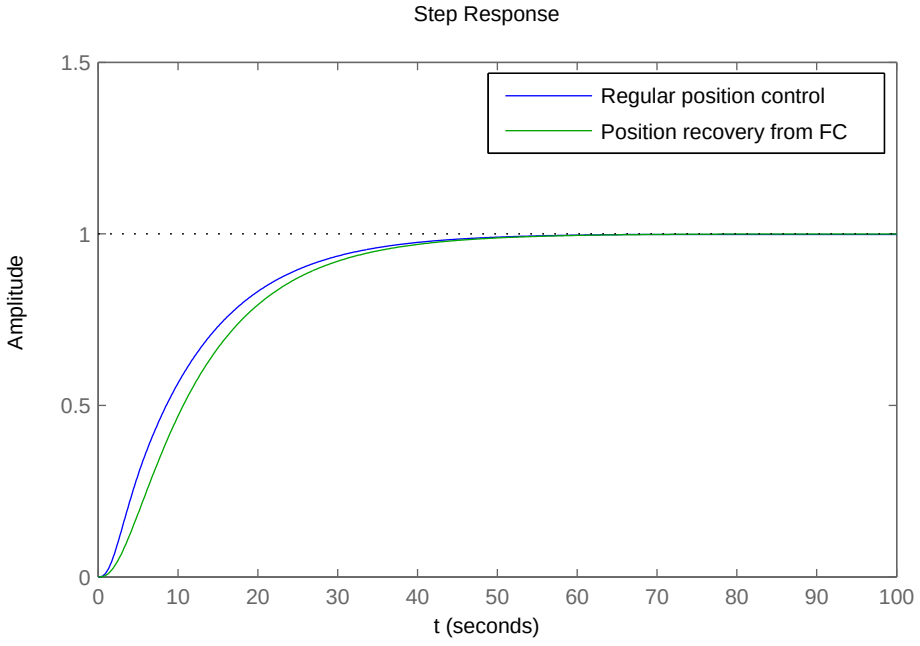

FIGURE 6.4: Reference response to a unit step in desired position.

TABLE 6.4: Relevant parameters for MRAC reference model

			Values	
Parameter	Unit	Description	MRAC	MRAC w/FC
ζ	$[\cdot]$	Reference model damping ratio	0.9	1.1
ω_0	[rad/sec]	Reference model resonant frequency	1.1	0.7

6.2.2 Reference PD-controller

A conventional non-linear PID controller with external force feed-forward is employed as a reference point for the two MRACs. The PID control law is given below.

$$\boldsymbol{F}_T = \boldsymbol{K}_p(\boldsymbol{\eta}_d - \boldsymbol{\eta}) + \boldsymbol{K}_i \int_0^t (\boldsymbol{\eta}_d - \boldsymbol{\eta}) d\tau + \boldsymbol{K}_d \frac{d}{dt}(\boldsymbol{\eta}_d - \boldsymbol{\eta}) - \boldsymbol{F}_C \tag{6.2}$$

Where the feed-forward term $\boldsymbol{F}_C$ is furnished by the estimator included in the NIT.

The control gains used in the PID controller are presented in Table 6.5. It is chosen to set the integral action gain to zero as any external disturbance is contained in the feed-forward term, giving a PD-controller with acceleration feed-forward (PD-AFF). However, in the following, it will be referred to as the PID controller.

TABLE 6.5: PID control gains

Direction	K_p	K_i	K_d
Surge	100	0	1000
Sway	100	0	1000
Yaw	200	0	3000

The PID controller (6.2) has shown good results in tests performed in the large ice tank of the HSVA in 2012 within the European R&D project DYPIC (Jenssen et al., 2012). Thus, it is considered to be a satisfactory point of reference for the demonstrated MRAC schemes.

6.2.3 Monitoring the parameter estimates

In addition to testing the performance of the MRAC schemes in terms of automatic vessel control, it is chosen to monitor the estimated values of the vessel inertia and damping matrices $\boldsymbol{M}, \boldsymbol{D}$ in (5.1) as well as the corresponding matrices for environment inertia and damping $\boldsymbol{M}_c, \boldsymbol{D}_c$ in (5.2).

Even though correct estimates are not required by the control scheme in order to achieve desired performance in terms of automatic control, it is interesting to study the effect of changing environment parameters in terms of vessel behavior in the ice field. Moreover, monitoring the sea ice parameters in different sections of the ice channel might shed som light over the problem of sea ice modelling in general.

6.2.3.1 Ideal Simulink simulation

It should be noted that, as the environmental parameters, as well as the vessel damping, are unknown and possibly varying, it is difficult to tune the estimation scheme in order to optimize convergence rates. To serve as a reference case, an ideal system with known and constant values for environmental mass and damping, as well as vessel damping, was simulated in Simulink. The reference case represents an ideal scenario, where both the vessel and the environment are completely decoupled in surge, sway and yaw. While this may be a highly unrealistic situation, the data gathered from the ideal case may serve as a reference for the estimator in terms of tuning.

In the ideal case, the environmental forces are modeled as a mass-damper dynamic system, with sinusoidal force inputs in each DOF. Furthermore, the force sinusoidals are subject to additive noise. This is done in order to more or less resemble the random nature of sea ice.

To satisfy the PE condition (4.16), excitation of the regressor signals (i.e. velocity and acceleration of vessel and ice) is ensured by frequent changes in desired vessel position. In addition, in order to resemble an actual case of noisy measurements, the regressor signals are contaminated with a small amount of additive noise.

The actual vessel parameter values for the ideal case are listed in Table 6.6. The vessel mass and moment of inertia are chosen identical to the corresponding parameters of the vessel simulated in the NIT. The damping parameters are chosen as purely experimental values.

Table 6.6: Actual vessel parameters, ideal case

Parameter	Unit	Description	Values
m_x	[kg]	Vessel mass surge	3060
m_y	[kg]	Vessel mass sway	3060
I_{zz}	$[\mathrm{kg} \cdot \mathrm{m}^2]$	Vessel moment of inertia yaw	7987.14
d_u	[kg/s]	Vessel damping surge	1000
d_v	[kg/s]	Vessel damping sway	500
d_ψ	$[\mathrm{kg} \cdot \mathrm{m/s}]$	Vessel damping yaw	1000
δ_v	$[\cdot]$	Dynamic normalization term factor	10

Table 6.7 shows the chosen values for the environmental mass, moment of inertia and damping for the ideal case. Similar to the vessel damping parameters, the environmental parameters are purely experimental values chosen solely so that convergence of the estimated parameters can be confirmed.

TABLE 6.7: Actual environment parameters, ideal case

Parameter	Unit	Description	Values
m_{Cx}	[kg]	Added environmental mass surge	100
m_{Cy}	[kg]	Added environmental mass sway	300
I_{Czz}	[kg $\cdot$ m^2]	Added environmental moment of inertia yaw	200
d_{Cu}	[kg/s]	Environmental damping surge	100
d_{Cv}	[kg/s]	Environmental damping sway	300
$d_{C\psi}$	[kg $\cdot$ m/s]	Environmental damping yaw	300
δ_C	[$\cdot$]	Dynamic normalization term factor	10

Table 6.8 summarizes the initial values and adaption gain matrices for the estimation scheme in the MRAC system. The initial values are set to experimental values, in the same size of order as the expected or actual parameter values. The gain matrices applies for one single DOF.

6.2.4 Execution of tests

The case study trials are executed in the following manner. The vessel is situated at an initial desired position $\boldsymbol{\eta}_d = 0$, outside of the ice field in open water. Figure 6.5 shows the initial vessel position.

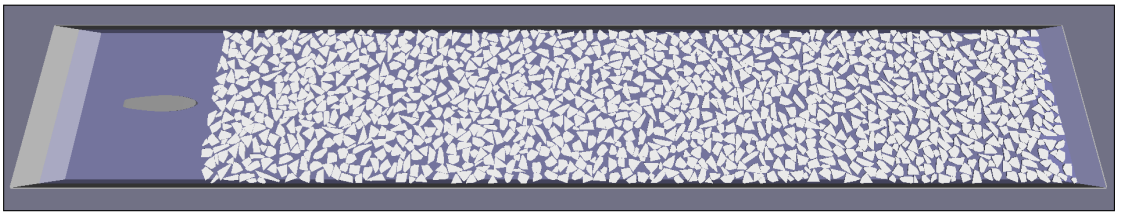

FIGURE 6.5: Vessel initial position.

The vessel hits the ice field ridge at approximately $t = 30$ [s]. To fully simulate a vessel enclosed in the ice field for all t, all results are trimmed to start at $t = 50$ [s], and all time instants in the results for positioning and observed forces are therefore offset with an amount of $t_{off} = 50$ [s]. This does not have any influence on the comparison of the control schemes, however, as their performance in open water are equal.

TABLE 6.8: Relevant parameters for MRAC estimation scheme

Parameter	Unit	Description	Values
$\mathbf{\Gamma}_v$	[·]	Vessel adaptive gain	$\left[\begin{smallmatrix}6100 & 0\\ 0 & 200\end{smallmatrix}\right]$
$\mathbf{\Gamma}_c$	[·]	Environment adaptive gain	$\left[\begin{smallmatrix}700 & 0\\ 0 & 200\end{smallmatrix}\right]$
m_{x0}	[kg]	Initial vessel mass estimate surge	2000
d_{x0}	[Ns/m]	Initial vessel damping estimate surge	1
m_{y0}	[kg]	Initial vessel mass estimate sway	2000
d_{y0}	[Ns/m]	Initial vessel damping estimate sway	1
m_{zz0}	[kg/m^2]	Initial vessel moment of inertia	7800
$d_{\psi 0}$	[Ns/m]	Initial vessel damping estimate yaw	1
M_{0vdu}	[·]	Upper leakage tolerance vessel damping	10000
M_{0vmu}	[·]	Upper leakage tolerance vessel mass/moment of inertia	10000
M_{0vdl}	[·]	Lower leakage tolerance vessel damping	0
M_{0vml}	[·]	Lower leakage tolerance vessel mass/moment of inertia	200
m_{cx0}	[kg]	Initial environment mass estimate surge	30
d_{cx0}	[Ns/m]	Initial environment damping estimate surge	1
m_{cy0}	[kg]	Initial environment mass estimate sway	30
m_{czz0}	[kg/m^2]	Initial environment moment of inertia estimate	30
$d_{c\psi 0}$	[Ns/m]	Initial damping estimate yaw	1
M_{0cdu}	[·]	Upper leakage tolerance environment damping	10000
M_{0cmu}	[·]	Upper leakage tolerance environment mass/moment of inertia	10000
M_{0cdl}	[·]	Lower leakage tolerance environment damping	0
M_{0cml}	[·]	Lower leakage tolerance environment mass/moment of inertia	10
δ	[·]	Dynamic normalization constant, vessel estimation	10
δ_c	[·]	Dynamic normalization constant, environment estimation	10

After penetrating the ice field ridge, the vessel tracks the reference position, or the reference interaction force in the force controlled case. In the case of force control, the desired interaction force is chosen to be equal to the ice force. That is,

$$\boldsymbol{F}_d = \boldsymbol{F}_C \tag{6.3}$$

Setting the desired force of interaction to be equal to the environmental forces, will lead to a reduction in the vessel thruster force when the environmental forces exceeds the force tolerance, resulting in a vessel responding solely to the forces off the ice. Together with the low force tolerance, this is believed to decrease the total environmental force on the vessel, reducing the total thruster force required to counteract the environmental

forces. The idea is that, by "giving in" for the environment at an early stage, excessive build-up the environmental forces can be avoided.

Table 6.9 shows the desired positions at the corresonding time instants of change in the case of waypoint tracking. The heading is kept at zero degrees for all t. This is done to maintain the vessel ice breaking capabilities with respect to the incoming ice.

TABLE 6.9: Desired positions for waypoint tracking scenario

t [s]	Surge [m]	Sway [m]	Yaw [deg]
$0-50$	0	0	0
$50-100$	0	2	0
$100-150$	1	2	0
$150-200$	1	0	0
$200-250$	0	0	0

6.2.5 Performance measurement methodology

In the case study, the performance of the control schemes is measured with respect to two aspects. The first aspect is accuracy with respect to positioning along the three actuated DOFs. For the stationkeeping scenario, this performance aspect will be measured using the standard deviation of the discrepancy, and the median of the position in each direction. For waypoint tracking the positioning accuracy is measured as a the sum of the squared errors.

The second aspect of performance is the measure of the magnitude of the applied thrust forces, as well as the magnitude of the environmental forces observed over time.

The following sections clarifies the measurement methodology used in the case study.

6.2.5.1 Standard deviation of discrepancy

For the stationkeeping case, positioning performance is measured in terms of the standard deviation σ of the discrepancy from the reference, given by

$$\sigma^2 = \frac{1}{n-1}\sum_{i=1}^{n} e^2(i) \tag{6.4}$$

where n is the number of time steps in the simulation, i denotes the ith sample and e is the discrepancy from the reference, given by

$$e^2 = e_x^2 + e_y^2 \tag{6.5}$$

where e_x, e_y is the error in surge and sway respectively.

6.2.5.2 Median of position

In addition to the standard deviation of the error, the median of the positions in North, East and yaw is used as a measure of positioning performance in the stationkeeping scenario. The median is used, as it is a robust statistic and gives a good measure on the vast majority of position samples. The median $\tilde{N}$ of the North position is calculated as

$$\tilde{N} = \frac{n+1}{2} \tag{6.6}$$

6.2.5.3 Sum of square error

For the waypoint tracking case, positioning performance is measured as a sum of the squares error (SSE) σ_α^2, given by

$$\sigma_\alpha^2 = \sum_{i=1}^{n} e^2(i) \tag{6.7}$$

Furthermore, by replacing the translational error e in Equations (6.4), (6.7) with the error in heading angle e_ψ, a similar measure of the positioning accuracy in yaw motion can be found for stationkeeping and waypoint tracking respectively.

6.2.5.4 Mean of absolute value

The second performance measure addresses the amount of thrust force applied by the vessel thrusters. Moreover, the amount of force applied on the vessel by the environment is used as a measure of wear and tear on mechanical equipment. The mean of the absolute value of forces acting on the vessel is used as a measure for both the thruster force and environmental force. The mean $|\bar{F}_T|$ of the absolute values of thruster force is calculated as

$$|\bar{F}_T| = \frac{1}{n} \sum_{i=1}^{n} |F_T(i)| \tag{6.8}$$

6.2.5.5 Variance of thrust force

The variance of the thrust forces is used as a measure on how much the thrust forces varies in value and time. A large variance in thrust force may be the source of excessive wear of thruster engines. Thus, the variance may be a proper indication of wear and tear

of actuating equipment. The variance $Var(F_T)$ of the thrust force is calculated as follows

$$Var(F_T) = \frac{1}{n}\sum_{i=1}^{n}(F_T(i) - \bar{F}_T)^2 \tag{6.9}$$

6.2.5.6 Energy calculations

In addition to the mean of absolute values of forces, the case study carried out in this chapter will attempt to do an analysis of the energy consumed by the vessel thrusters, as well as the amount of energy dissipated in the vessel by the environment. With regards to the former, the NIT does not output any data of engine power. Therefore, it is chosen to look at the cumulative amount of force applied by the vessel thrusters. That is, it is argued that a measure of consumed energy is given by

$$\bar{\boldsymbol{E}} = \sum_{i=0}^{n-1} |\boldsymbol{F}_T(i)| \geq 0 \tag{6.10}$$

where $\bar{\boldsymbol{E}}$ contains a measure of the consumed energy in each DOF. Furthermore, the expression

$$\bar{E}_{total} = \sum_{i=1}^{3} \bar{\boldsymbol{E}}_i \tag{6.11}$$

is a measure on the total amount of energy consumed by the vessel thrusters. In (6.11) i denotes the ith direction contained in $\bar{\boldsymbol{E}}$. By the theory in Appendix A.1, and from conversations with Professor Lars Imsland (Imsland, 2013), the above expressions gives a reasonable indication on the energy consume of the vessel thrusters.

In Chapter 7, the results gathered form the case study will be presented.

Chapter 7

Results and analysis

This chapter presents the results gathered from the case study carried out in Chapter 6. For each main case, starting with the case of stationkeeping, the positioning performance of each controller is presented first. Thereafter, results regarding the estimated forces acting on the vessel is presented.

The second main case, where waypoint tracking is conserned, will include the results conserning the estimation of system parameters. This is the only case where the requirement of persistent excitation of the input signals can be sufficiently satisfied, and thus the only case where the estimates are expected to converge to real values.

The results presented in this chapter are constructed from data gathered from the NIT simulator software. In the process of testing, several vessel towing tests were conducted in the NIT. The test from which the presented results are obtained, was considered as a good choice of data source, as it illustrates the behavior and the performance of the control systems in a adequate manner. Nevertheless, the performance of the controllers may not be optimal, as further tuning may improve the performance even more.

7.1 Stationkeeping

7.1.1 Surge and sway

7.1.1.1 Positioning

Figure 7.1 presents the position plots for the stationkeeping case for each controller. It can be observed from the plots that the MRAC controller performs well in keeping the vessel at the reference position.

In the plot showing positions for the vessel using the MRAHFC, green signifies position control, while brown signifies that the vessel is force controlled. The MRAHFC is seen to have a higher variance in sway, a direction in which force control may be activated. In particular, relatively large deviations in sway is observed at approximately $t = 75$ and $t = 120$ [s]. It can be observed that the vessel is force controlled during these drift-offs.

The reference PID controller is observed to have an offset in surge, resulting the vessel to be slightly off the reference position.

TABLE 7.1: Statistical observations of positioning error during stationkeeping.

Measure	Unit	PID	MRAC	MRAHFC
σ_{xy}	[m]	0.00490	0.00320	0.00760
$\tilde{N}$	[m]	8.364×10^{-4}	1.900×10^{-3}	2.200×10^{-3}
$\tilde{E}$	[m]	-6.7577×10^{-5}	-2.4675×10^{-6}	3.4061×10^{-5}

A quantitative measure of the performance of the different controllers are presented in Table 7.1. The table presents the standard deviations of the stationkeeping errors, as well as the median values in N and E direction for each controller. The MRAC controller is seen to perform superior to the two others in terms of small deviations from the reference position.

The results for the MRAHFC shows a considerably higher standard deviation for this controller. The MRAC and PID controller proves superior in terms of a small median value in the E direction. In particular, the classic MRAC is shown to obtain a median value superior to the two other controllers both in N and E..

The relatively large standard deviation and median value in sway for the MRAHFC is to be expected, as in this case the controller is intended to let the vessel drift off the reference position if the environmental forces are excessive. The relatively high median value of the PID controller in surge is believed to partly be a result of the offset in surge, observed in Figure 7.1 for this controller.

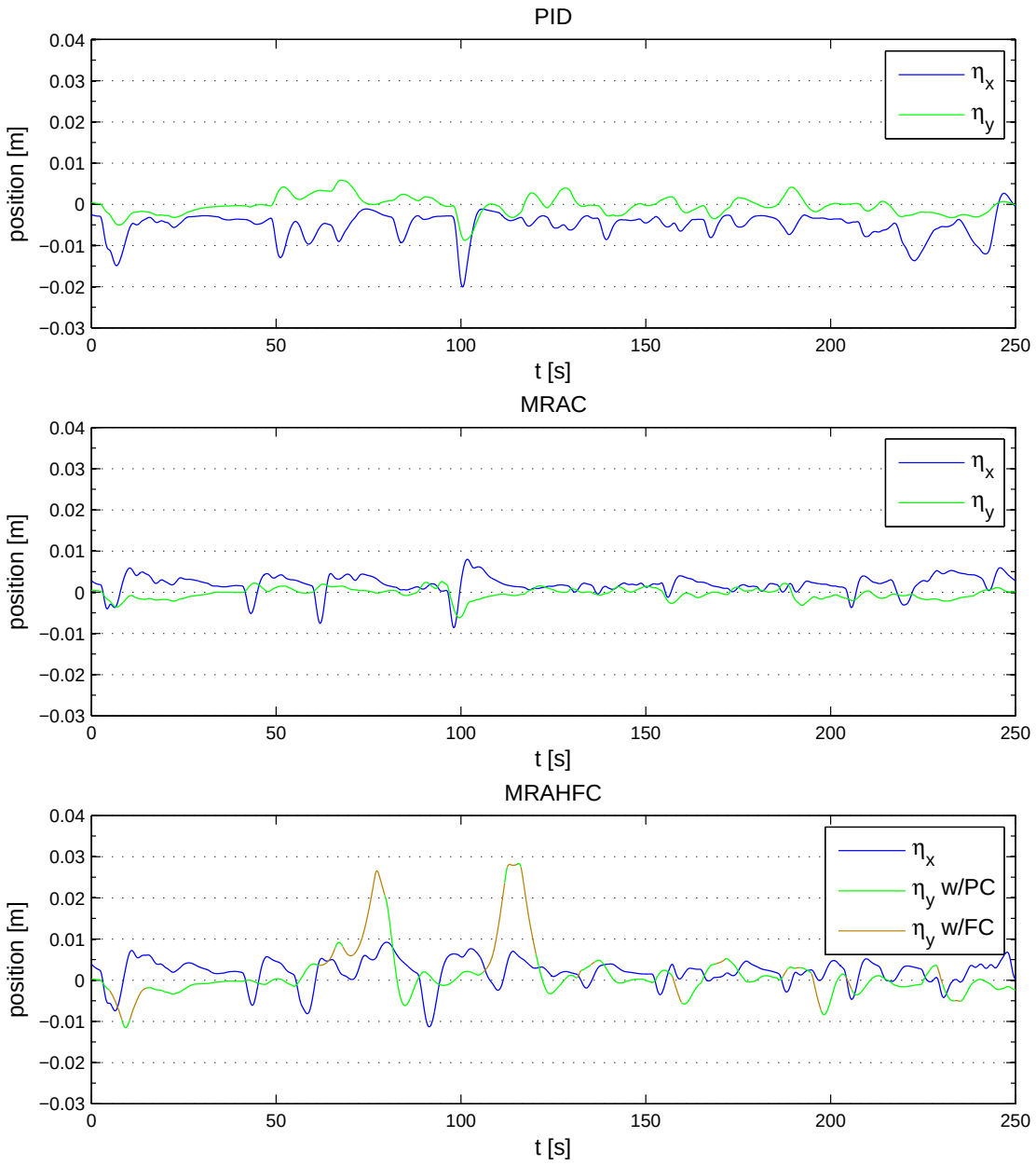

FIGURE 7.1: Positioning performance in surge and sway.

Figure 7.2 shows the trace of the vessel during stationkeeping. The deviations in sway in the case of MRAHFC, is clearly visible as rather large eastward drift-offs, extending to an error in sway of about 0.029 [m].

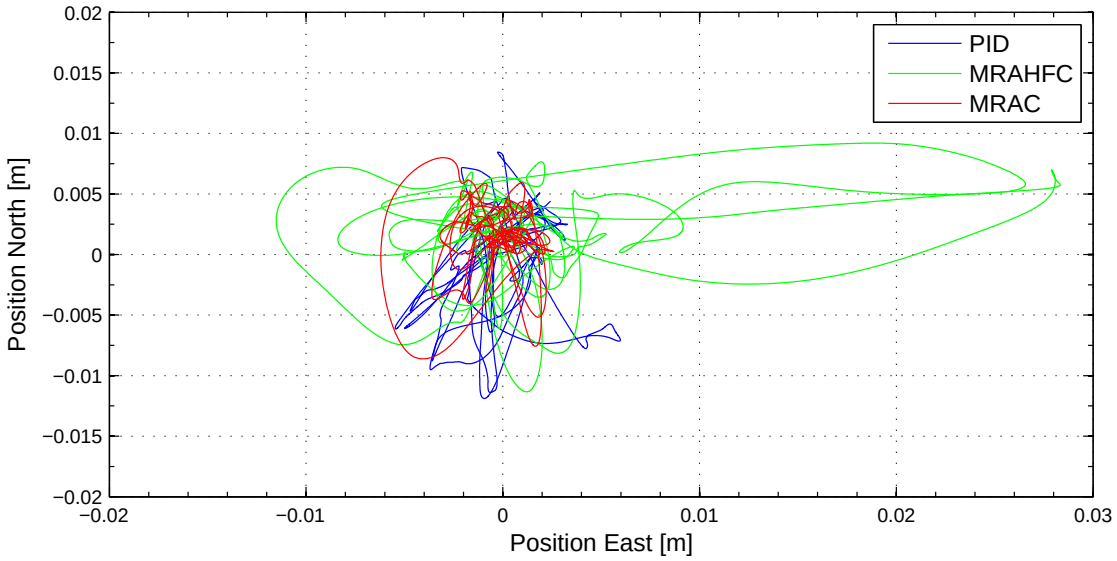

FIGURE 7.2: Trace plot of DP vessel during stationkeeping.

7.1.1.2 Observed forces

Figure 7.3 shows the environmental forces acting on the vessel from the environment in surge and sway. It can be observed that for the PID controlled vessel the high levels of environmental forces spans over longer time intervals. On the contrary, the pure MRAC is seen to experience the environmental forces in shorter intervals, though with higher peak values.

Table 7.2 shows the mean value of the environmental forces in surge and sway during stationkeeping.

TABLE 7.2: Statistical observations of environmental forces during stationkeeping.

Measure	Unit	PID	MRAC	MRAHFC
$\lvert\bar{F}_{Cx}\rvert$	[N]	11.4891	10.9205	11.3437
$\lvert\bar{F}_{Cy}\rvert$	[N]	1.3009	1.2055	1.3118

The MRAHFC controlled vessel is seen to be influenced by the environment in a similar way as the PID controller. However, as with the pure MRAC case, the environmental forces is seen to be divided into shorter intervals of time.

The PID controller manages the sea ice environment by feed-forwarding the environmental forces. Thus, to counteract the environment, the vessel thrusters in the PID case actuates a thrust force equal to the environment force for all t. It is of the author's belief that this results in the more severe environmental influence observed in the plots.

The actuating signal from the MRAC controllers is calculated based on the estimated coupled dynamics, resulting in precise control of the thrust force. It is seen that the pure

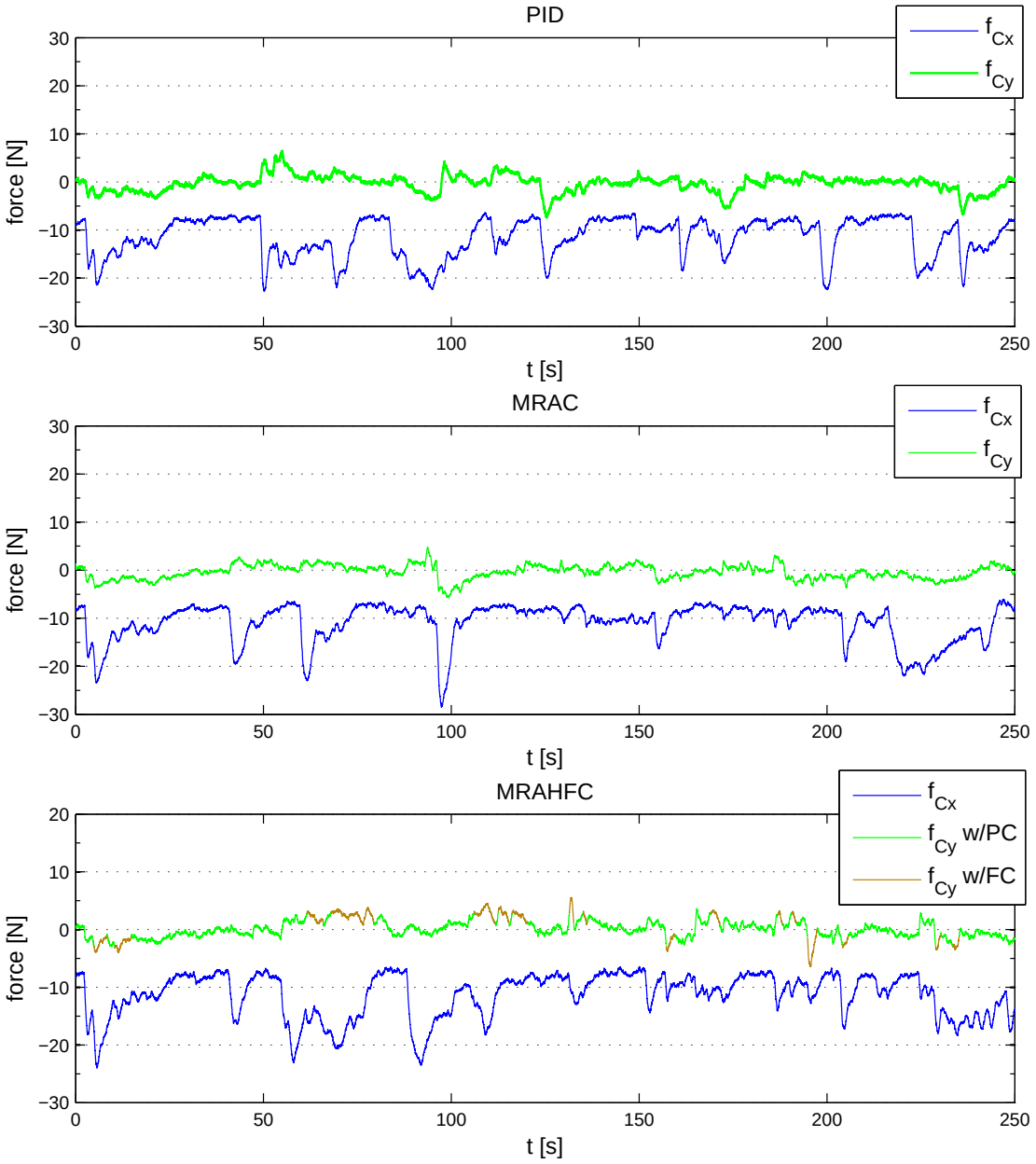

FIGURE 7.3: Perceived environment forces.

MRAC controlled vessel, as opposed to the PID controlled vessel, keeps the environmental forces at a low level during most of the trial, while experiencing some peaks in perceived force lasting a shorter amount of time.

The MRAHFC, on the other hand, is more similar to the PID. It is believed that the environmental influence in this case, comes from the fact that as the controller lets the vessel drift off the reference position during force control. This implies that when the environmental forces decreases, in order to regain position, the vessel has to track a longer trajectory through the surrounding fluid. This results in the relatively high observed environmental influence over time compared to the pure MRAC.

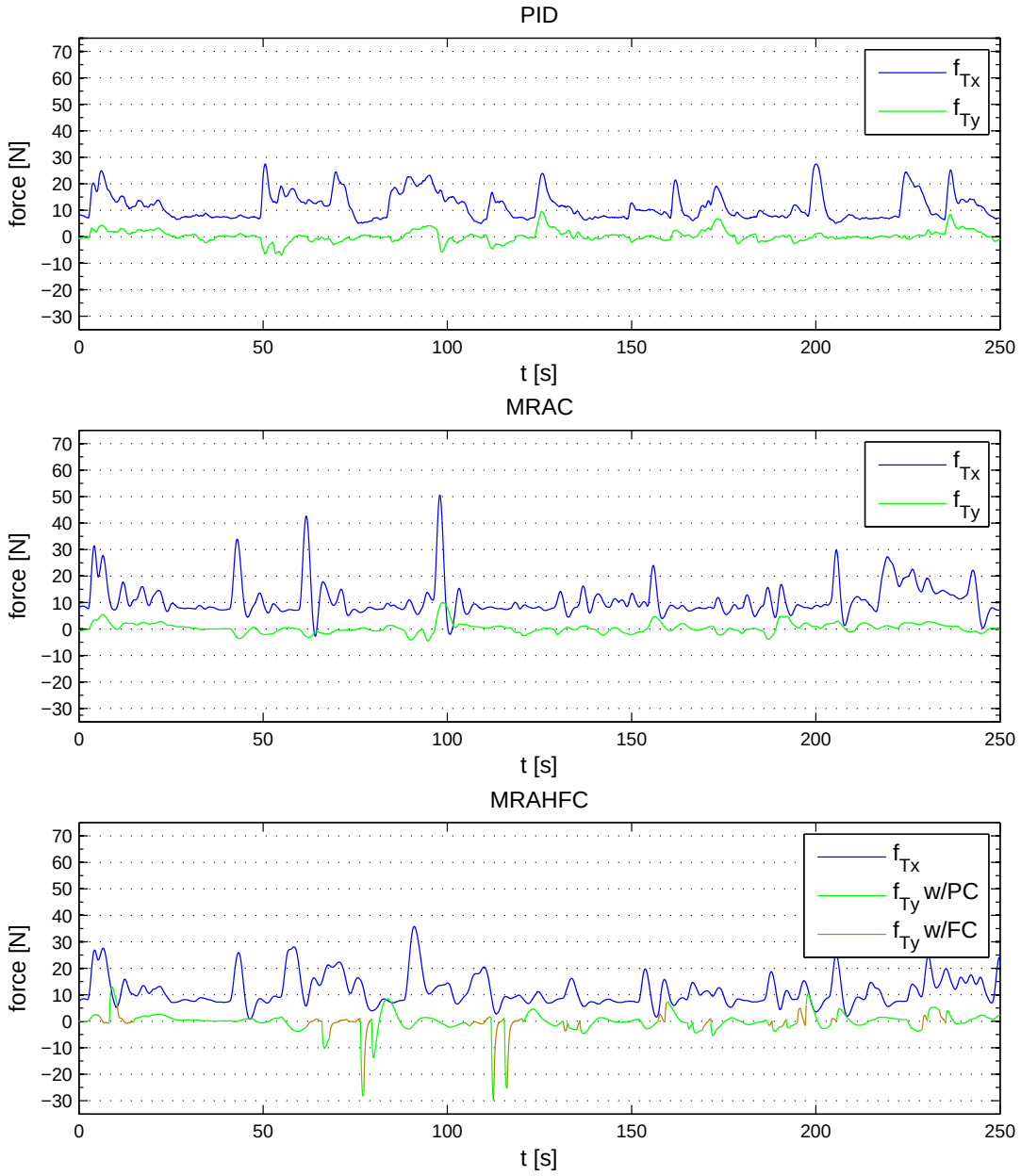

FIGURE 7.4: Actuated thruster forces.

Even though force control is only activated in sway and yaw, the above observations are particularly clear in surge, as this is the direction of the incoming sea ice, and thus inhabits most of the environmental influence in the case of zero heading stationkeeping. The slight increase of environmental force in sway at $t = 75$ and $t = 120$ [s], resulted in the drift-offs for the MRAHFC controlled vessel, observed in the position plots of Figures 7.1 and Figure 7.2.

Figure 7.4 shows the forces actuated from the thrusters in the surge and sway. Similar to the tendency of shorter, more frequent peaks in force, observed in the plots showing environmental forces, the MRAC controller actuates higher thrust force in shorter periods of time, keeping the overall thrust at a low level compared to the PID. However, due to

this, rather large thrust rates can be observed for both MRAC controllers. In particular, the drift-offs seen in the position plots for the MRAHFC can be observed as four rather sharp, negative peaks in sway at approximately $t = 75$ and $t = 120$ [s].

Table 7.3 presents the variance, as well as the mean value of the actuating forces in surge and sway.

TABLE 7.3: Statistical observations of thrust forces during stationkeeping.

Measure	Unit	PID	MRAC	MRAHFC
$Var(F_{Tx})$	[N]	25.2956	39.9014	32.1994
$Var(F_{Ty})$	[N]	4.6140	3.6000	12.9576
$\lvert\bar{F}_{Tx}\rvert$	[N]	11.4961	10.9490	11.3680
$\lvert\bar{F}_{Ty}\rvert$	[N]	1.4957	1.3704	1.9809

7.1.2 Yaw

7.1.2.1 Positioning

Figure 7.5 presents the plots showing the heading angle in each case, measured in degrees. The trend from the translational directions repeats, as it is seen that the MRAHFC tends to vary more from the reference heading than the MRAC and the PID reference controller. In the plot showing the performance of the MRAHFC, green signifies force control, while red signifies position control.

Table 7.4 shows the standard devations of the error in heading angle each of the controllers.

TABLE 7.4: Statistical observations in yaw angle during stationkeeping.

Measure	Unit	PID	MRAC	MRAHFC
σ_ψ	[deg]	0.00230	0.00220	0.00500
$\tilde{\psi}$	[deg]	6.5113×10^{-5}	6.9398×10^{-12}	7.9264×10^{-4}

From Table 7.4, presenting the mean value and standard deviation of the error in yaw, it is evident that the accuracy in in terms of positioning in yaw of the MRAHFC is inferior compared to the pure MRAC and the reference controller. However, as for positioning in surge and sway, this is to be expected, as force control activates when environmental forces gets excessive, resulting in slight drift-offs from the reference heading.

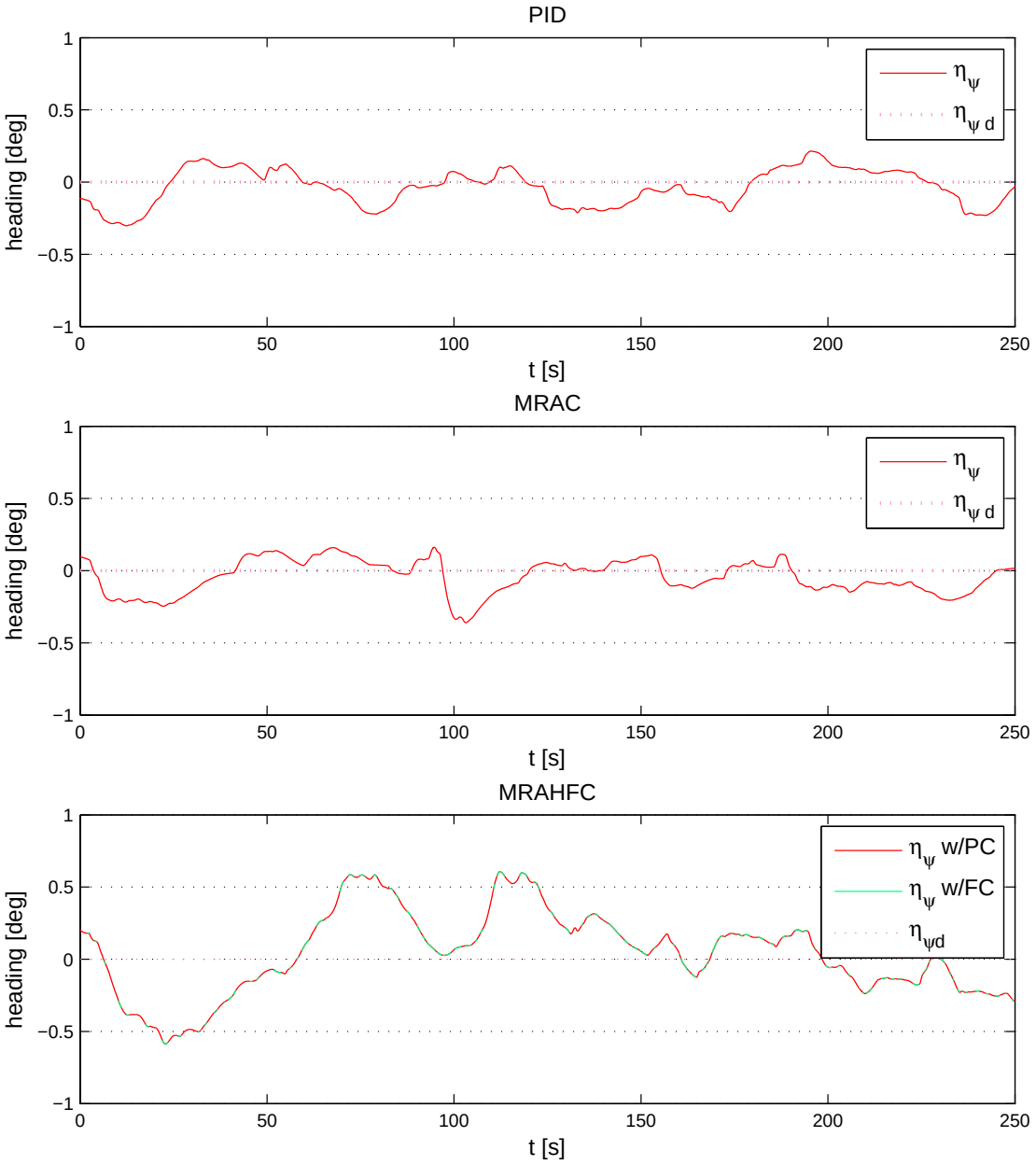

FIGURE 7.5: Positioning performance in yaw.

7.1.2.2 Observed moments

Figure 7.6 shows the measured moments applied by the environment in yaw. It is seen that for the two MRAC controllers, the moments are at a lower level than the PID reference controller. Moreover, the moments acting on the PID controlled vessel is seen to vary more in amount relative to the MRACs. It is believed that this is due to the control strategy of the feed-forward PID controller.

Table 7.5 presents the mean values of the environmental forces in yaw.

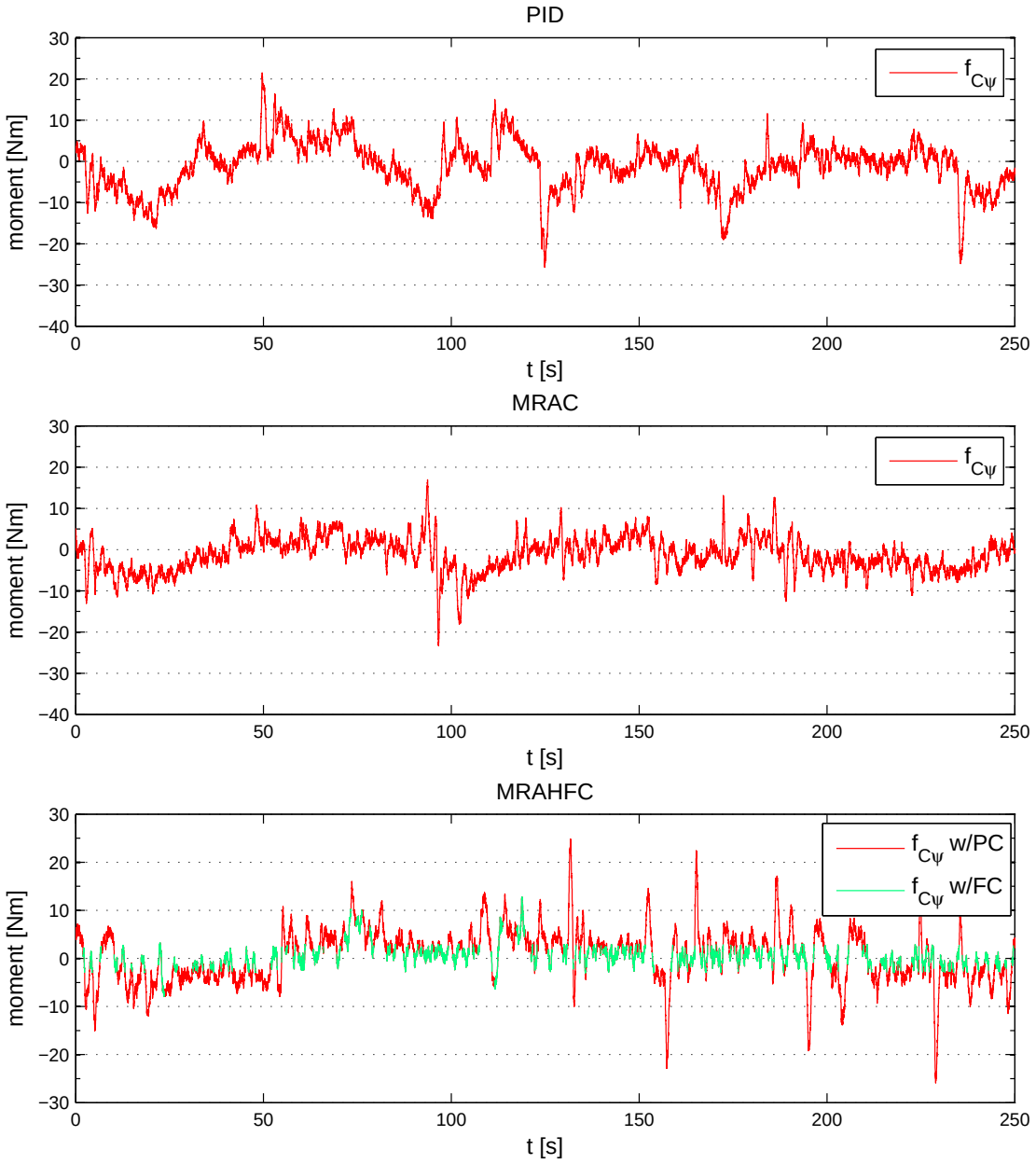

FIGURE 7.6: Perceived environment moment.

TABLE 7.5: Statistical observations of environmental moments in yaw during station-keeping.

Measure	Unit	PID	MRAC	MRAHFC
$\lvert\bar{F}_{C\psi}\rvert$	[Nm]	4.5636	3.3889	3.8357

Figure 7.7 shows the thruster actuated moment in yaw. The pure MRAC is seen to be represented by a smoother moment profile, relative to the reference PID controller, varying less with time.

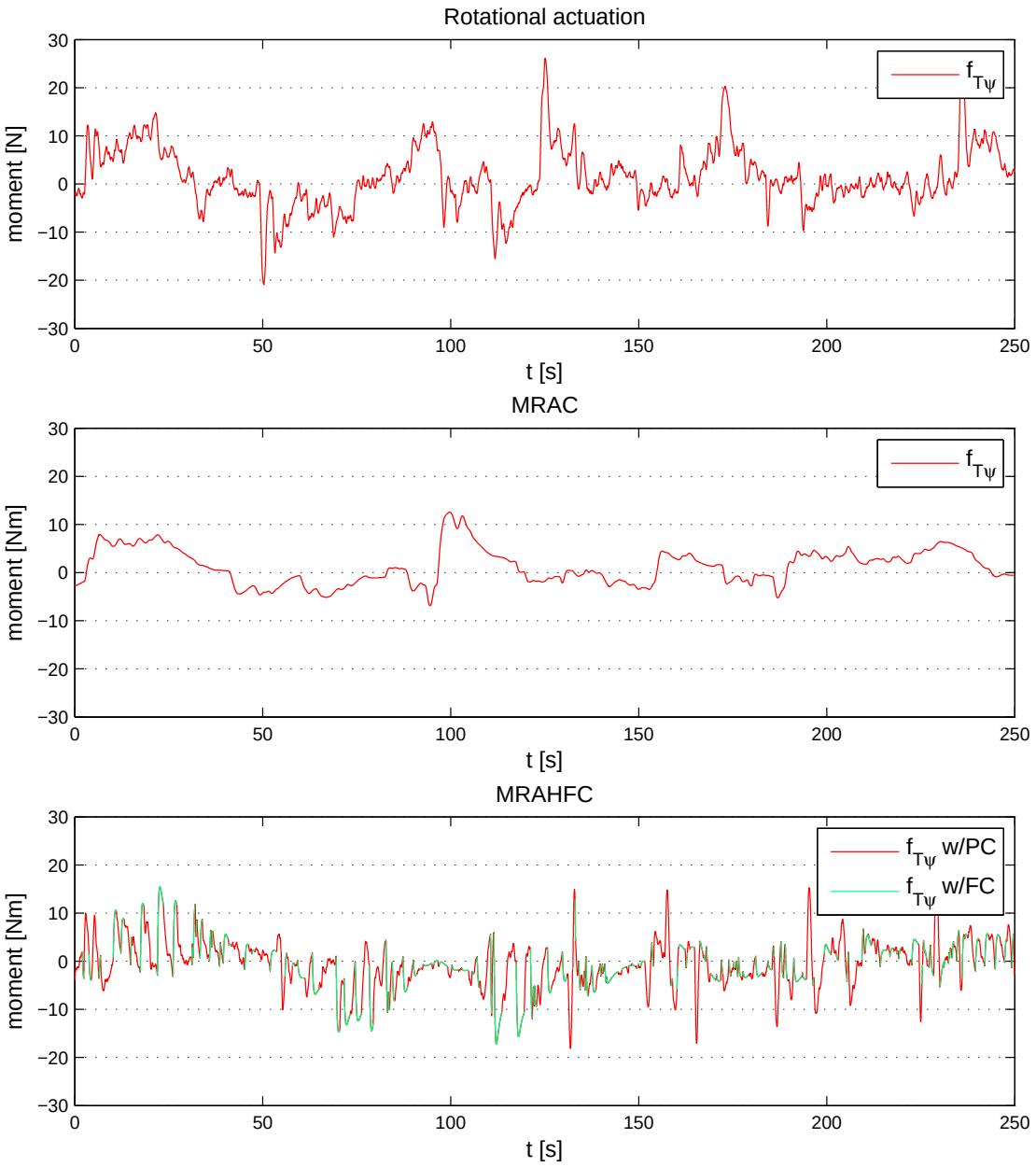

FIGURE 7.7: Actuated thruster moment.

The MRAHFC is seen to vary rather extensively both in value and time as the environmental forces frequently deactivates position control. It is of the authors belief, that the variations in yaw moment in the case of MRAHFC, is due to the small drift-offs causing the controller to repeatedly regain the heading. This, in turn, causes the vessel to track a longer trajectory through the surrounding fluid in this case, as well as exerting seemingly oscillating values in thrust moment.

Table 7.6 presents the variance, as well as the mean value of the actuating moments in yaw.

TABLE 7.6: Statistical observations of thrust induced moments in yaw during stationkeeping.

Measure	Unit	PID	MRAC	MRAHFC
$Var(F_{T\psi})$	[Nm]	37.5822	13.8771	26.1775
$\lvert\bar{F}_{T\psi}\rvert$	[Nm]	4.5085	3.1847	3.8405

7.1.3 Cumulative force measurements

The cumulative values of the measured environmental forces, shown in Figure 7.8, is chosen as a measure of the performance with regards to wear and tear on mechanical equipment, as it is approximately proportional to the total energy dissipated on the vessel by the environment. As seen in the plot, the MRAC is influenced by less environmental forces in total. Similar tendencies is observed for each individual DOF. The MRAHFC is influenced more than the MRAC, while the PID controlled vessel is seen to be significantly more influenced by the environment than both the proposed control schemes.

The total cumulative applied thrust force, shown in Figure 7.9, is chosen as a measure of the total energy consumed by the vessel thrusters, as the force applied is approximately proportional to the energy consumed by the vessel engines. The heavy influence the environment has on the PID controlled vessel, results in a significantly higher applied cumulative thrust force relative to the MRAC in this case, as seen in Figure 7.9. Relative to the total amount of environmental influence, the MRAHFC is seen to apply more thrust force in total, than both the MRAC and the reference controller. The pure MRAC is seen to perform superior to the other two in terms of total applied force as well as cumulative thrust force in all DOFs.

Table 7.7 presents the cumulative environmental forces observed at the end of the stationkeeping scenario.

TABLE 7.7: Cumulative environmental forces and moments during stationkeeping.

Direction	Unit	PID	MRAC	MRAHFC
Surge	[N]	2.8724×10^5	2.7302×10^5	2.8360×10^5
Sway	[N]	3.2524×10^4	3.0138×10^4	3.2796×10^4
Yaw	[Nm]	1.1409×10^5	8.4725×10^4	9.5896×10^4
Total	[N, Nm]	4.3385×10^5	3.9041×10^5	4.1229×10^5

Table 7.8 presents the cumulative thrust forces applied at the end of the stationkeeping scenario.

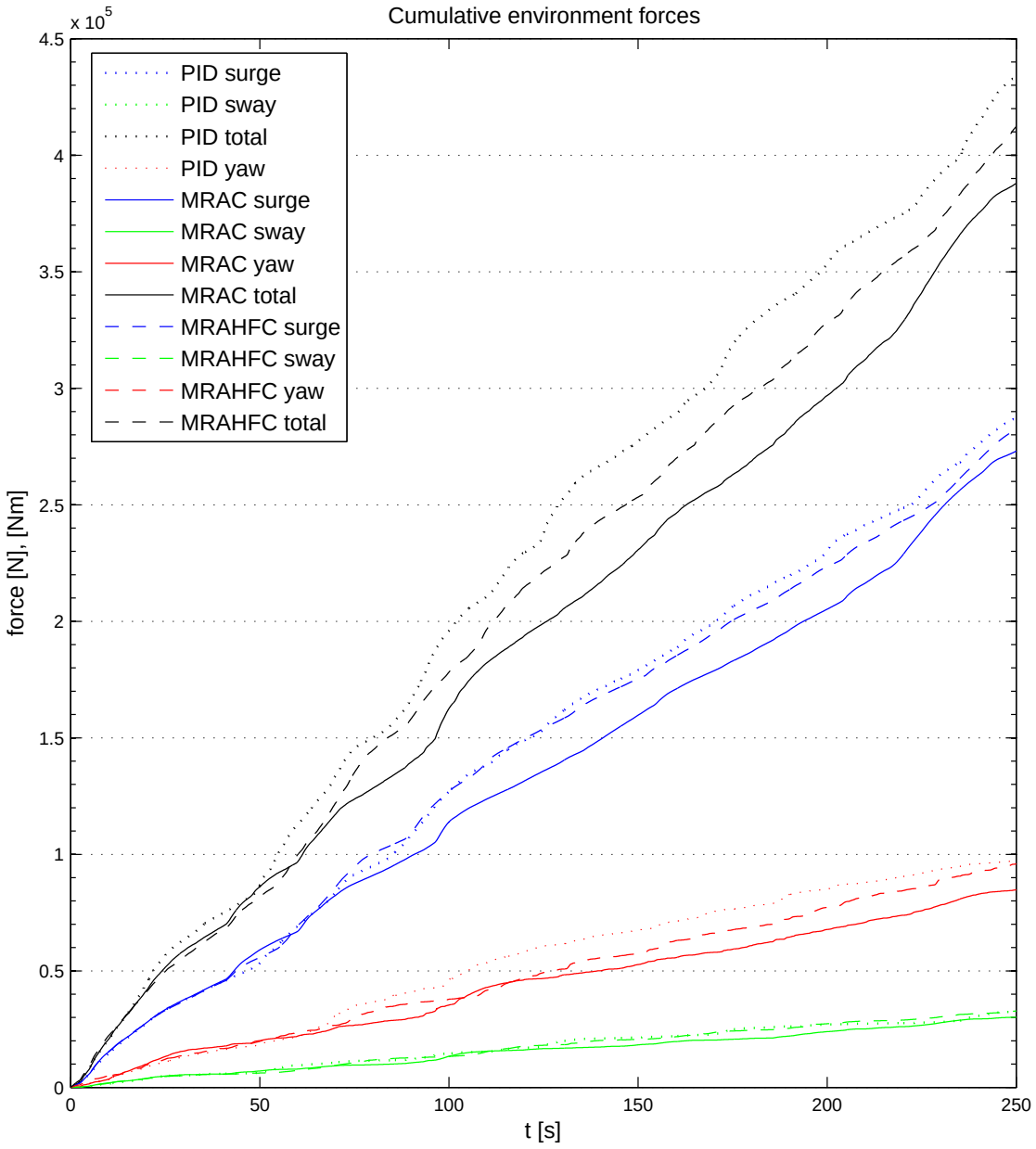

FIGURE 7.8: Cumulative forces and moments acted by the environment during station-keeping.

TABLE 7.8: Cumulative thrust forces and moments during stationkeeping.

Direction	Unit	PID	MRAC	MRAHFC
Surge	[N]	2.8741×10^5	2.7374×10^5	2.8421×10^5
Sway	[N]	3.7393×10^4	3.4262×10^4	4.9523×10^4
Yaw	[Nm]	1.1272×10^5	7.9622×10^4	9.6015×10^4
Total	[N, Nm]	4.3752×10^5	3.8762×10^5	4.2546×10^5

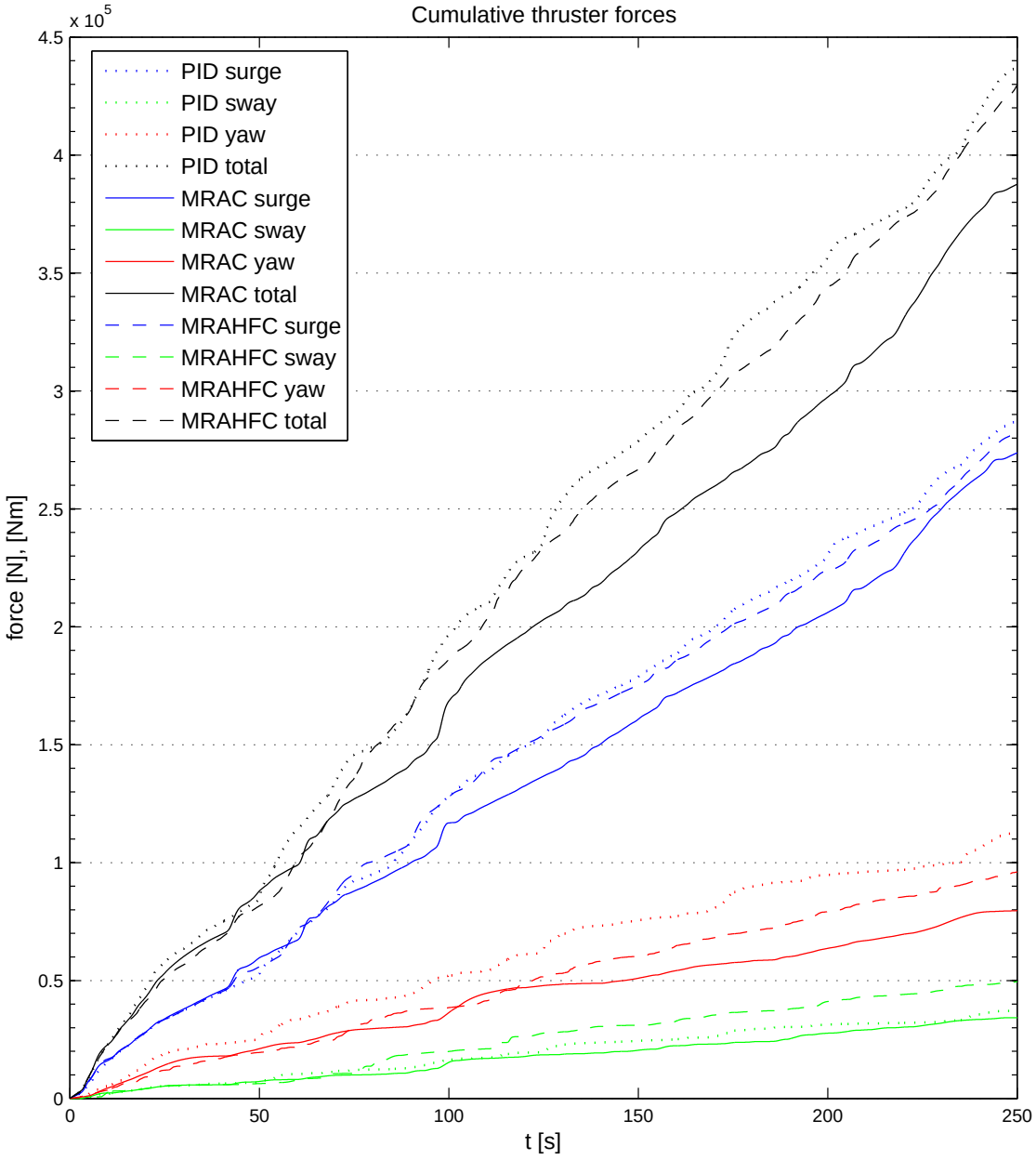

FIGURE 7.9: Cumulative applied thrust forces and moments during stationkeeping.

7.2 Waypoint tracking

7.2.1 Surge and sway

7.2.1.1 Positioning

Figure 7.10 shows the positioning performance of the controllers in the case of waypoint tracking through the managed ice channel.

TABLE 7.9: Sum of square error in surge and sway position in the case of waypoint tracking.

	PID	MRAC	MRAHFC
$\sigma_{\alpha ss}$ [m]	57.9185	72.4902	84.8742

Table 7.9 shows the SSE in position in the case of waypoint tracking. It is seen that the PID controller performs better than the MRACs in terms of a small SSE.

From the plot it is seen that the PID controlled vessel converges faster to the desired position than the MRACs, resulting in a smaller SSE over time. This might be due to the choices of the parameters ζ and ω_0 for the MRAC reference model, causing the MRAC to converge to the desired position at a slower rate. The parameter choices are seen to result in a fast initial convergence rate which decreases as the vessel is approaching the desired position. The overall convergence rate is thus seen to be lower relative to the PID controlled vessel. However, the vessel controlled by the pure MRAC scheme is seen to follow the reference trajectory well, converging fairly fast to the desired position. To what extent the choices of ζ and ω_0 influences the results, is discussed further in Section 7.2.1.2, as well as in Chapter 9.

The MRAHFC is observed to drift away from the reference position in sway when the vessel is situated within the position tolerance limit of ± 0.5 [m]. This occurs as a result of force control, whenever excessive environmental forces is experienced within these constraints. The drift-offs in sway is seen to influence the surge motion as well, as deviations in sway will affect the motion in yaw, resulting in a slight momentarily lag in surge. This is further discussed in Section 7.2.2.

Figure 7.11 shows a trace plot of the vessel in the case of waypoint tracking. It can be seen from the plot, that the two MRAC controlled vessels deviates more from the straight lines between the waypoints than the PID controlled vessel. This is due to the slower convergence rate of the MRAC schemes in general, as well as the drift-offs during force control for the MRAHFC. This confirms the observations made from Figure 7.10 and from Table 7.9.

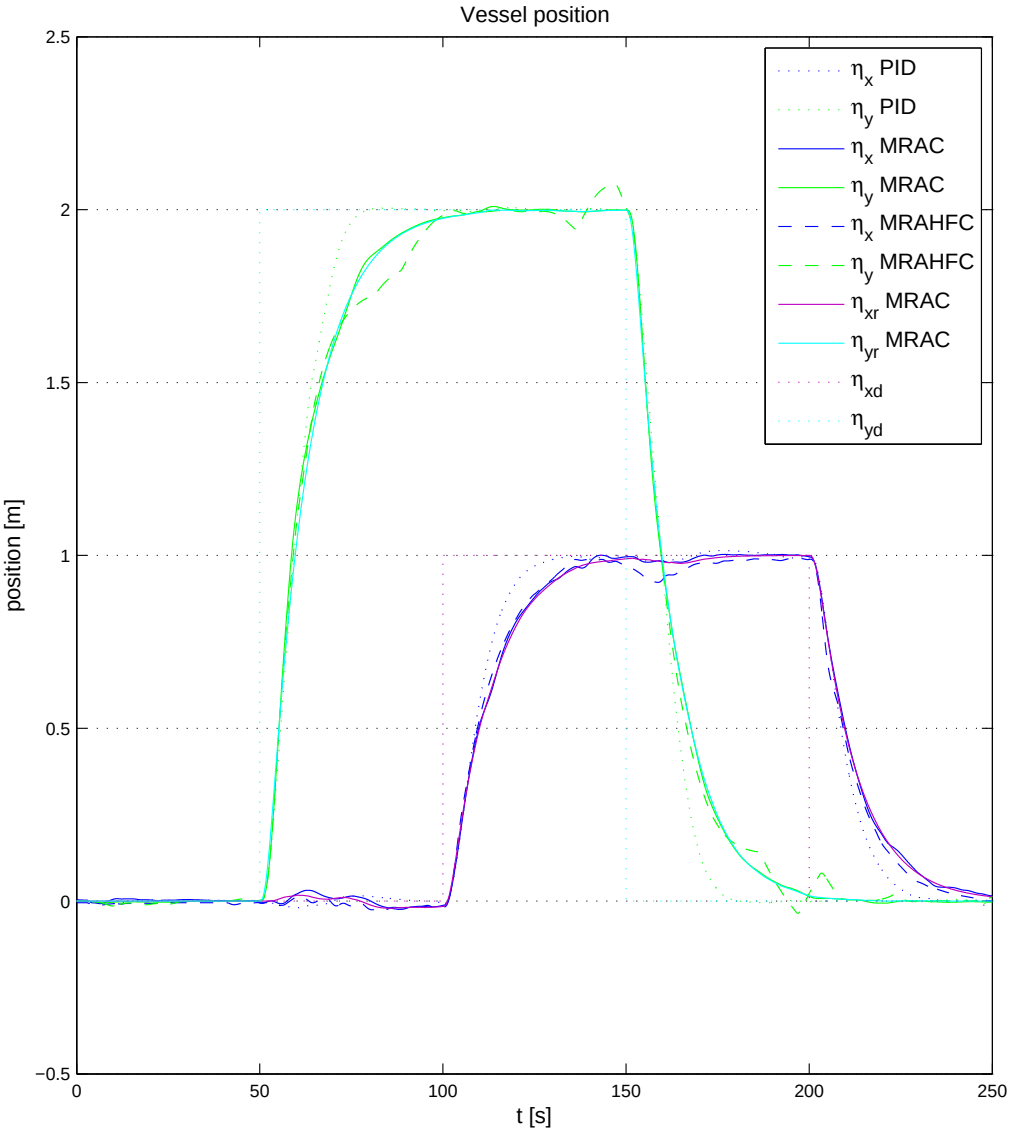

FIGURE 7.10: Positioning performance in surge and sway, waypoint tracking

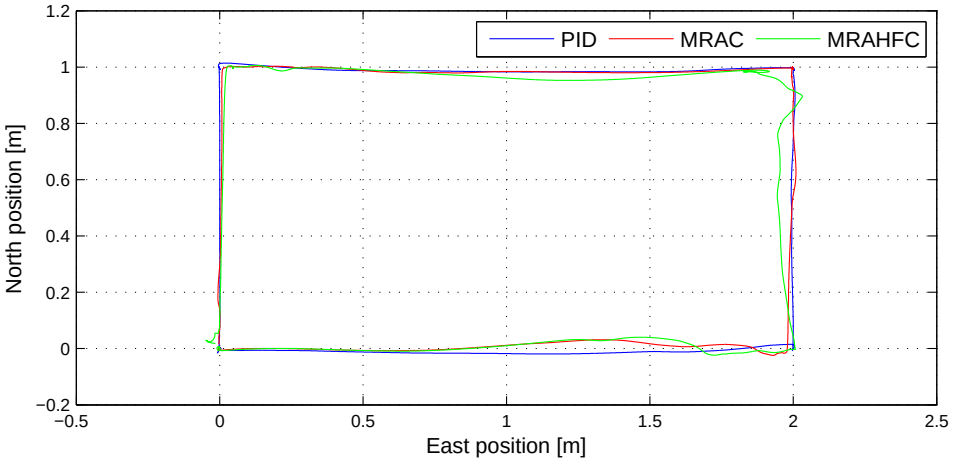

FIGURE 7.11: Trace plot, waypoint tracking

7.2.1.2 Observed forces

Figure 7.12 shows the observed environmental forces acting on the vessel in surge and sway during the waypoint tracking case. For all controllers, an increase in environmental force in sway is seen to occur at approximately $t = 55$ and $t = 160$ [s]. Similarly, alltough to a smaller extent this is also observed in surge at approximately $t = 105$ and $t = 205$ [s]. These increases in environmental force arises from the vessel motion, as a result of the change in desired position.

Table 7.10 shows the mean value of the environmental forces in surge and sway during stationkeeping.

TABLE 7.10: Statistical observations of environmental forces during stationkeeping.

Measure	Unit	PID	MRAC	MRAHFC
$\lvert\bar{F}_{Cx}\rvert$	[N]	14.3064	15.7159	14.3170
$\lvert\bar{F}_{Cy}\rvert$	[N]	10.8589	7.7029	8.9744

The PID controlled vessel is seen to experience more environmental influence relative to the MRAC schemes. In particular, the pure MRAC shows a considerably low environmental influence from a similar change of position, as opposed to the PID controlled vessel. It could be argued that this observation arises from the fact that the PID has a faster overall convergence rate. However, the time constant of the two schemes are similar, meaning the initial thrust force are the same for the two cases. This is observed in Figure 7.13 as well, showing the thrust forces applied in surge and sway. The fact that the convergence rate of the MRAC is decreasing as the vessel is approaching the desired position, is seen to lower the environmental forces at a faster rate, compared to the PID. This results in less environmental influence and less thrust force applied over time.

In the bottommost plot, green signifies that the vessel is position controlled, while brown signifies force control. It can be observed that the vessel is force controlled in the occurence of excessive environment forces, until these are lowered to a sufficiently low level. Nonetheless, the vessel does not experience any noteworthy reduction in environmental force relative to the pure MRAC.

From Figure 7.13 the same tendencies as in the stationkeeping scenario can be observed. The MRAC schemes applies thrust force in shorter periods of time than the PID controller. This results in an overall lower level of thrust force for the MRAC schemes.

Table 7.3 presents the variance, as well as the mean value of the actuating forces in surge and sway during waypoint tracking.

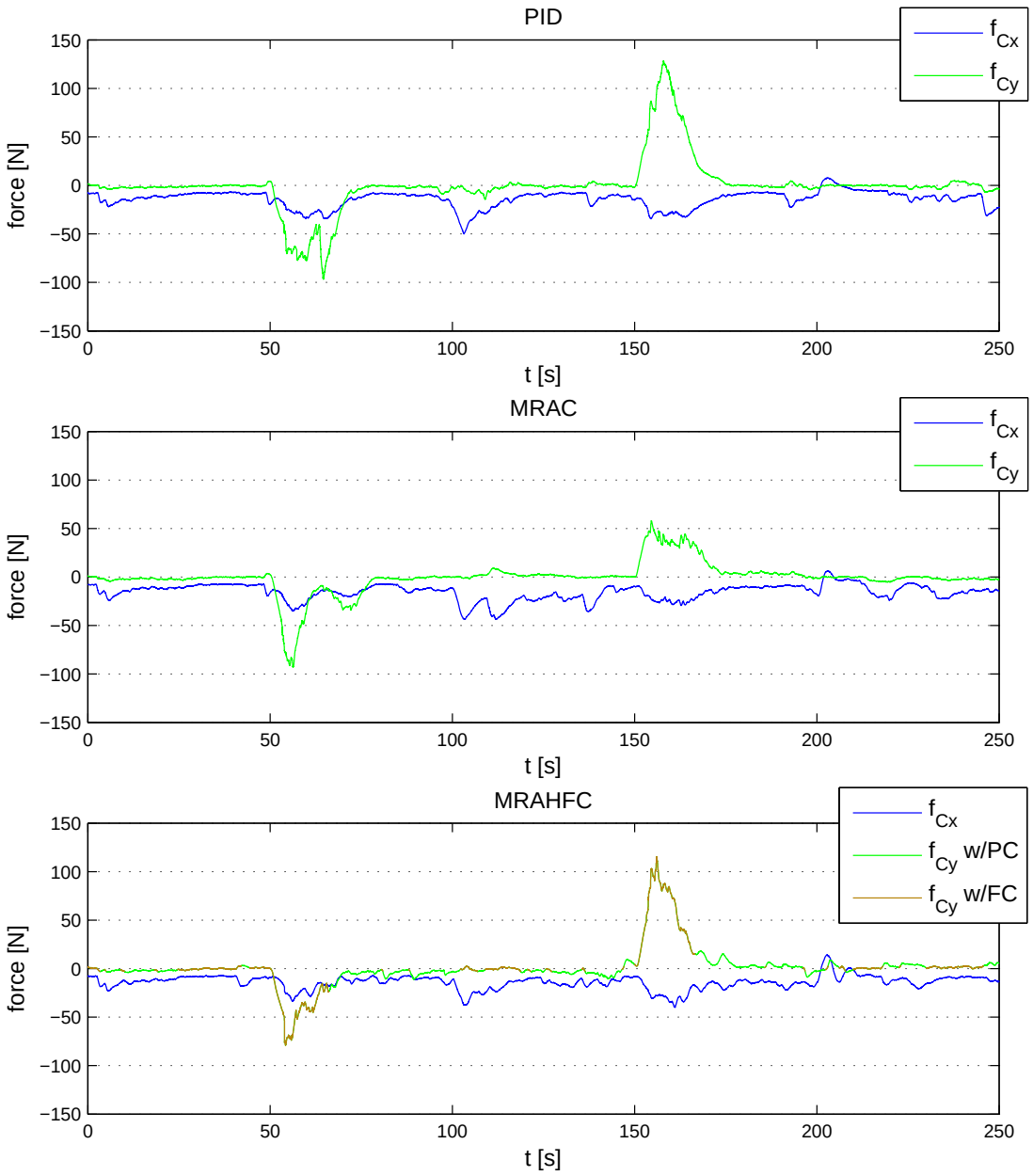

FIGURE 7.12: Environment forces, waypoint tracking.

TABLE 7.11: Statistical observations of thrust forces during waypoint tracking.

Measure	Unit	PID	MRAC	MRAHFC
$Var(F_{Tx})$	[N]	254.0878	250.6444	461.3053
$Var(F_{Ty})$	[N]	1056.6000	898.3447	1087.0000
$\lvert\bar{F}_{Tx}\rvert$	[N]	16.0594	17.2564	18.0474
$\lvert\bar{F}_{Ty}\rvert$	[N]	12.5499	9.7752	11.9414

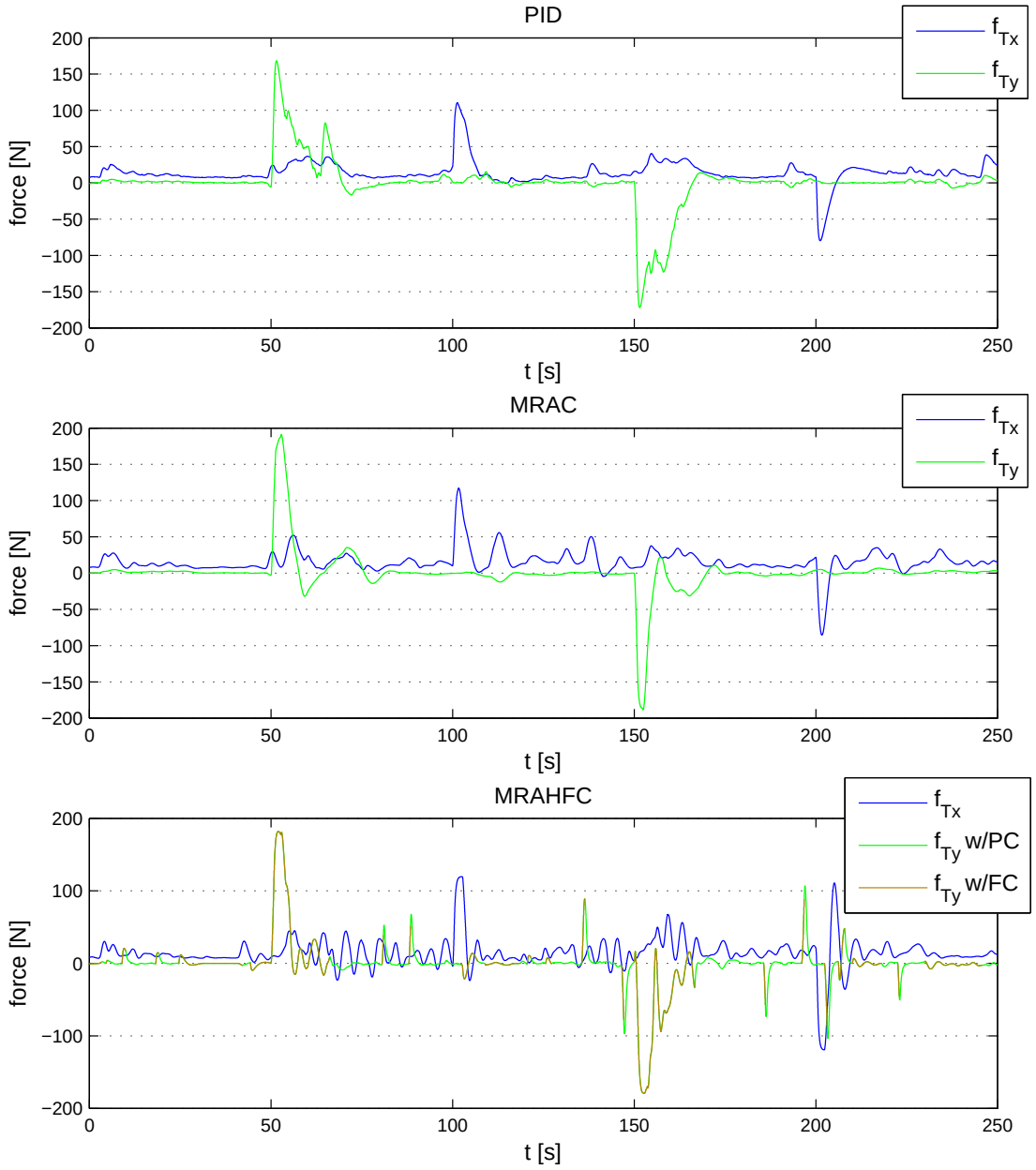

FIGURE 7.13: Actuated thruster forces, waypoint tracking.

7.2.2 Yaw

7.2.2.1 Positioning

Figure 7.14 shows the heading angle in the case of waypoint tracking. From the plots it is observed that the performance of the PID controller proves superior relative to the MRAC schemes in terms of keeping a constant yaw angle at 0 [deg]. The decrepancies for the MRAHFC can be explained by the force control, which allows the vessel to drift away from the heading reference by a small amount in the case of excessive environmental forces. This is not the case for the pure MRAC, however. The pure MRAC shows a rather poor performance relative to the PID controller in keeping a constant heading.

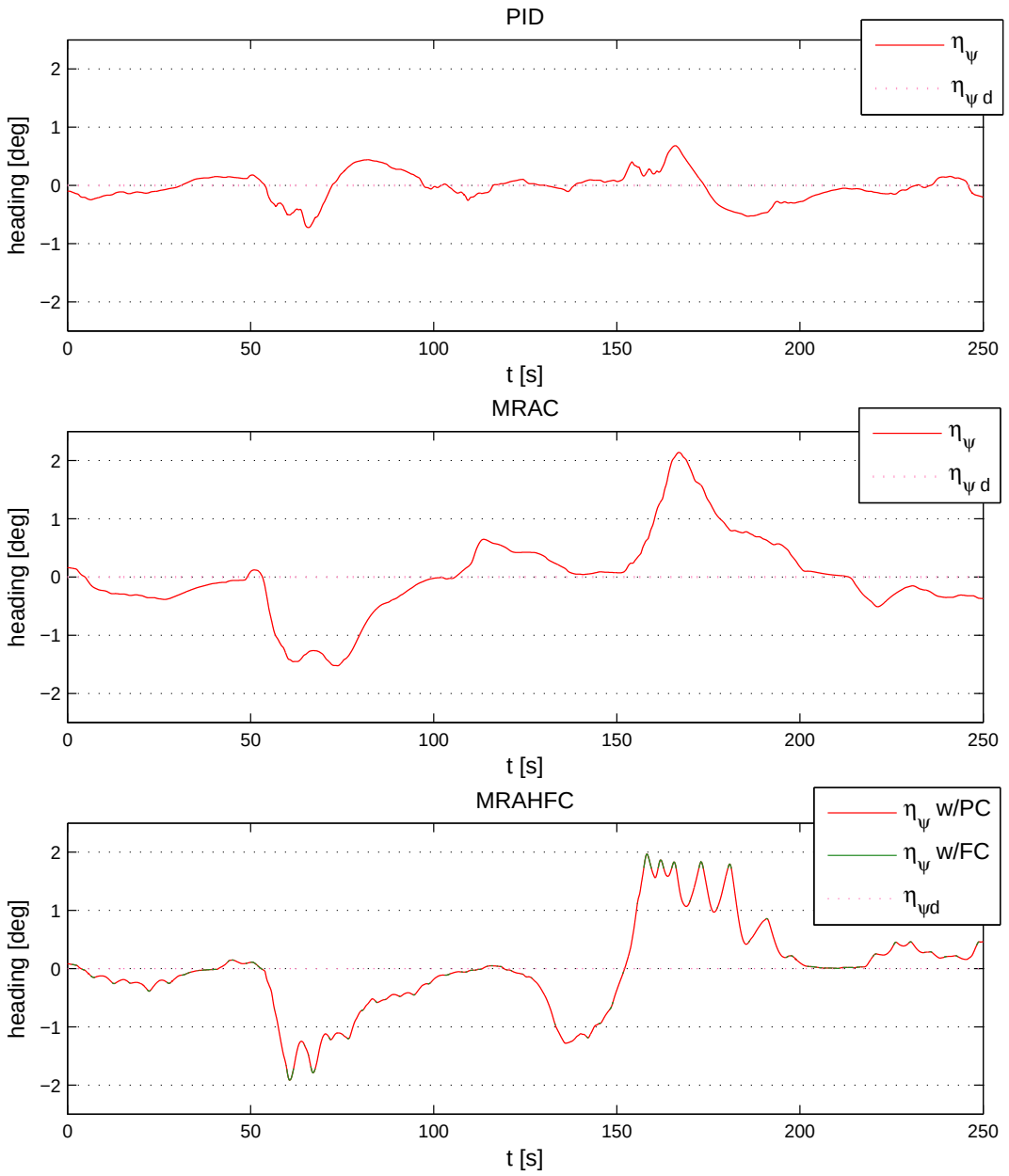

FIGURE 7.14: Positioning performance in yaw, waypoint tracking

Table 7.12 shows the standard deviations, as well as the mean value of the heading angle for each controller during waypoint tracking.

TABLE 7.12: Statistical observations in yaw angle during stationkeeping.

Measure	Unit	PID	MRAC	MRAHFC
σ_ψ	[deg]	0.0043	0.0120	0.0119
$\bar{\psi}$	[deg]	-5.2×10^{-5}	-1.9×10^{-5}	-3.5×10^{-4}

The drift-offs in yaw for the MRAC controlled vessels is seen to occur as the vessel experiences an acceleration in sway, due to a change in desired position. This can be explained by the environmental added mass matrix presented in Section 2.2.3. The added mass matrix includes cross terms in yaw due to motion in sway. Thus, motion in sway induces moments about the yaw axis. Furthermore, due to the simplifying (and crude) assumption of completely decoupled environmental forces, such effects are not modeled in the MRAC scheme. Thus, sway induced moments in yaw might explain the drift-offs in heading observed for the MRAC controlled vessels.

7.2.2.2 Observed moments

Figure 7.15 shows the environmental moment acting on the vessel for the waypoint tracking case. The PID controlled vessel is seen to experience more environmental influence in yaw relative to the MRAC schemes. Nevertheless, as discussed in the previous section, the PID controller proves superior in terms of keeping the heading at a constant angle.

Table 7.13 presents the mean values of the environmental forces in yaw.

TABLE 7.13: Statistical observations of environmental moments in yaw during waypoint tracking.

Measure	Unit	PID	MRAC	MRAHFC
$\lvert\bar{F}_{C\psi}\rvert$	[Nm]	11.2162	9.2911	12.1370

Figure 7.16 shows the applied thrust forces in yaw. The pure MRAC is recognized by a noticeable smooth thrust profile, relative to the other schemes. The reference PID is seen to mimic the environmental forces, leaving a thrust profile reflecting the environmental influence observed for the PID controlled vessel in Figure 7.15. As was the case for the thrust forces in surge and sway, this is due to the feed-forward term in the PID control law (6.2). The MRAHFC can be recognized by a more fragmented thrust profile disrupted by occasional smooth curve segments at approximately $t = 60$ and $t = 130$ [s].

The reason for the fragmented thrust curve segments of the MRAHFC vessel might be the frequent alternation between force- and position control. As the environmental forces vary rapidly between the upper and lower force thresholds, a moderate shattering effect occurs. The shattering might be avoided by increasing the force interval between the upper and lower force threshold. As the environmental forces exceeds the upper force threshold due to motion in sway, force control is activated for a longer period of time, resulting in the dispersed smooth curve segments.

Table 7.14 presents the variance, as well as the mean value of the actuating moments in yaw during waypoint tracking.

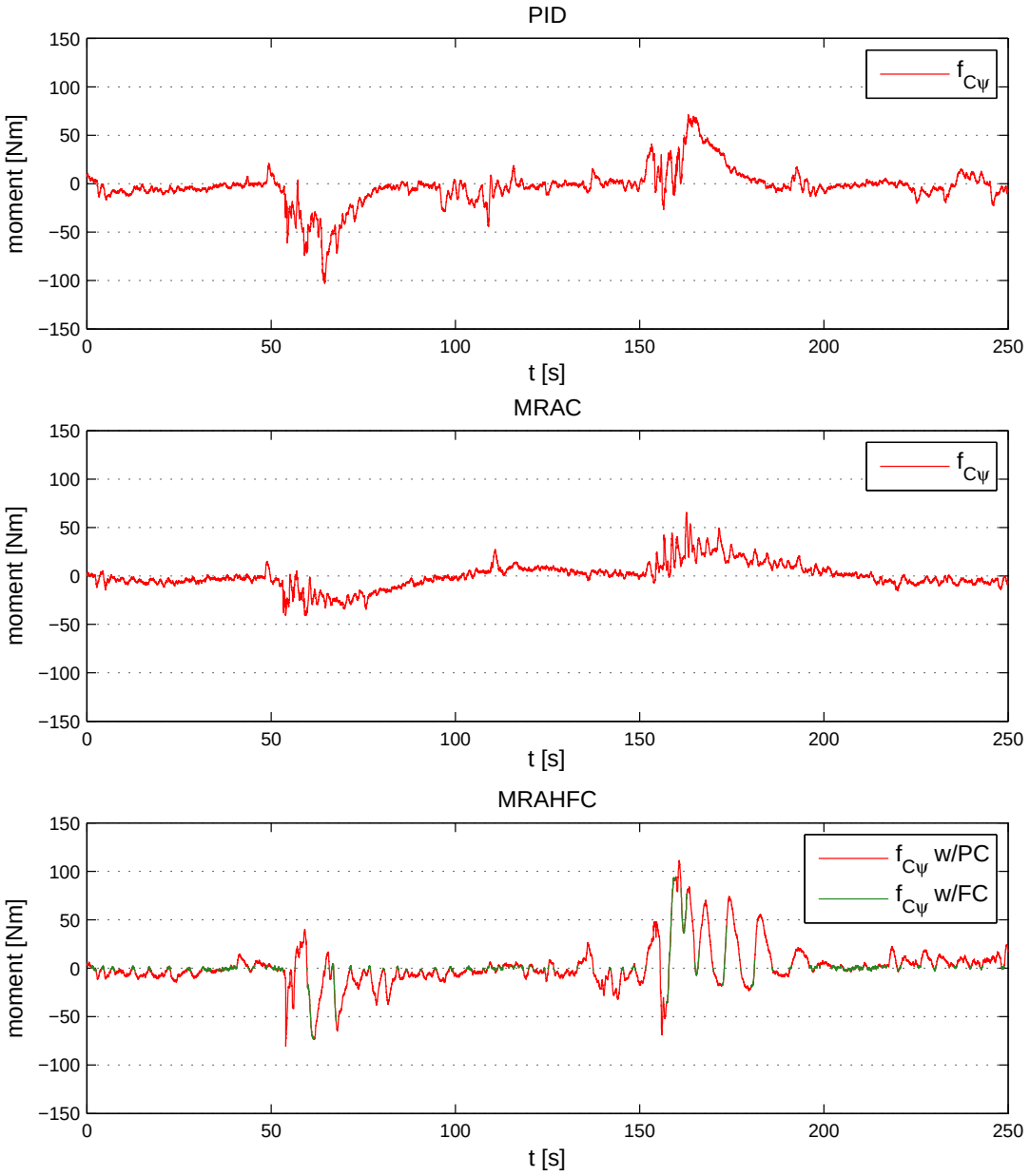

FIGURE 7.15: Perceived environment moment, waypoint tracking.

TABLE 7.14: Statistical observations of thrust induced moments in yaw during station-keeping.

Measure	Unit	PID	MRAC	MRAHFC
$Var(F_{T\psi})$	[Nm]	376.4092	168.0529	876.0512
$\lvert\bar{F}_{T\psi}\rvert$	[Nm]	11.3306	9.0590	15.1788

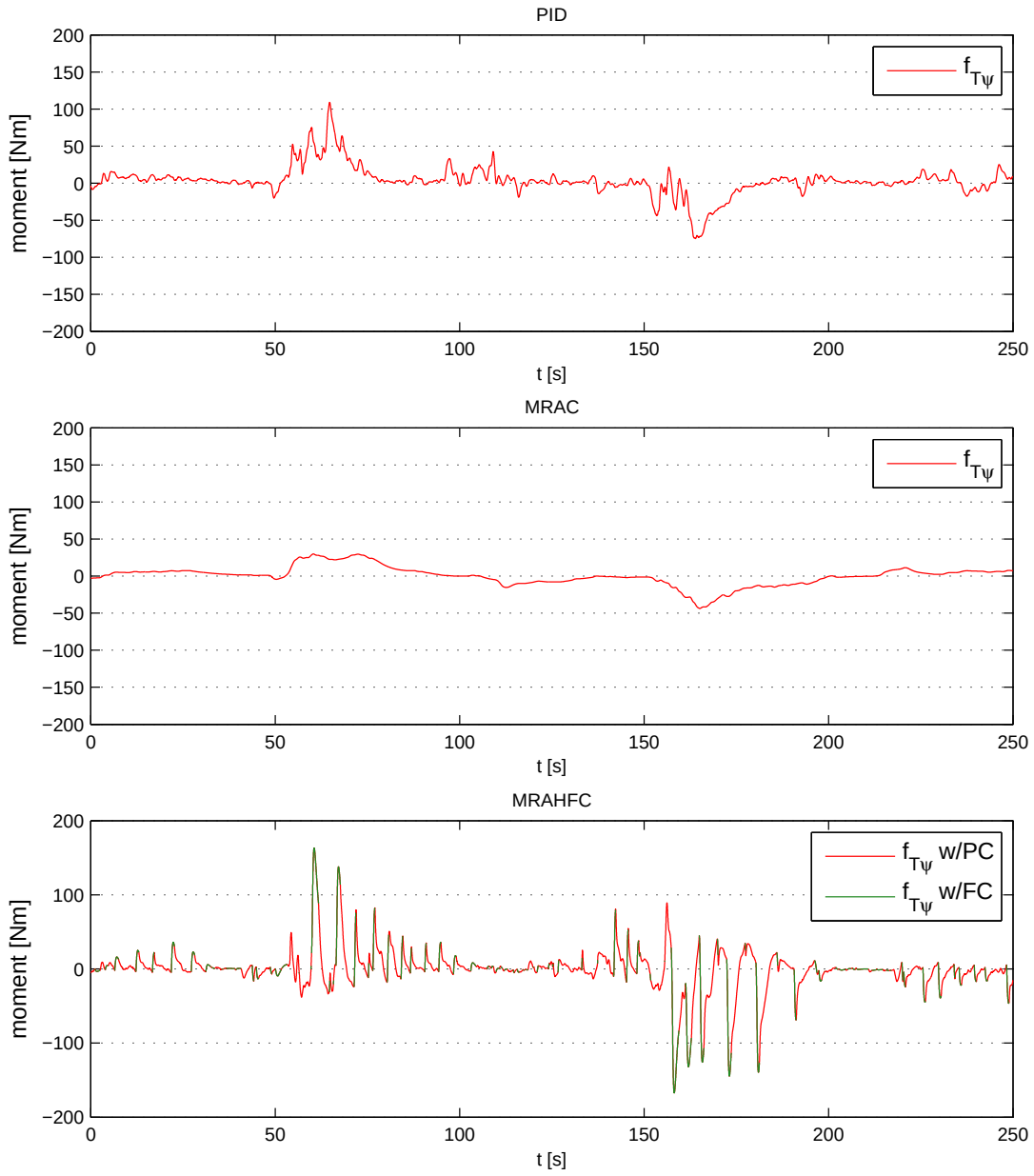

FIGURE 7.16: Actuated thruster moment, waypoint tracking.

7.2.3 Cumulative force measurements

Figure 7.17 presents a plot showing the cumulative environmental forces for the case of waypoint tracking. The two MRAC schemes are seen to result in less total environmental force acting on the vessel relative to the PID controller. Furthermore, the pure MRAC is seen to be superior to the other two controllers in terms of small environmental influence in sway and yaw. However, the curves for the PID controller and MRAHFC shows less environmental influence in surge for these two relative to the MRAC.

Table 7.15 presents the cumulative forces observed at the end of the waypoint tracking scenario.

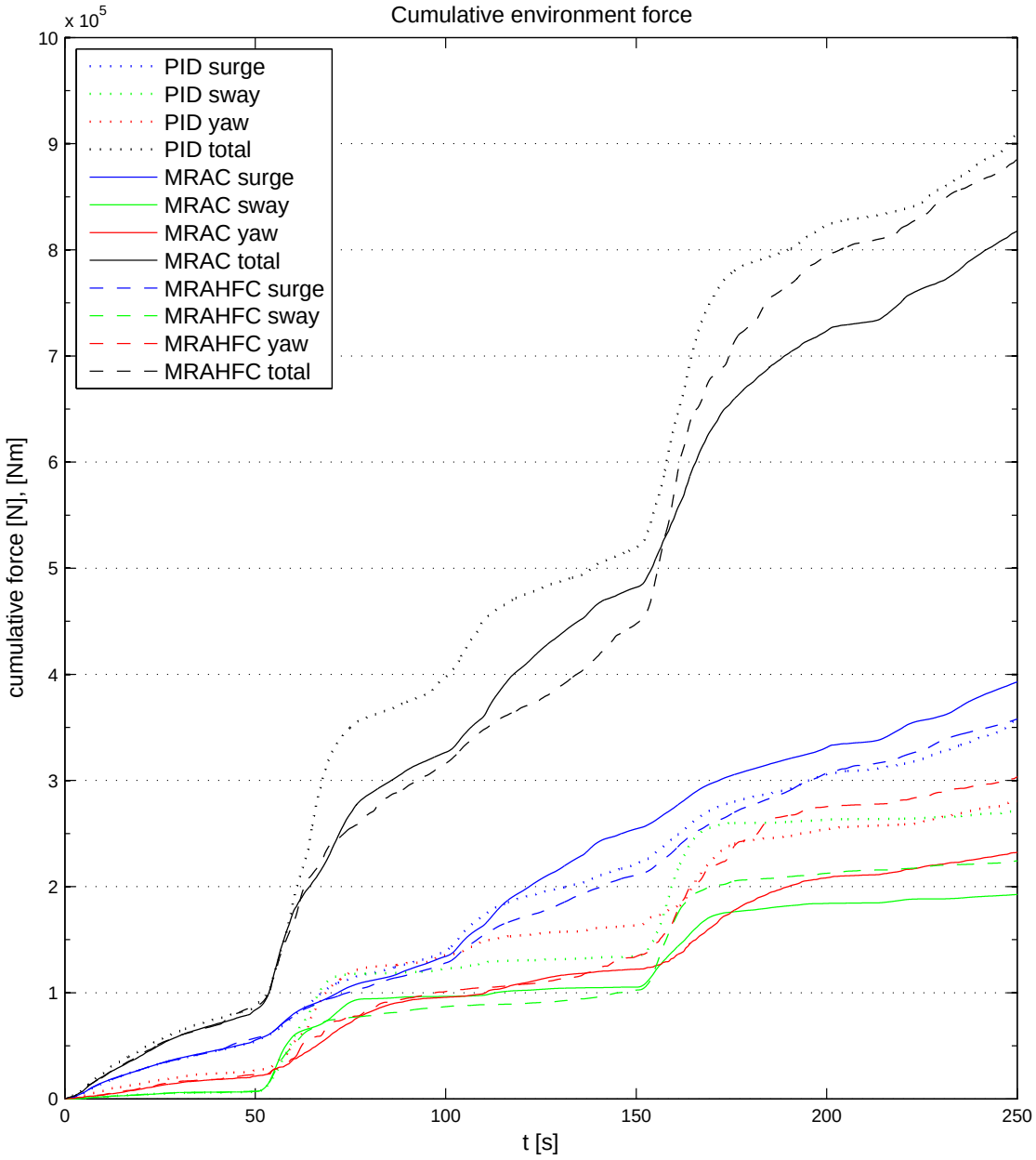

FIGURE 7.17: Cumulative perceived forces and moments applied by the environment.

The results for cumulative environmental influence is seen to reflect the observed cumulative applied thrust forces, presented in Figure 7.18. As seen in the results for the stationkeeping case, the MRAHFC is observed to apply more thrust force per environmental force, relative to the PID controller and the pure MRAC. Even though the MRAC is seen to apply more thrust force in surge relative to the PID, it proves superior compared to the PID in sway and yaw. Finally, the pure MRAC is observed to apply less thrust force in total relative to the other control schemes.

Table 7.16 presents the cumulative thrust forces observed at the end of the waypoint tracking scenario.

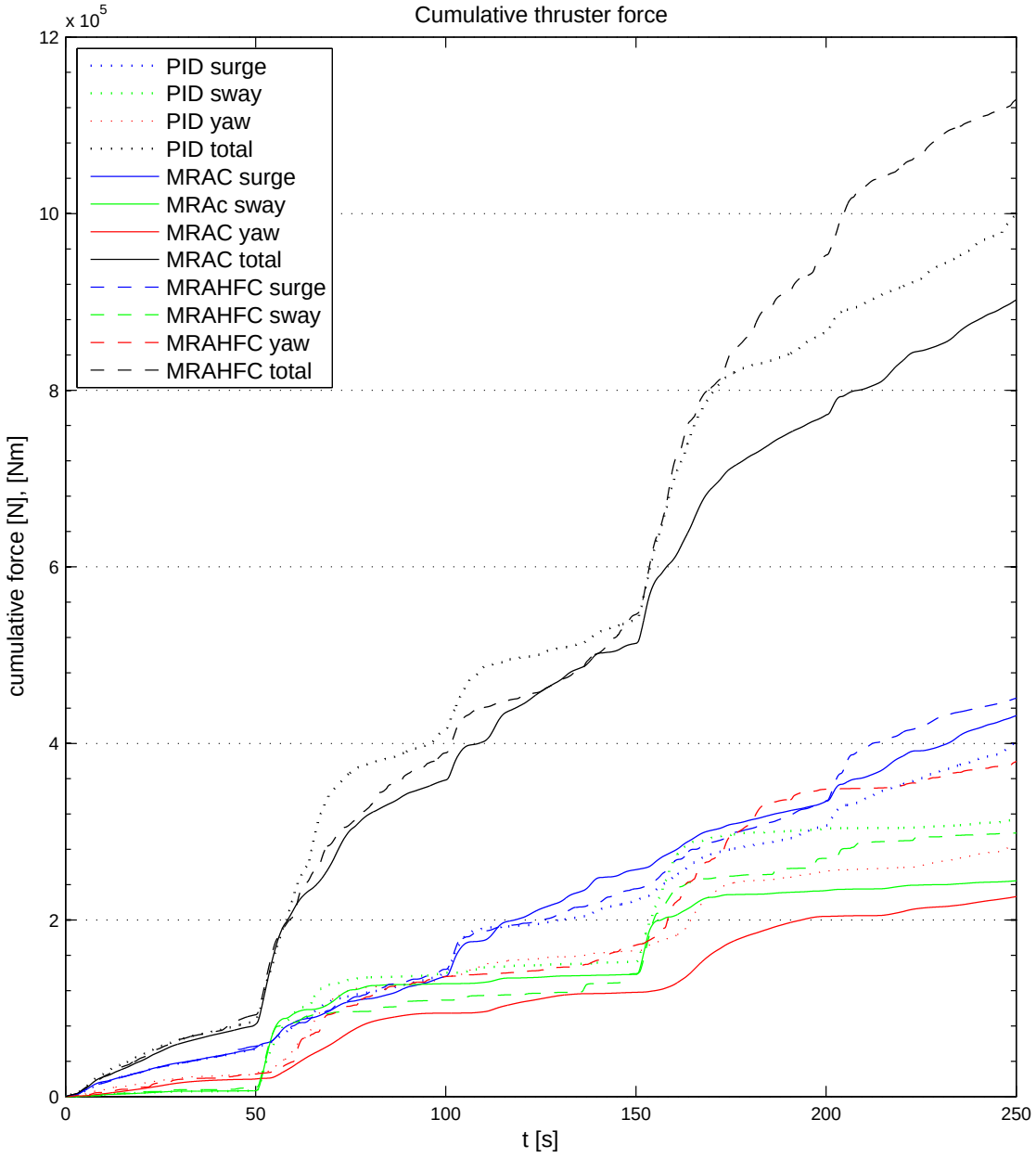

FIGURE 7.18: Cumulative applied thruster forces and moments.

TABLE 7.15: Cumulative environmental forces and moments during waypoint tracking.

Direction	Unit	PID	MRAC	MRAHFC
Surge	[N]	3.5767×10^5	3.9289×10^5	3.5794×10^5
Sway	[N]	2.7148×10^5	1.9258×10^5	2.2437×10^5
Yaw	[Nm]	2.8042×10^5	2.3229×10^5	3.0344×10^5
Total	[N, Nm]	9.0957×10^5	8.1776×10^5	8.8575×10^5

TABLE 7.16: Cumulative thrust forces and moments during stationkeeping.

Direction	Unit	PID	MRAC	MRAHFC
Surge	[N]	4.0150×10^5	4.3143×10^5	4.5120×10^5
Sway	[N]	3.1376×10^5	2.4439×10^5	2.9855×10^5
Yaw	[Nm]	2.8328×10^5	2.2648×10^5	3.7949×10^5
Total	[N, Nm]	9.9854×10^5	9.0230×10^5	11.2924×10^5

7.3 System adaption and parameter estimates

The MRAC control laws are calculated based on estimates of the system parameters. The estimates are provided by the MRAC system identification scheme, and includes estimates of vessel and environment mass, damping and moment of inertia.

The results from the parameter estimation in the waypoint tracking case are preceded by results gathered from an ideal case simulated in Simulink. In this case parameter convergence is ensured by proper excitation of input signals.

One thing to note from the results regarding the parameter estimates is that data from $t = 0$ to $t = 300$ [s] are presented in the plots. Thus, the plots starts $t = 50$ [s] ahead of the results presented for position, thrust- and environmental forces. This is done in order to capture any initial transient period in the estimates, and will besides this not affect the results.

7.3.1 Ideal case

7.3.1.1 Vessel parameters

The data from the ideal case are gathered from a Simulink model simulation of an MRAC controlled vessel that resembles the model simulated in the NIT. The estimation scheme utilized in the ideal simulation is identical to the scheme included in the MRAC tested in the NIT.

The vessel mass estimates from the ideal case is presented in Figure 7.19. Figure 7.20 shows the vessel moment of inertia.

The estimates for vessel linear damping for surge and sway is shown in Figure 7.21. Figure 7.22 shows the estimate of vessel damping in yaw.

All estimates are seen to converge to a value in close proximity to the actual values listed in Tables 6.6 and 6.7. Any discrepancies are caused by the noise contamination of the regressor signals.

7.3.1.2 Environment parameters

Figures 7.23-7.26 shows the corresponding environmental parameter estimates for the ideal Simulink simulation. The parameters are seen to converge to a value in close proximity to their actual values. As for the vessel parameters, any discrepancies is caused by noise contaminated input signals.

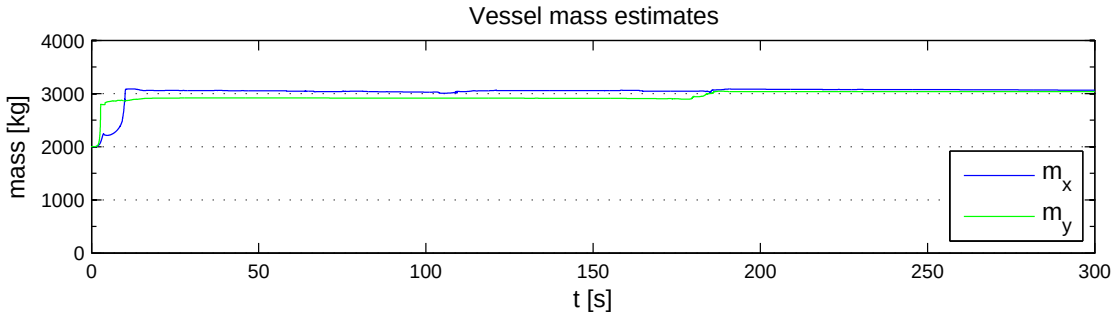

FIGURE 7.19: Vessel mass estimates, ideal case.

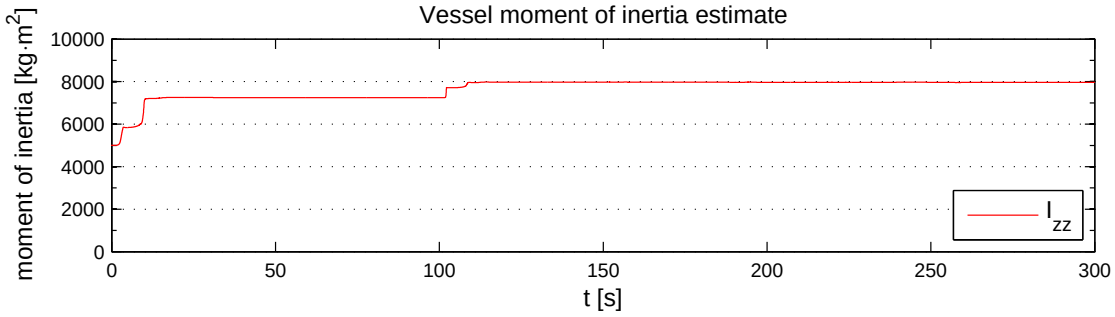

FIGURE 7.20: Vessel moment of inertia estimate, ideal case.

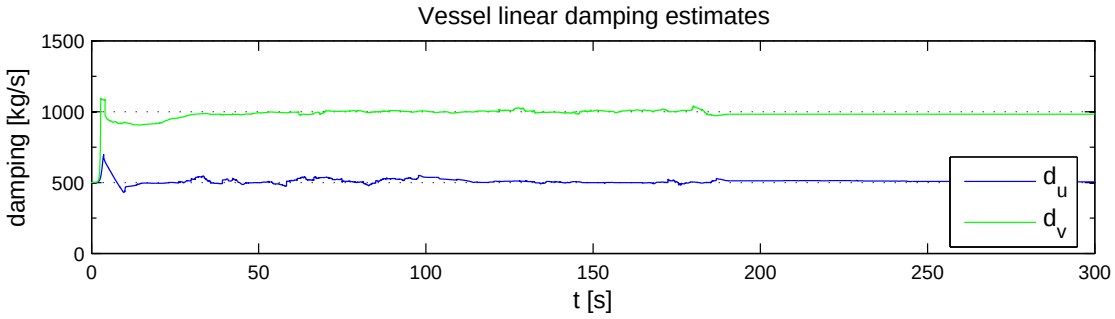

FIGURE 7.21: Vessel linear damping estimates, ideal case.

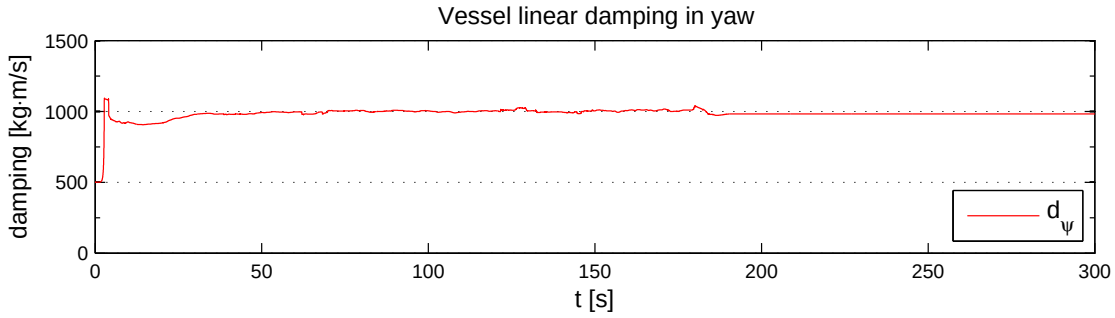

FIGURE 7.22: Vessel damping in yaw estimate, ideal case.

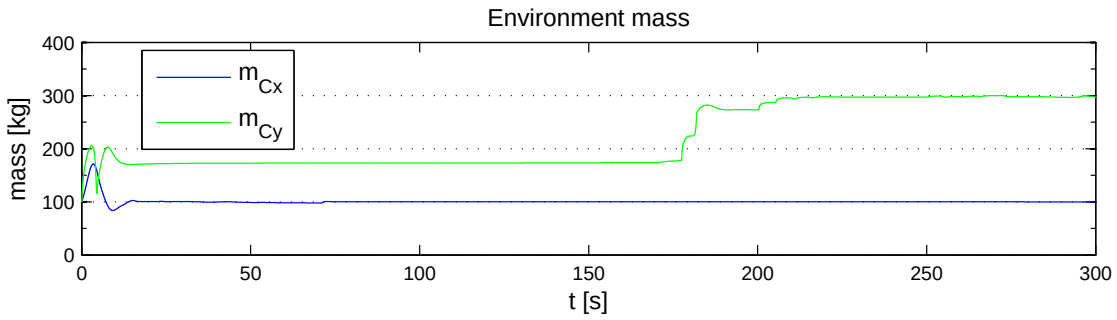

FIGURE 7.23: Environmental mass, ideal case.

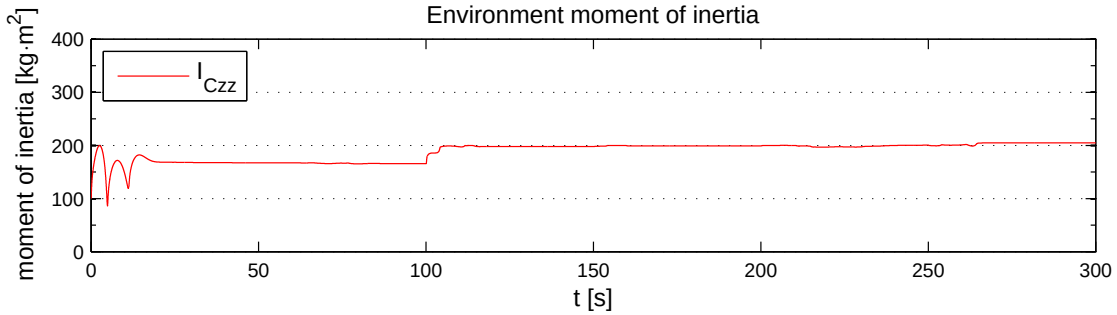

FIGURE 7.24: Environmental moment of inertia, ideal case.

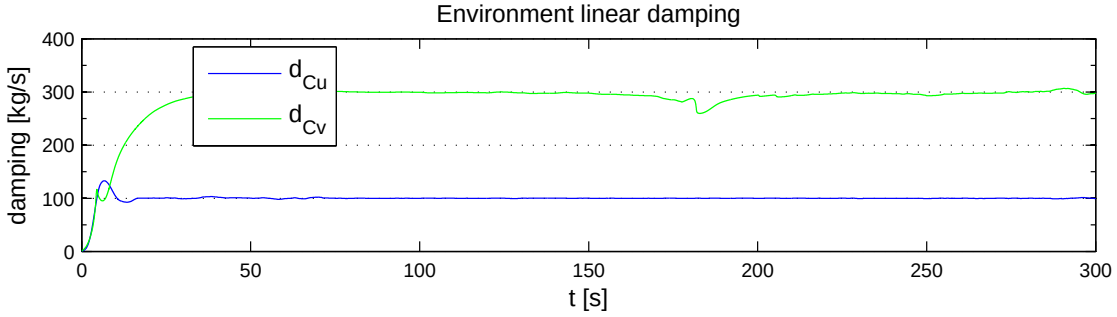

FIGURE 7.25: Environmental damping in surge and sway, ideal case.

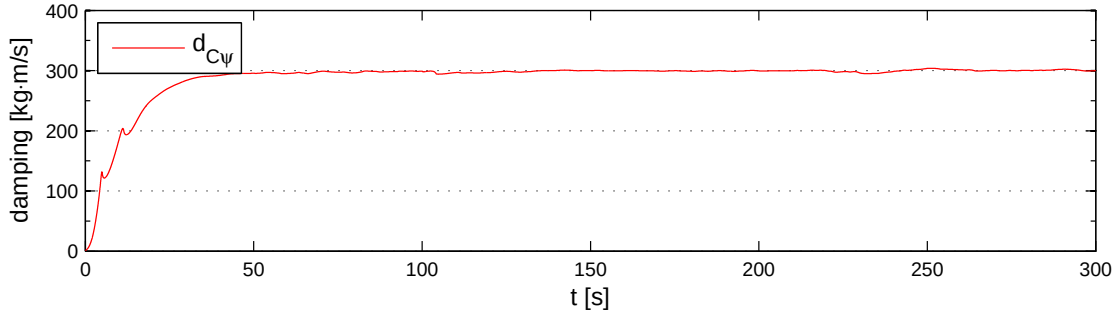

FIGURE 7.26: Environmental damping in yaw, ideal case.

7.3.2 NIT simulations

Having approved the MRAC performance in terms of parameter convergence for the ideal case, the parameter estimates for the simulations conducted in the NIT can be presented. These are the estimates applied to calculate the MRAC control law at any time t. Except from the vessel mass and moment of inertia, all parameters are unknown and possibly varying. Furthermore, the NIT simulations differ from the ideal case in that the environmental forces in sway and yaw cannot be assumed decoupled. Therefore, the parameter estimates might be deficient. This is something to keep in mind when analyzing the estimates gathered from the simulations. It is, however, expected, that the results presented gives a good view of how the forces act on the vessel, and, finally, how the total forces are broken into inertial, resistive and capacitive parts.

7.3.2.1 Vessel parameters

Table 7.17 shows the actual vessel mass and moment of inertia as it is modeled in the NIT. These are constant vessel parameters, and the estimates are expected to converge to these values.

TABLE 7.17: Actual vessel parameters

Parameter	Unit	Description	Values
m_x	[kg]	Vessel mass surge	3060
m_y	[kg]	Vessel mass sway	3060
I_{zz}	[kg $\cdot$ m^2]	Vessel moment of inertia yaw	7987.14

The estimates for vessel mass, presented i Figure 7.27, shows that convergence occurs for the mass estimate for surge and sway motion. The estimates are, however, slightly high; approximately $m = 3200$ [kg].

Figure 7.28 shows the estimated vessel moment of inertia. The estimate for this parameter is observed to converge to the actual value. However, its convergence rate is rather poor. As stated in Section 4.2.2, the property of persistent excitation is required in order for a parameter to undergo convergence to the actual value. By introducing proper excitation in yaw, the convergence properties of this parameter might be improved. However, motion in yaw might not be desirable, as this is known to induce large environmental forces in all DOF. Thus, a trade-off have to be made between achieving parameter convergence and keeping a constant yaw angle.

The vessel damping parameters (i.e. the elements of the matrix $\boldsymbol{D}$ in the DP model (5.1)) are dependent on the angle of attack of the relative current as well as the perceived environmental forces, and is therefore to be considered unknown and varying. Figure 7.29

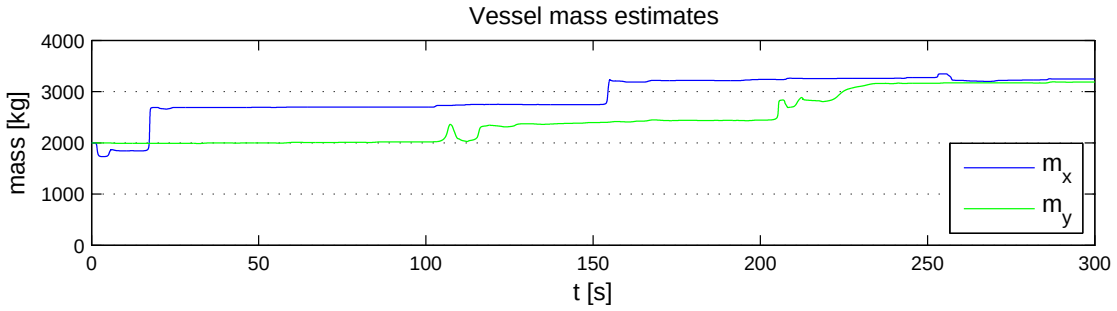

FIGURE 7.27: Vessel mass estimates, NIT simulations.

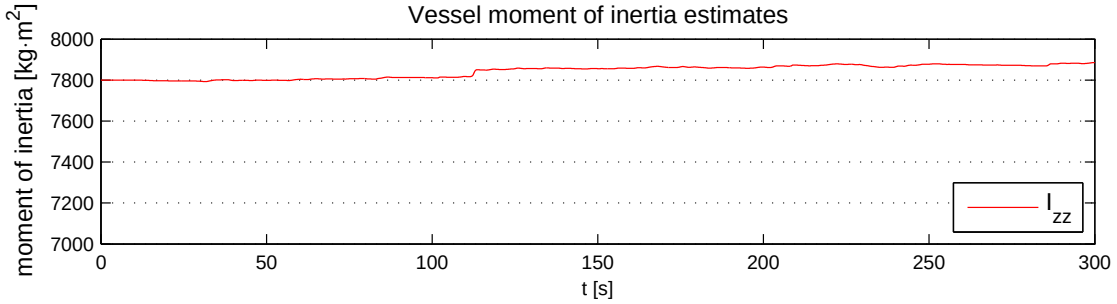

FIGURE 7.28: Vessel moment of inertia estimates, NIT simulations.

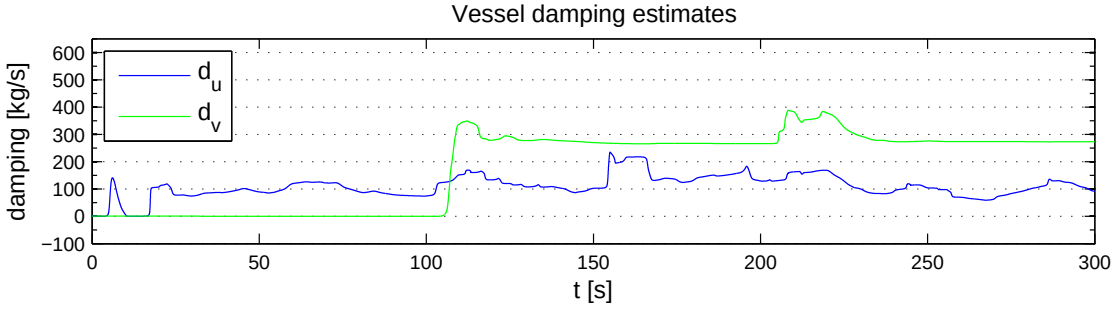

FIGURE 7.29: Vessel damping estimates for surge and sway, NIT simulations.

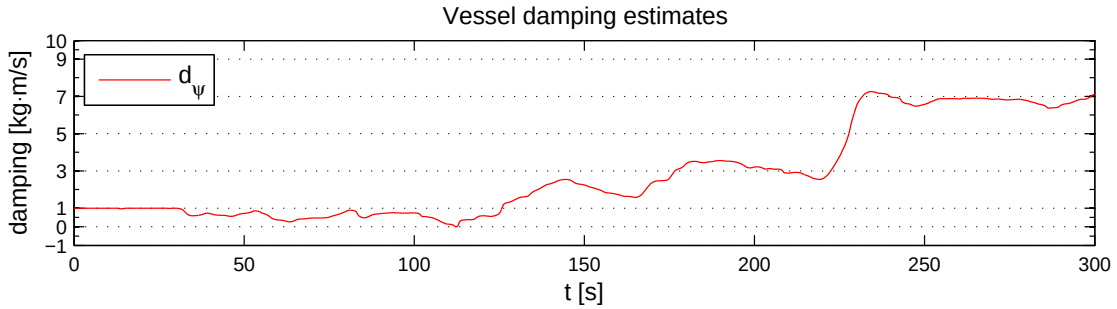

FIGURE 7.30: Vessel damping estimates for yaw motion, NIT simulations.

shows the damping estimates for the vessel simulated in the NIT. In surge, where the drift speed of the ice field results in a moderate degree of PE, the vessel damping is seen to vary about approximately 100 [kg/s].

In sway, the estimate is seen to converge to a constant value at approximately 280 [kg/s] after an initial value of 0 [kg/s]. At the time instants where the vessel undergoes a change in desired position i sway, the estimate is seen to increase. The estimate in sway might be poor though, due to little degree of PE, and some reservations have to be made when analyzing this estimate value.

The vessel damping estimate in yaw motion, presented in Figure 7.30, is shown to converge to approximately 7 [kg $\cdot$ m/s]. However, similar to the estimate of moment of inertia, the estimate of damping in yaw might suffer from poor PE properties.

7.3.2.2 Environment parameters

7.3.2.2.1 Mass and damping

The environment mass estimates is presented in Figure 7.31. The plot shows that after an initial transient, which is caused by initialization of the force estimator included in the NIT, and the initial acceleration in surge, the added mass in surge stabilizes at a value approximately at $m_{Cx} = 800$ [kg].

In sway the estimate is seen to experience an increase in environment mass at the time instant of position change from $\eta_y = 0$ to $\eta_y = 2$ [m]. At the time instant when the vessel drifts back to the initial position, the environmental mass estimate decreases. The higher level in value between $t = 100$ and $t = 200$ [s] might be due to increased friction as the vessel pushes the ice masses against the ice channel ridge.

The environmental moment of inertia, presented in Figure 7.32, is shown to converge to approximately 140 [kg $\cdot$ m^2]. However, as a consequence of poor excitation of the input signals, the results showing the environmental parameters in yaw might be dubious.

The environmental damping in surge and sway, presented in Figure 7.33, shows that both the initial acceleration in surge, and the penetration of the ice ridge, occurring at approximately $t = 30$ [s], results in sudden increases in surge damping. Moreover, the changes in desired position in surge occurring at $t = 150$ [s] and $t = 250$ [s] increases surge damping.

In sway, the damping estimates is seen to keep a low value until excitation of input signals is experienced due to the first change in position at $t = 100$ [s]. The value then converges to a value at about $d_{Cy} = 390$ [kg/s]. Another transient is seen at the second position change at $t = 200$ [s], before the estimate converges to approximately $d_{Cy} = 250$ [kg/s]. This might indicate that the environmental damping in sway is higher in the areas close

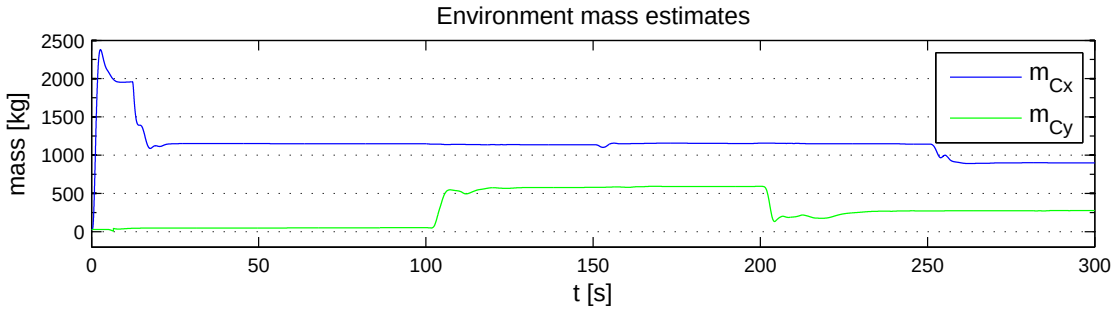

FIGURE 7.31: Environmental added mass estimates, NIT simulations.

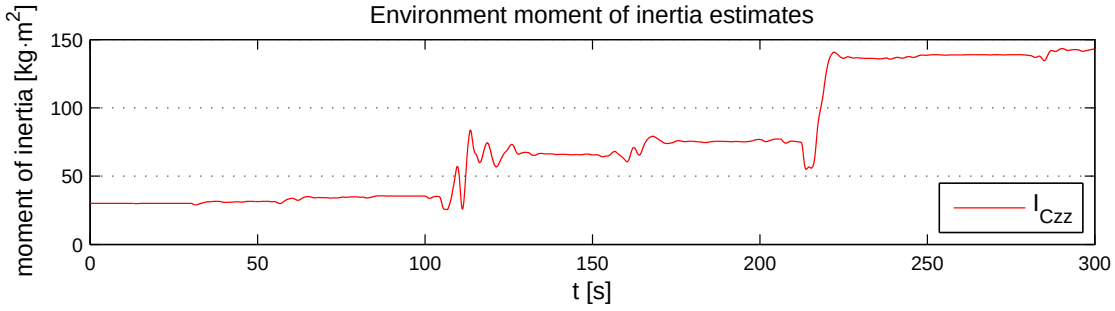

FIGURE 7.32: Environmental added moment of inertia estimates, NIT simulations.

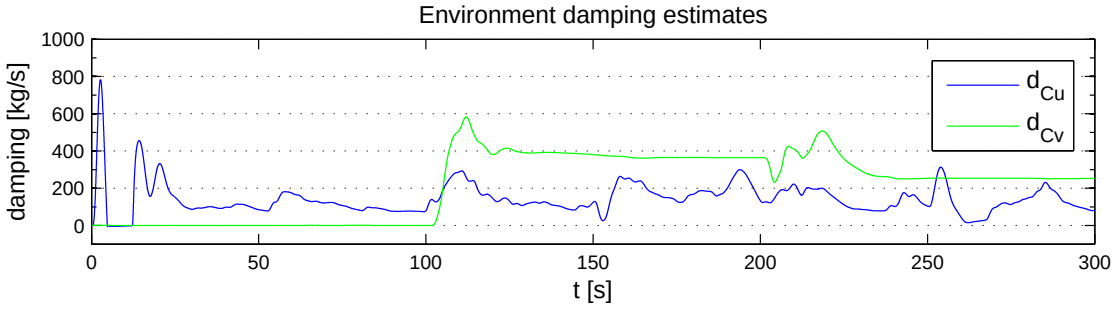

FIGURE 7.33: Environmental damping estimates in surge and sway, NIT simulations.

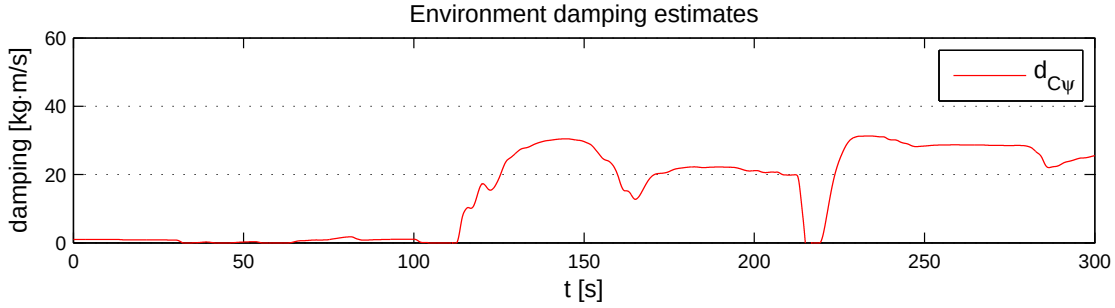

FIGURE 7.34: Environmental damping estimates in yaw, NIT simulations.

to the ice channel ridge. However, due to the lack of persistent excitation in sway, the parameter estimates might be questionable.

Changes in the damping estimates in yaw, presented in Figure 7.34, is seen to occur approximately at the time instants of position change in sway. A convergence to approximately 25 [kg · m/s] is observed, both preceding and subsequent to the sway position changes. This might indicate a rather constant environmental damping in yaw.

7.3.2.2.2 Stiffness

When the ice forces exceeds the force threshold, the environment is modeled using the model (5.6), where the stiffness parameter $\boldsymbol{K}_C$ is calculated using (5.28). Figures 7.35 and 7.36 show the estimated stiffness value k_C for sway and yaw respectively.

The plots shows that k_C increases both in sway and yaw as a result of a change in desired sway position. The sway-yaw interaction is due to the introduction of the cross terms discussed earlier. Furthermore, the plot in Figure 7.35 shows that a slightly higher level of stiffness in sway is observed between the two peaks (i.e. when the vessel is situated at $\eta_y = 2$ [m], close to the ice ridge). This slight rise in stiffness level is reflected in Figure 7.36, where the stiffness in yaw is seen to increase between $t = 100$ and $t = 220$ [s].

This may indicate that a vessel closer to the ice ridge tends to be subject to a stiffer environment relative to being situated in the middle of the ice channel.

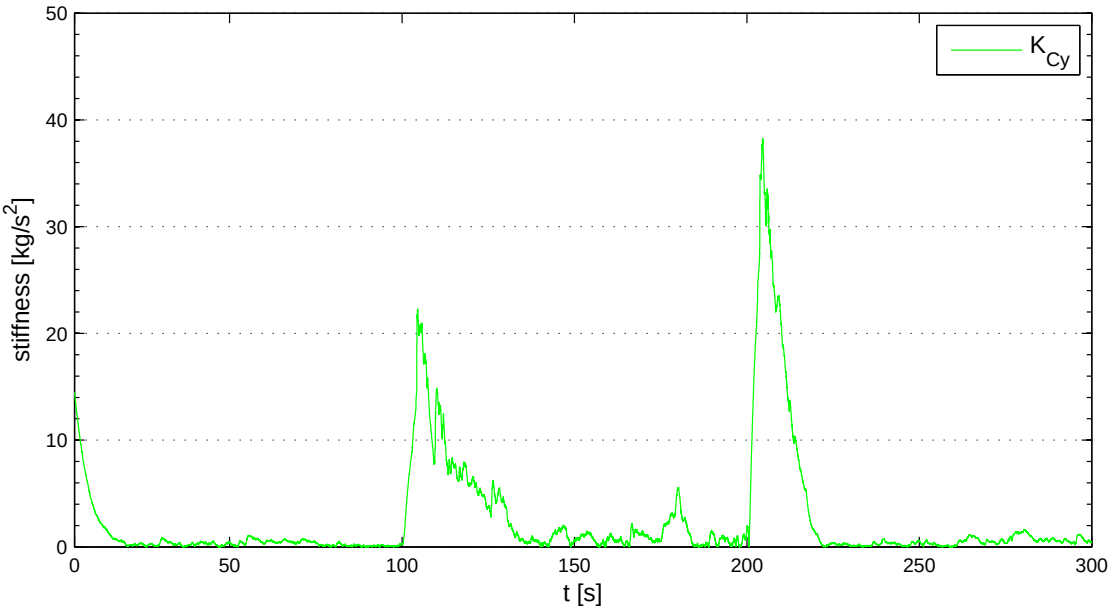

FIGURE 7.35: Environmental stiffness estimates sway, NIT simulations.

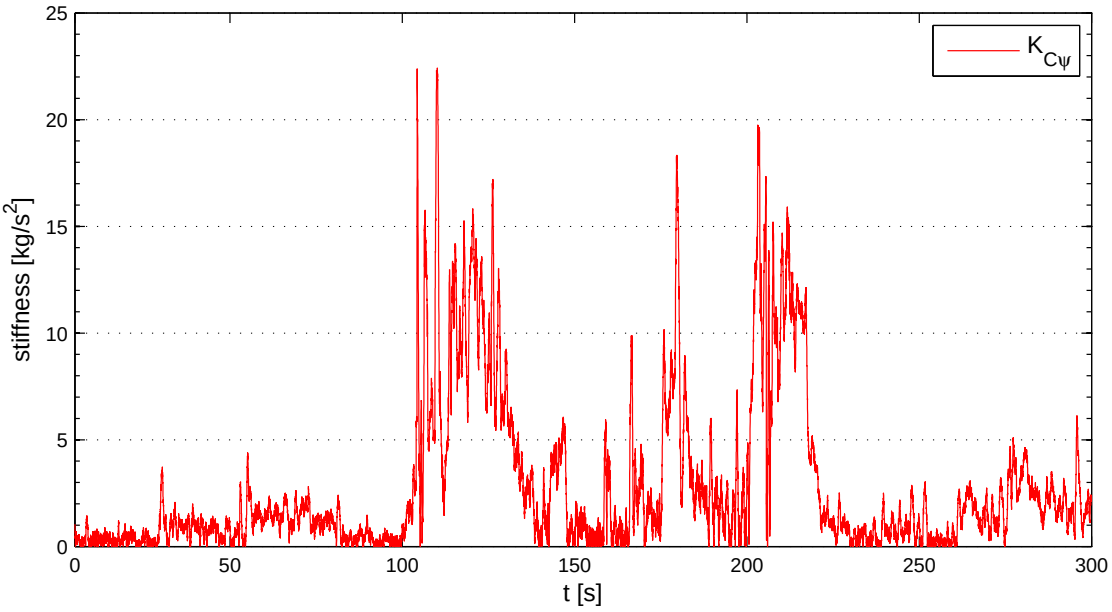

FIGURE 7.36: Environmental stiffness estimate yaw, NIT simulations.

Chapter 8

Discussion

The motivation for this work was to investigate the feasibility of adaptive control designs for DP systems in managed ice. Such designs would enable an ice going vessel to adapt to the environment in which it is situated, and might result in decreased energy consume compared to a conventional open-water system.

Furthermore, incorporating concepts from force control into the adaptive scheme was believed to alleviate the environmental forces acting on the vessel, leading to an even lower energy consume, as well as reduced wear and tear on mechanical equipment.

In Chapter 5 the implementation of the modified MRAC scheme was carried out. The modified MRAC had the possibility to incorporate force control in the DP system by the means of making the MRAC reference model condition dependent. The aim was to deactivate position control, and regulate the ice load induced forces by controlling the vessel-ice interaction force dynamics, if the external forces exceeded a given threshold.

Chapter 6 presented a case study, where the control scheme was to be tested using the Numerical Ice Tank simulator software. Two implementations of the modified MRAC were tested; one in which only position control was allowed (referred to as the MRAC), and one having the possibility to force control the vessel in the case of excessive ice loads (referred to as the MRAHFC). The NIT was set to resemble two test scenarios: stationkeeping and waypoint tracking. During the case study, the proposed control schemes were compared to a reference PID controller with acceleration feed-forward.

In Chapter 7 the results with regards to positioning performance, as well as the observed forces from each test scenario in the case study, were presented. In addition, calculations of cumulative environmental forces and thrust forces were analyzed.

8.1 Performance during stationkeeping

The results from the stationkeeping scenario showed that the MRAC scheme proved superior to the reference PID controller in terms of position control. This was shown by comparison of standard deviations of the positioning error for each case, where it was evident that the total MRAC error was 34.6 [%] smaller in the translational directions of N and E than the PID error with respect to keeping a zero reference.

The results for the MRAHFC showed that the force control functionality caused the vessel to drift off the reference position, resulting in a larger error standard deviation. This was to be expected, however, as the limitations of force control, carried out in Section 3.2, implies that force and position cannot be controlled independently at the same time.

The results presenting the actuating thrust forces, showed that the PID controller actuated counteracting forces over longer intervals in time compared to the MRAC. The MRAC force profile was recognized by short force peaks. The results indicated that the MRAC control law distributes the applied thrust force in a manner that reduces the force level over time. This was the case for the MRAHFC as well. However, the force control mode of the MRAHFC resulted in longer intervals of high-level thrust force compared to the MRAC. The reason for this is believed to be that drift-offs from the reference position results in a longer vessel trajectory in total. Thus, despite the intentions of using less power by letting the vessel drift off the reference position in the case of excessive ice loads, the results indicates that tracking a longer trajectory through the environment requires the vessel to apply more thrust force than staying at the reference point.

In addition, frequent shifts between control domains lead to high thrust rates in the case of the MRAHFC, resulting in an oscillating behavior of the applied thrust forces. It is believed that this behavior might be improved by increasing the upper force threshold, escalating the hysteresis effect of the control algorithm.

Similar tendencies to the ones observed in N and E, were observed from the results in yaw motion. The MRAC proved superior in keeping a stationary angle in terms of standard deviation of the error. However, opposed to the performance in the translational directions, the PID controller performed approximately equal to the MRAC in yaw. The results for the MRAHFC showed that force control in yaw resulted in some drift-off from the reference heading.

The plots presenting the force observations in yaw, showed similar results to the translational directions. The force profile of the PID controlled vessel showed that a relatively high amount of thrust force was applied in order to keep the reference heading. The results for the MRAC showed a much smoother force profile. The MRAHFC showed a fragmented force profile with scattered smooth segments. This was believed to be a result of the frequent change in control domain, which causes the vessel to constantly recover

to the reference heading after repeated drift-offs. Again, this behavior might be fixed by rising the upper force threshold, and increase the hysteresis effect of the controller. However, rising the force threshold too much will lead to a more extensive build-up of external forces before the controller activates force control. This might therefore undermine the initial purpose of force control, which is to avoid the excessive ice loads by controlling the forces of interaction to a minimum.

Despite the untidy behavior of the extended MRAHFC and the fact that force control implies a longer vessel trajectory, the results of the calculation of the cumulative thrust forces showed that both MRAC schemes applied less thrust force in total relative to the PID. Moreover, the plots presenting results for cumulative perceived environmental forces, indicated that both proposed control schemes were less influenced by environmental forces over time. By the theory in Appendix A, this suggests that the MRAC approach of calculating a control law based on vessel-environment parameters, results in decreased energy consume. In addition, reduced wear on mechanical equipment is expected as a result of the less severe environmental influence.

8.2 Performance during waypoint tracking

The waypoint tracking scenario shared many tendencies with the stationkeeping case. The MRAC scheme was shown to perform well in regulating the vessel to the desired way points. However, a slightly lower convergence rate relative to the PID controller, resulted in an extended time consume in terms of converging to desired positions. The elongated transient was due to the shape of the reference trajectory, which is generated by the choice of the damping ratio ζ and the resonant frequency ω_0. A more optimal choice of these parameters may alter the shape. However, the dynamics of the thruster engines plays a major role in shaping the reference trajectory, outweighing the reference model parameters beyond a certain point. Moreover, if, for instance, one was to decrease the damping ratio in order to achieve a higher convergence rate towards the end of the transient, this might result in an imprecise system. The reason for this is that the reference model parameters not only shape the output of the reference model; they also define the mechanical impedance of the system relative to the environment. A small damping ratio and resonant frequency will produce a system that is more susceptible to environmental influence. This, in turn, might cause the vessel to drift unintentionally off the reference trajectory, showing poor performance in terms of position accuracy.

The MRAHFC scheme had a behavior similar to the MRAC until the vessel reached within the boundaries of the position tolerances. Once situated within these boundaries, force control was activated whenever the environmental forces satisfied the requirements set by the force thresholds. In the event of excessive ice loads, the vessel drifted off the reference position until the limits were reached, or the ice loads decreased to a near zero value, whereupon the vessel recovered to the reference position.

The observed forces showed that increased environmental forces were experienced for all control schemes whenever the vessel performed a change in desired position. However, these force peaks were rather modest for the two MRAC controlled vessels relative to the vessel controlled by the PID. This may indicate that the MRAC schemes perform the position changes in a more cautious manner than the PID. This indication is supported by the lower convergence rate shown in the position plots, and suggsts that a more time consuming convergence rate may alleviate the environmental influence.

It may be argued, however, how much role the slightly decreased convergence rate actually plays in reducing the environmental influence. It was shown in the stationkeeping case, where convergence rates were not an issue, that the MRAC schemes alleviated the environmental influence relative to the PID. Thus, despite the relatively modest convergence rate of the MRACs, it is reasonable to believe that the precise MRAC approach of calculating its control signals plays a major role in the decreased environmental forces observed in the plots.

As for the applied thrust force in the stationkeeping scenario, the thrust forces for the MRAC schemes in the case of waypoint tracking were recognized by short force peaks. In particular, the MRAHFC was observed by the many small impulses in force, resulting from the force control in sway.

In yaw, the positioning performance was influenced by the motion in sway. In Section 2.2.3, cross terms in the equations of motions for sway and yaw, caused by environmental forces, were introduced. In the case of sway motion, these cross terms were evident to arise, as the results showed that the vessel was seen to experience environmental influence in yaw, and drift from the reference heading whenever a change in sway position was conducted.

The MRAC schemes are modeled from the simplification that both vessel motion and environmental forces are decoupled in surge, sway and yaw. Thus, the sway-yaw cross terms are not accounted for in the MRAC models. This results in drift-offs in yaw for both the MRAC controlled vessel and the vessel controlled by the MRAHFC scheme. However, as the forces in yaw were rather moderate for both MRAC schemes, a satisfactory performance was observed for both controllers. Nevertheless, in situations where sway-yaw motion interaction is more excessive, an MRAC control approach might require the knowledge of motion induced cross terms. This implies that, in such cases, an MRAC scheme for multi variable (MIMO) systems needs to be developed.

The cumulative force plots showed that the MRAC schemes proved superior compared to the PID, both in terms of perceived environmental influence and applied thrust forces. Again, the higher convergence rate of the PID controller might explain some of the superfluous applied and perceived forces in this case. However, it is reasonable to believe that the MRAC tendency to apply less force, demonstrated in the stationkeeping case, is further amplified with increased system motion.

Even though both MRAC schemes proved superior to the PID controller in terms of a lesser cumulative thrust force, the vessel controlled by the MRAHFC consumed more force in total than the vessel controlled by the classic MRAC. It may be argued, as in the stationkeeping scenario, that the force control implication of longer vessel trajectories results in increased thrust force over time. The results thus suggest that taking the shortest path to a desired position is preferable over taking the path of least resistance. This may depend on the situation, of course, as very excessive hard packed sea ice might not be possible to overcome. However, such events was not simulated in the tests conducted in this work, and might be the focus of future work on the subject.

8.3 System adaption and parameter estimates

The vessel-environment estimates was presented in Section 7.3.2. The task of estimating the system parameters, was shown to be a challenging task. Due to the fact that the system was regulated to keep a constant position, sufficient richness of input signals were difficult to obtain. The vessel mass estimates were the only estimates expected to converge to a constant value. Convergence was achieved in this case. However, for vessel damping and the environment parameters, this was not the case, and the parameters were observed to vary in value with time. In this case, the environmental parameters were not expected to be constant, and the results gathered from the simulations might reveal some of the behavior of sea ice. However, the lack of persistent excitation in the system, make the results dubious. Especially the parameters dependent on the motion in yaw were shown to have poor convergence properties in the cases where the actual value was known.

The lack of knowledge of the environmental parameters results in a purely qualitative analysis of the estimates. Nevertheless, some correlation between the environmental parameter estimates and the moton of the vessel was pointed out, as the environmental mass and damping was seen to increase as the vessel changed position in the ice field. It is believed that this might be due to increased friction on the vessel hull. Furthermore, the calculated stiffness parameter increased in the cases where the vessel was situated close to the ice ridge, signifying a stiffer environment in these areas of the managed ice channel.

In hindsight, as estimating the environment parameters was shown to be a challenging task due to poor PE conditions, a direct implementation of the MRAC schemes might be preferable. In the direct approach, the control law parameters are calculated directly, without estimating the system parameters. Furthermore, as convergence to actual parameter values is not required in general to achieve good performance in terms of automatic control, soly focusing on acquiring good control properties might be a just as good approach as attempting to monitor the environment. The direct MRAC approach is well covered in the literature (Ioannou and Sun, 1996), (Kaufman et al., 1998).

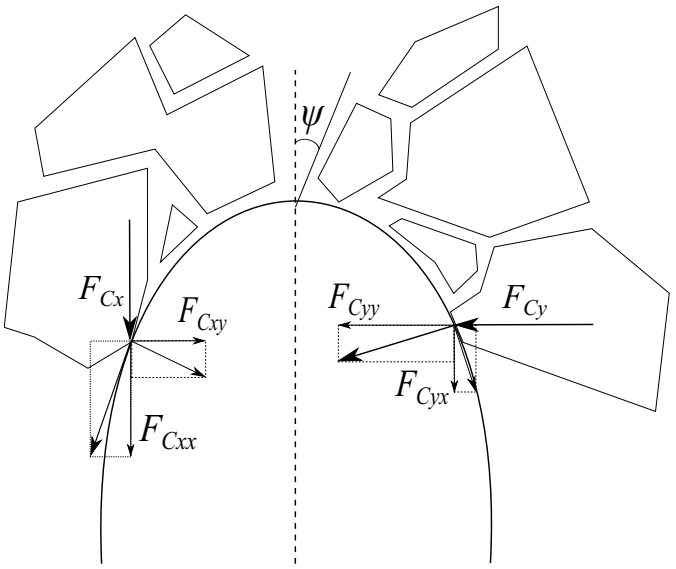

FIGURE 8.1: Coupled environmental forces acting on vessel hull.

8.4 Limitations of MRAC model

The MRAC control laws (5.10) and (5.11) are calculated from the coupled vessel-environment system, consisting of the linearized DP model (5.1) and a simplified model of the environment (i.e. either (5.2) in the case of position control, or (5.6) in the case of force control), as well as the MRAC reference model of choice.

In the process done in order to derive the MRAC control structure, several simplifications have been made to the system models. These simplifications results in certain limitations to the MRAC performance. One of the simplifications made, was the assumption of decoupled vessel dynamics. This assumption might be unrealistic. However, it is plausible if one assumes xz plane, as well as yz plane, symmetry. This is the case if the center of origin CO of the BODY coordinate system coincides with the center of gravity CG of the vessel. Such a situation, however, is certainly an ideal scenario as load conditions and general vessel design often violates the symmetry properties in the yz plane. Symmetry in the xz plane, however is more realistic, and thus it is common to only decouple the surge motion from the sway-yaw equations (Fossen, 2011). The vessel model simulated in the NIT, however, inhabits symmetry properties in both the xz- and yz plane. Thus, the decoupling of the vessel DOFs done in this work is a plausible assumption

The assumption of decoupled environmental forces is believed to be a considerably more unrealistic one, and it is likely that this simplification has the biggest influence on the MRAC performance. Figure 8.1 presents a conceptual illustration showing two points of attack of the forces acting on a vessel hull. It is seen from the figure, that both the ice loads F_{Cx} acting from an angle of attack of 0 [deg], and the ice loads F_{Cy} acting from an angle of attack of 90 [deg], induces forces in all DOFs. However, only the force F_{Cxx} and F_{Cyy} are accounted for in the estimated environmental model.

The effects resulting from the neglect of sway-yaw cross terms in the environmental added mass matrices have already been revealed in the results presented in Chapter 7. It was observed that any motion in sway induced a moment acting about the z axis. Moreover, it is believed that increasing the angle of attack of the incoming ice, will amplify these effects even further. Eliminating the issues related to sway-yaw motion coupling, requires the inclusion of these cross terms in the MRAC model. This implies that the MRAC scheme has to be implemented as a multi variable (MIMO) system.

The implementation of MRAC schemes for MIMO plants has been done in the case of direct MRACs in Li and Tao (2010) and Hsu et al. (2013). The choice of implementing an indirect MRAC for the purpose of this thesis originated in the desire to monitor the ice force parameters. Not much literature with regards to multi variable indirect MRAC systems have been found, and it was therefore focused on simplifying the system to consist of three decoupled SISO systems. Furthermore, if the angle of attack of the incoming ice is small, the sway-yaw cross terms may be considered small enough to be regarded as disturbance terms. In this case the robustness properties of the implemented MRAC scheme will guarantee for stability and ensure a small positioning error. Nevertheless, it is recommended to focus on multi variable MRAC schemes in any further work on the subject, in order to derive a comprehensive adaptive control scheme for the purpose of vessel control in managed ice.

Another simplification was made with regards to the modeling of the environment in the case of excessive ice forces. The stiffness term in (5.6) was found from the monitored lateral distance from the vessel to the ice channel ridge. It was argued that the location of the channel ridge could function as the originating pivot point of the environmental stiffness force. However, excessive ice forces may be caused by event loads originating in any area of the ice channel, not just from vessel-ridge ice clogging. The location of such an originating point in the general case is difficult to establish. Thus, some method to predict and detect points of origin of event loads might be beneficial to develop in order to generate proper time varying environmental models.

Despite the model simplifications, and the limitations these entails, the implemented MRAC schemes proved well suited for the scenarios in which they were tested. As these scenarios resembled managed ice operations where the angle of attack of the incoming ice could be considered small, the robustness properties of the control structures ensured adequate performance in terms of vessel control. Furthermore, the results showed that the thrust force profile of the MRAC schemes resulted in less environmental influence compared to the reference PID controller.

8.5 Limitations of testing environment

The NTNU Numerical Ice Tank was used as a testing environment for the demonstrated control schemes. The tool resembles a towing tank experiment, in which the towing tank may be covered in an ice field inhabiting different parameters of choice, including coverage, thickness and density. The tool includes an extensive hydrodynamical model, as well as a model of sea ice behavior that does indeed capture most of the effects sea ice interaction entails (Scibilia et al., 2014). It should be mentioned, however, that the NIT in its present version does not simulate dynamic ice forces not initiated by the vessel. That is, if the vessel velocity in some direction is zero, the external forces acting on the vessel in this direction will be small. Furthermore, phenomenons including the discussed event loads, including vessel-ridge ice clogging are only simulated to some extent. Thus, even though the NIT is a powerful tool, fully suited for model scale simulations of ice going vessels, the results gathered from the simulations are numerical simplifications of full scale effects. This needs to be kept in mind when analyzing the results.

In addition, the lack of a proper model of the propulsion system, and data from such a model, results in a truncated qualitative analysis of power consume and the energy consumption over time. The simulation tool in its present version is not intended for such analysis, and thus some degree of critical approach has to be made when studying the results regarding these aspects of the case study.

This concludes the discussion part of this thesis. The next chapter will draw conclusions from the discussions on the results, and present ideas and recommendations for further work on the subject.

Chapter 9

Conclusion and further work

The work of this thesis was carried out in order to test the hypotheses presented in Chapter 1, stating that an adaptive control system would be a beneficial utilization for marine operations in Arctic environments, increasing positioning performance and reducing energy consumption. Furthermore, it was alleged that incorporating concepts from force control would lower the energy consume over time even further.

9.1 Main conclusions

The results presented in this thesis suggested that

- Adaptive control is well suited for marine operations in Arctic environments.
- Force control in the implemented form does not decrease energy consume further.
- Cross terms should be included in the MRAC system models.

9.1.1 Performance of indirect MRAC

In light of the results presented in Chapter 7, and the discussion carried out in Chapter 8, it is reasonable to conclude that the proposed MRAC scheme was superior to the PID controller in keeping a floating vessel at a stationary setpoint. This was evident with regards to positioning performance in terms of a smaller error, but also in the observed environmental forces, as the MRAC controlled vessel tended to be influenced less by the environment. Moreover, it was argued that this was a result of less applied thrust force. In addition, the cumulative force observations over time showed a clear tendency of the MRAC to to utilize less force in total.

The MRAC tendency of less applied force was was even clearer in the case of waypoint tracking. However, the PID controlled vessel in this case showed a higher convergence

rate to desired positions, resulting in smaller error over time relative to the MRAC. Moreover, even though the MRAC were seen to perform very well in maintaining vessel position in the ice field, this scenario revealed limitations to the MRAC controller, as sway induced moments in yaw was seen to result in drift-offs from the reference heading. This was a result of unmodeled coupled sway-yaw dynamics in the environmental model.

9.1.2 Performance of hybrid force control scheme

The MRAHFC scheme performed as expected in terms of positioning the vessel, drifting away from the reference position in the case of excessive ice loads. However, the control scheme was shown to perform inferior relative to the classic MRAC and the PID controller in terms of applied thrust force. It was observed that the strategy of drifting off the reference position in the case of excessive ice loads resulted in increased thrust forces, as the drift-offs implied an extended trajectory through the surrounding sea ice environment. This was shown for both the stationkeeping scenario, and for the case of waypoint tracking. Moreover, the results suggest that staying at the setpoint, and choosing the shortest path to a desired position, results in less applied thrust force in total, relative to taking the path of least resistance. Thus, the results indicate that force control in the implemented form, and for the scenarios tested, does not decrease energy consume over time.

9.1.3 Adaptive properties and parameter estimates

The estimated parameters for vessel mass was seen to converge to a value close to the actual value. Moreover, correlations between vessel motion through the ice field and the estimate parameters were shown. However, due to poor PE properties of input signals, the results are believed to be somewhat dubious. Thus, the estimates merely indicates sea ice behavior, and better properties in terms of PE is required to generate better parameter convergence, and draw final conclusions.

9.2 Recommendations for further work

In light of the above conclusions, and the fact that setpoint regulation is the most likely scenario for an MRAC system in this regard, a direct MRAC approach might be sufficient for DP control. This is because achieving proper convergence of parameter estimates in the indirect MRAC approach might be a challenging task. Moreover, further work on the subject should focus on the implementation of adaptive control schemes for multi-variable systems, accounting for cross terms in the system models. Finally, it is recommended to further optimize such a control scheme with respect to fuel consumption and choice-of-route through the ice.

Appendix A

Energy calculations and model scaling

This chapter will briefly go through some considerations related to energy calculations, as well as practical aspects related to the model scaling used in the execution of the case study presented in Chapter 6.

A.1 Energy calculations

In physics, energy is defined as the ability to perform work. Work, in turn, is the line integral of the resultant force F acting on a body along the line of integration s, given by (Freedman and Young, 2008)

$$W = \int Fds \tag{A.1}$$

As energy is defined as the ability to do work, the work performed on a body b by an energy source a, can be thought of as a measure of the energy consumed by a in performing work on b.

The above is true for the ideal, frictionless case where the only force acting in the system, is the force exerted on b by a. However, when considering the energy consumed by a thruster propelling a vessel through some fluid, this is not the case. The amount of energy required to perform work on the vessel increases with the amount of hydrodynamic forces acting on the vessel from the fluid. In particular, if forces due to sea ice interference is concerned, the environmental forces might exceed the ceiling thrust force of the vessel in some direction, causing the resultant force acting on the vessel to become negative. This results in the sea ice performing work on the vessel, even though the vessel thrusters operate at full speed. Thus, the above equation gives a deficient measure of the energy consume in this case.

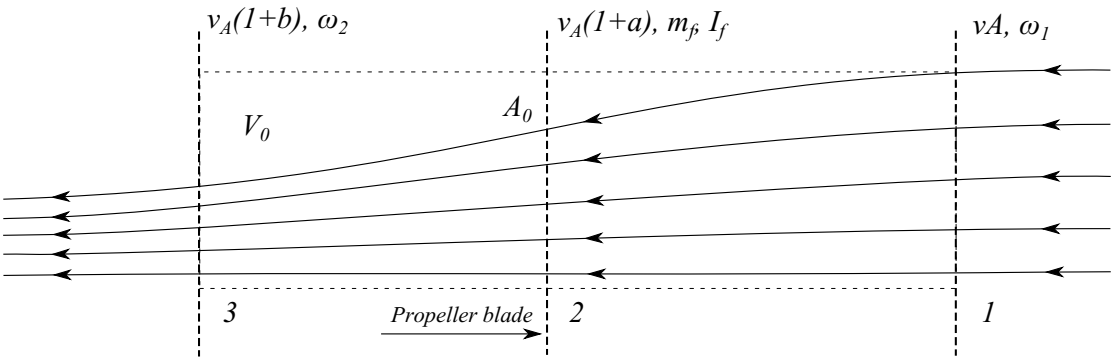

FIGURE A.1: Control volume containing thruster propeller, and depiction of variables.

When considering vessel propulsion, it makes sense to look at the absorbed *power* P of the thruster propellers. Power is defined as the rate of doing work. In terms of a thruster propeller advancing through some fluid, and rotating about some axis of rotation, the power P_p absorbed by the propeller can be calculated as (Van Manen and Van Oossanen, 1988)

$$P_p = T\omega \tag{A.2}$$

where T is the torque absorbed by the propeller and ω is the angular velocity.

Assume now, that the propeller is contained in an enclosing control volume V_0, as shown in Figure A.1. Furthermore, ν_A is the translational velocity of the fluid before entering V_0, $\nu_A(1+a)$ is the translational velocity of the fluid when it passes through the cross-sectional area A_0 of the propeller, and $\nu_A(1+b)$ is the final translational velocity of the fluid after it has left V_0. Assume further that ω_1 denotes the initial angular velocity of the fluid before it enters V_0, and that ω_2 denotes the final angular velocity as the fluid leaves V_0. Assuming the torque is distributed uniformly over the propeller blades (an ideal assumption), the absorbed torque T in Equation (A.2) can then be expressed as (Van Manen and Van Oossanen, 1988)

$$\begin{aligned} T &= I_f(\omega_2 - \omega_1) \\ &= m_f r^2(\omega_2 - \omega_1) \\ &= \rho A_0 \nu_A(1+a) r^2(\omega_2 - \omega_1) \end{aligned}$$

where I_f, m_f is the moment of inertia and mass respectively of the fluid passing through the cross-section of the control volume in unit time, ρ is the density of the fluid, and r is the radius of the propeller.

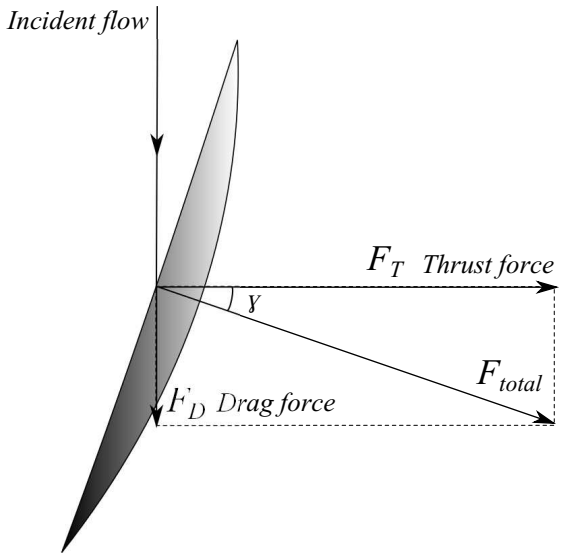

FIGURE A.2: Depiction of forces developed by a rotating propeller.

The torque T absorbed by the propeller, results in a force exerted on the surrounding fluid. This force can be decomposed into a force component called the *thrust*, that acts normal to the incident flow direction, and a force component called the *drag*, that acts tangent to the incident flow direction. Figure A.2 shows the propeller blade and the forces it exerts on the surroundings. The angle γ denotes the *thrust-to-drag ratio* (i.e. $\tan\gamma = F_D/F_T$), which is a measure of the efficiency of the propeller. The thrust F_T performs useful work on the vessel, and can be expressed as (Van Manen and Van Oossanen, 1988)

$$F_T = \rho A_0 \nu_A^2 (1+a) b \tag{A.3}$$

The total power absorbed by the propeller, given by Equation (A.2) can be decomposed into useful work performed by the propeller, and the energy losses to the surrounding fluid. Furthermore, the energy losses can be decomposed into losses due to the increase in kinetic translational and kinetic rotational energy of the surrounding fluid respectively. That is, the energy losses is given by

$$E_T = \frac{1}{2} m_f (\nu_A b)^2 \tag{A.4}$$

$$E_R = \frac{1}{2} I_f (\omega_2 - \omega_1)^2 \tag{A.5}$$

The useful work performed by the propeller in unit time is given by the product of the thrust F_T and the fluid velocity ν_A,

$$\bar{W} = F_T \nu_A \tag{A.6}$$

Finally, the energy balance for the propeller torque in unit time, gives

$$T = \bar{W} + E_T + E_R \tag{A.7}$$

Integrating Equation (A.7) over time, gives the total torque absorbed by the propeller

$$T_{tot} = \int \bar{W} dt + \int E_T dt + \int E_R dt \tag{A.8}$$

Equations (A.7), (A.8) shows that if W is assumed to be much larger than the energy losses E_T, E_R, then F_T is a good indication on energy consume in unit time, while the *cumulative* force $\int_0^t F_T d\tau$ can be used as a measure of total energy consumed over time.

A.2 Similarity considerations and scaling

The case study carried out in Chapter 6 includes the simulation of a towing tank experiment including a model-scale vessel in an ice basin. In order to compare results from the simulations to a real world scenario, dimensional analysis has to be applied.

In the engineering literature, the concept of *similarity* is used to relate a model behavior and a full-scale case. Complete similarity is difficult to achieve. Therefore, it is common to pursuit three main types of similarity in order to achieve a comprehensive model-prototype relation (White, 2007):

Geometric Similarity (GS)

Geometric similarity concerns the length dimension, and is a necessary requirement for the model to share any resemblance with the full-scale case. It requires that a linear scale ratio can be used to relate the length dimension in the model and the prototype. That is, all lengths has to be related by

$$L_m = \alpha L_p \tag{A.9}$$

where L_m is the model-scale length, L_p is the full-scale length, and α is the scale ratio.

Kinematic Similarity (KS)

Kinematic similarity concerns the scale ratio relating the velocities of the model and the velocities of the prototype. It requires geometric similarity, as well as equal time scale ratios of the model and the prototype. The so-called *Froude number* Fr is defined as the ratio of the inertia of a ship propagating through a fluid, to the gravitational wave traveling over the fluid surface, given by

$$Fr = \frac{U^2}{gL} \tag{A.10}$$

where U is the flow velocity in the x direction, g is the acceleration due to gravity and L is the fluid depth.

The model and the prototype are kinematically similar if their Froude numbers are equal. That is

$$Fr_m = \frac{U_m^2}{gL_m} = \frac{U_p^2}{gL_p} = Fr_p \tag{A.11}$$

From Equation (A.11) it can be observed that the velocity scale is

$$\frac{U_m}{U_p} = \left(\frac{L_m}{L_p}\right)^{1/2} = \sqrt{\alpha} \tag{A.12}$$

Similarily, the time scale can be shown to equal

$$\frac{T_m}{T_p} = \left(\frac{L_m/U_m}{L_p/U_p}\right)^{1/2} = \sqrt{\alpha} \tag{A.13}$$

Dynamic Similarity (DS)

The last type of similarity involves the forces acting on the model and the full-scale prototype. Dynamic similarity requires that geometric and kinematic similarity exists. In addition, DS requires that the model and prototype Reynolds numbers are equal. The last requirement is difficult to attain, as it requires the scaling of the viscosity of the fluid in which the model test is conducted. This means that if water is used both in the model and in the full scale experiment, DS is not achieved. For most practical uses, data on forces obtained in model-scale is typically estimated by extrapolation in order to retrieve full-scale comparable results.

Appendix B

Preliminaries

When dealing with adaptive control in an unknown environment, issues such as stability and boundedness plays an important role. This chapter will define and briefly describe these concepts in the context of this work. The definitions, lemmas and theorems in this chapter are used when analyzing the adaptive schemes in Appendix C, and are taken from Khalil and Grizzle (2002) and Ioannou and Sun (1996). The proofs for the theorems and lemmas presented in this chapter will not be proved here as this is outside the scope of this work.

B.1 Norms and $\mathcal{L}_p$ spaces

A norm is a mathematical function defined as the vector analog of the absolute value

Definition B.1 (Vector norm). The norm $|x||$ of a vector x is a real valued function with the following properties

(i) $|x| \geq 0$ with $|x| = 0$ if and only if $x = 0$

(ii) $|\alpha x| = |\alpha||x|$ for any scalar α

(iii) $|x + y| \leq |x| + |y|$ (the triangle inequality)

The norm can be thought of as the size or length of the vector.

An extension of the concept of the vector norm is the *induced* norm or the *matrix* norm defined next

Definition B.2 (Induced norm). Let $|\cdot|$ be a given vector norm. Then for each matrix $A \in \mathcal{R}^{m \times n}$, the quantity $||A||$ defined by

$$||A|| \triangleq \sup_{\substack{x \neq 0 \\ x \in \mathcal{R}^n}} \frac{|Ax|}{|x|} = \sup_{|x| \leq |} |Ax| = \sup_{|x|=1} |Ax| \tag{B.1}$$

is called the *induced (matrix) norm* of A corresponding to the vector norm $|\cdot|$.

With the above definition of norms, the notion of $\mathcal{L}_p$ spaces can be defined.

Definition B.3 ($\mathcal{L}_p$ **norm).** For functions of time, the $\mathcal{L}_p$ norm is defined as

$$||x||_p \triangleq \left(\int_0^\infty |x(\tau)|^p d\tau\right)^{\frac{1}{p}} \tag{B.2}$$

for $p \in [1, \infty)$. We say that $x \in \mathcal{L}_p$ when $||x||_p$ exists. The $\mathcal{L}_\infty$ norm is defined as

$$||x||_\infty \triangleq \sup_{t \geq 0} |x(t)| \tag{B.3}$$

and we say that $x \in \mathcal{L}_\infty$ when $||x||_\infty$ exists.

B.1.1 $\mathcal{L}_{2\delta}$ norm

An extension of the notion of the $\mathcal{L}_2$ norm is the $\mathcal{L}_{2\delta}$ norm. This norm and its properties, which are presented in the next section, is introduced to simplify the stability analysis of the robust adaptive scheme with dynamic normalization introduced in Section 4.4.2 and analyzed in Appendix C.

Definition B.4 ($\mathcal{L}_{2\delta}$ **norm).** The $\mathcal{L}_{2\delta}$ norm is defined as

$$||x_t||_{2\delta} \triangleq \left(\int_0^t e^{-\delta(t-\tau)} x^\top(\tau) x(\tau) d\tau\right)^{\frac{1}{2}} \tag{B.4}$$

where $\delta \geq 0$ is a constant. If $||x_t||_{2\delta}$ exists, $x \in \mathcal{L}_{2\delta}$. The $\mathcal{L}_{2\delta}$ norm has the same properties as the norm given by (i)-(iii) in Definition B.1.

B.2 Input/output stability

Consider the linear system

$$y(s) = H(s)u(s) \tag{B.5}$$

where $H(s)$ is the transfer function that maps the Laplace transform of the input signal $u(s)$ to the Laplace transform of the output signal $y(s)$.

Definition B.5 ($\mathcal{L}_p$ **stability).** The system B.5 is stable in the $\mathcal{L}_p$ sense if $u \in \mathcal{L}_p \Rightarrow y \in \mathcal{L}_p$ and $||y||_p < c||u||_p$ for some constant $c \geq 0$ and any $u \in \mathcal{L}_p$. When $p = \infty$, $\mathcal{L}_p$ stability is also referred to as bounded-input bounded-output (BIBO) stability.

Lemma B.6. *Let $H(s)$ in B.5 be proper. If $H(s)$ is analytic in Re[s] $\geq -\frac{\delta}{2}$ for some $\delta \geq 0$ and $u \in \mathcal{L}_2$ then*

(i)

$$||y_t||_{2\delta} \leq ||H(s)||_{\infty\delta}||u_t||_{2\delta}$$

where

$$||H(s)||_{\infty\delta} \triangleq \sup_{\omega} \left| H\left(j\omega - \frac{\delta}{2}\right)\right|$$

(ii) Furthermore, when $H(s)$ is strictly proper, we have

$$|y(t)| \leq ||H(s)||_{2\delta}||u_t||_{2\delta}$$

where

$$||H(s)||_{2\delta} \triangleq \frac{1}{\sqrt{2\pi}} \left\{ \int_{-\infty}^{\infty} \left| H\left(j\omega - \frac{\delta}{2}\right)\right|^2 d\omega \right\}^{\frac{1}{2}}$$

The norms $||H(s)||_{2\delta}$, $||H(s)||_{\infty\delta}$ are related by the inequality

$$||H(s)||_{2\delta} \leq \frac{1}{\sqrt{2p-\delta}}||(s+p)H(s)||_{\infty\delta} \tag{B.6}$$

for any $p > \frac{\delta}{2} \geq 0$.

B.3 Bounded functions

The following definitions, lemmas and their proofs can be found in Ioannou and Sun (1996).

Definition B.7. A continuous function $\xi : [0, r] \to \mathcal{R}^+$ (or a continuous function $\xi : [0, \infty) \to \mathcal{R}^+$) is said to belong to class $\mathcal{K}$, i.e., $\xi \in \mathcal{K}$ if

(i) $\xi(0) = 0$

(ii) ξ is strictly increasing on $[0, r]$ (or on $[0, \infty)$)

Definition B.8. A continuous function $\xi : [0, \infty) \to \mathcal{R}^+$ is said to belong to class $\mathcal{KR}$, i.e., $\xi \in \mathcal{KR}$ if

(i) $\xi(0) = 0$

(ii) ξ is strictly increasing on $[0, r]$ (or on $[0, \infty)$)

(iii) $\lim_{r\to\infty} \xi(r) = \infty$

Lemma B.9. *The following is true for scalar valued functions:*

(i) A function $f(t)$ that is bounded from below and is non-increasing has a limit as $t \to \infty$

(ii) Consider the nonnegative scalar functions $f(t), g(t)$ defined for all $t \geq 0$. If $f(t) \leq g(t)$, $\forall t \geq 0$ and $g \in \mathcal{L}_p$, then $f \in \mathcal{L}_p$ for all $p \in [1, \infty]$

Lemma B.10 (Barbălat's lemma). *If $\lim_{t\to\infty} \int_0^t f(\tau)d\tau$ exists and is finite, and $f(t)$ is a uniformly continuous function, then $\lim_{t\to\infty} f(t) = 0$.*

Now, consider the general system

$$\dot{x} = f(t, x), \;\; x(t_0) = x_0 \tag{B.7}$$

Definition B.11 (Boundedness). A solution $x(t; t_0, x_0)$ of B.7 is *bounded* if there exists a $\beta > 0$ such that $|x(t; t_0, x_0)| < \beta$ for all $t \geq t_0$, where β may depend on each solution.

Definition B.12 (Uniformly boundedness). The solutions of B.7 are said to be *uniformly bounded* if for any $\alpha > 0$ and $t_0 \in \mathcal{R}^+$, there exists a $\beta = \beta(\alpha)$ independent of t_0 such that if $|x_0| < \alpha$, then $|x(t; t_0, x_0)| < \beta$ for all $t \geq t_0$.

Definition B.13 (Uniformly ultimately boundedness). The solutions of B.7 are *uniformly ultimately bounded* (with bound B) if there exists a $B > 0$ and if corresponding to any $\alpha > 0$ and $t_0 \in \mathcal{R}^+$, there exists a $T = T(\alpha) > 0$ (independent of t_0) such that $|x_0| < \alpha$ implies $|x(t; t_0, x_0)| < B$ for all $t \geq t_0 + T$.

Theorem B.14. *Assume that B.7 possesses unique solutions for all $x_0 \in \mathcal{R}^n$. If there exists a function $V(t, x)$ defined on $|x| \geq R$ (where R may be large) and $t \in [0, \infty)$ with continuous first-order partial derivatives with respect to x, t and if there exists $\xi_1, \xi_2 \in \mathcal{KR}$ such that*

(i) $\xi_1(|x|) \leq V(t, x) \leq \xi_2(|x|)$

(ii) $\dot{V}(t, x) \leq 0$

for all $|x| \geq R$ and $t \in [0, \infty)$, then, the solutions of B.7 are uniformly bounded. If in addition there exists $\xi_3 \in \mathcal{K}$ defined on $[0, \infty)$ and

(iii) $\dot{V}(t, x) \leq -\xi_3(|x|)$ *for all* $|x| \geq R$ *and* $t \in [0, \infty)$

then, the solutions of B.7 are uniformly ultimately bounded.

Appendix C

Proofs

The following proofs and analysis are taken from Ioannou and Sun (1996). It uses the definitions, lemmas and theorems presented in Appendix B.

C.1 Proof of Theorem 4.5

C.1.1 Part (i) and (ii)

Considering Equation 4.14 and assuming the actual parameter vector θ^* can be treated as constant in every time step, the update of the parameter error $\tilde{\theta} = \theta - \theta^*$ can be written as

$$\dot{\tilde{\theta}} = \Gamma \epsilon \phi \tag{C.1}$$

where

$$\epsilon = -\frac{\tilde{\theta}^\top \phi}{m^2} \tag{C.2}$$

Choosing the Lyapunov function candidate

$$V(\tilde{\theta}) = \frac{\tilde{\theta}^\top \Gamma^{-1} \tilde{\theta}}{2} \geq 0 \tag{C.3}$$

Differentiating C.3 along the solution of C.1 gives

$$\begin{aligned} \dot{V}(\tilde{\theta}) &= \tilde{\theta}^\top \Gamma^{-1} \dot{\tilde{\theta}} \\ &= \tilde{\theta}^\top \Gamma^{-1} (\Gamma \epsilon \phi) \\ &= \tilde{\theta}^\top \epsilon \phi \end{aligned} \tag{C.4}$$

Now, by noting from C.2 that $\epsilon m^2 = -\tilde{\theta}^\top \phi$ this gives

$$\dot{V} = -\epsilon^2 m^2 \leq 0 \tag{C.5}$$

Thus, $V, \tilde{\theta} \in \mathcal{L}_\infty$, which, together with Equation C.2, θ^* constant, and the assumption $\frac{\phi}{m} \in \mathcal{L}_\infty$ implies that $\epsilon, \epsilon n_s, \theta, \dot{\theta} \in \mathcal{L}_\infty$. Now, $V \geq 0$ is a nonincreasing function, and thus, from Lemma B.9, V_∞ exists. Furthermore, from Definition B.3 of the $\mathcal{L}_2$ norm

$$\lim_{t\to\infty} \int_0^t \epsilon^2 m^2 d\tau = -\left(\int_0^\infty \dot{V}^2(\tau) d\tau\right)^{\frac{1}{2}} = V(0) - V(\infty) \tag{C.6}$$

exists. This implies that $\epsilon m \in \mathcal{L}_2$ which in turn implies $\epsilon, \epsilon n_s \in \mathcal{L}_2$. Now, from C.1

$$|\dot{\tilde{\theta}}| = |\dot{\theta}| \leq ||\Gamma|||\epsilon m|\frac{|\phi|}{m} \tag{C.7}$$

which, since $\frac{|\phi|}{m} \in \mathcal{L}_\infty$ and $\epsilon m \in \mathcal{L}_2 \cap \mathcal{L}_\infty$, implies that $\dot{\theta} \in \mathcal{L}_2 \cap \mathcal{L}_\infty$. This completes the proof for (i) and (ii). The reader is referred to p. 236 in Ioannou and Sun (1996) for the proof of (iii) as this is long and complicated and uses theory beyond the scope of this work. □

C.2 Analysis of the adaptive law 4.51

Following is the analysis of the robust adaptive law 4.51 rewritten below for reference

$$\dot{\theta}_p = \Gamma\bar{\epsilon}\phi - \Gamma w\theta_p \tag{C.8}$$

This can be written in terms of the parameter error just as in the case with the unmodified adaptive law 4.14.

$$\dot{\tilde{\theta}} = \Gamma\bar{\epsilon}\phi - \Gamma w\theta_p, \;\; \bar{\epsilon} = -\frac{\tilde{\theta}_p\phi + \sigma}{m^2} \tag{C.9}$$

where $\tilde{\theta}_p = \theta_p - \theta_p^*$. The time derivative of the diagonal Lyapunov function candidate $V(\tilde{\theta}_p) = \frac{\tilde{\theta}_p^\top \Gamma^{-1}\tilde{\theta}_p}{2}$ along the solution of C.9 becomes

$$\dot{V} = -\bar{\epsilon}^2 m^2 + \bar{\epsilon}\sigma - w\tilde{\theta}_p^\top\theta_p \leq -\frac{\bar{\epsilon}^2 m^2}{2} - w\tilde{\theta}_p^\top\theta_p + \frac{\sigma^2}{2m^2} \tag{C.10}$$

Now, the term $-w\tilde{\theta}^\top\theta$ can be written

$$\begin{aligned} -w\tilde{\theta}_p^\top\theta_p = w(\theta_p - \theta_p^*)\theta_p &\geq w|\theta_p|^2 - w|\theta_p||\theta_p^*| \\ &\geq w|\theta_p|(|\theta_p| - M_0 + M_0 - |\theta_p^*|) \end{aligned}$$

and thus

$$w\tilde{\theta}_p^\top\theta_p \geq w|\theta_p|(|\theta_p| - M_0) + w|\theta_p|(M_0 - |\theta_p^*|) \geq 0 \tag{C.11}$$

since $w \geq 0, w(|\theta_p| - M_0) \geq 0$ and $M_0 \geq |\theta^*|$. Thus, the term $-w\tilde{\theta}^\top\theta \leq 0$, $\forall t$. Moreover,

$$-w\tilde{\theta}_p^\top\theta_p \leq -w_0\tilde{\theta}_p^\top\theta_p + 2w_0M_0^2 \tag{C.12}$$

which, when inserted in C.10, gives

$$\dot{V} \leq -\frac{\epsilon^2 m^2}{2} - w_0 \tilde{\theta}_p^\top \theta_p + 2w_0 M_0^2 + \frac{\sigma^2}{2m^2} \tag{C.13}$$

Now, by completing the square, the term $-w_0 \tilde{\theta}_p^\top \theta_p$ can be written

$$-w_0 \tilde{\theta}_p^\top \theta_p = -w_0 \tilde{\theta}_p (\tilde{\theta}_p + \theta_p^*) \leq -w_0 \tilde{\theta}_p^\top \tilde{\theta}_p + w_0 |\tilde{\theta}_p||\theta_p^*| \leq -\frac{w_0 \tilde{\theta}_p^\top \tilde{\theta}_p}{2} + \frac{w_0 |\theta_p^*|^2}{2} \tag{C.14}$$

This gives

$$\dot{V} \leq -\frac{\epsilon^2 m^2}{2} - \frac{w_0 \tilde{\theta}_p^\top \tilde{\theta}_p}{2} + 2w_0 M_0^2 + \frac{\sigma^2}{2m^2} + \frac{w_0 |\theta_p^*|^2}{2} \tag{C.15}$$

Now, adding and subtracting $\alpha V = \alpha \frac{\tilde{\theta}_p^\top \Gamma^{-1} \tilde{\theta}_p}{2}$, for some $\alpha > 0$, gives

$$\dot{V} \leq -\alpha V - \frac{\epsilon^2 m^2}{2} - \left(I w_0 - \alpha \Gamma^{-1}\right) \frac{\tilde{\theta}_p^\top \tilde{\theta}_p}{2} + 2w_0 M_0^2 + \frac{\sigma^2}{2m^2} + \frac{w_0 |\theta_p^*|^2}{2} \tag{C.16}$$

where I is the identity matrix. Now, by choosing $0 < I\alpha < w_0 \Gamma$, this gives

$$\dot{V} \leq -\alpha V + 2w_0 M_0^2 + \frac{\sigma^2}{2m^2} + \frac{w_0 |\theta_p^*|^2}{2} \tag{C.17}$$

This implies that $\tilde{\theta}_p$ converges exponentially to the set

$$D_s = \left\{ \tilde{\theta}_p \;\middle|\; |\tilde{\theta}_p|^2 \leq \Gamma \alpha \left(\frac{\sigma^2}{m^2} + w_0 |\theta_p^*|^2 + 4w_0 M_0^2 \right) \right\} \tag{C.18}$$

Thus, the parameter error in the case of the modified adaptive law C.8, is dependent on the upper bound d_0 of the disturbance σ. The boundedness of $\tilde{\theta}_p$ implies, by Theorem, that $\theta_p, \dot{\theta}_p, \epsilon \in \mathcal{L}_\infty$. Thus the property (i) of Theorem 4.5 is preserved. It can be shown (Ioannou and Sun, 1996) that property (ii) cannot be extended to the modified adaptive law case, but that C.8 guarantees that $\epsilon, \dot{\theta}_p$ is are $(\frac{\sigma^2}{m^2})$-small in the mean square sense, that is

$$\epsilon, \dot{\theta}_p \in \mathcal{S}\left(\frac{\sigma^2}{m^2} + w \right) \tag{C.19}$$

and $\epsilon, \dot{\theta}_p$ keeps within the bounds of the disturbance σ.

This completes the analysis of the modified adaptive law, and shows that C.8 guarantees bounded output signals which is crucial for stability of any adaptive control scheme.

References

Šabanović, A. and Ohnishi, K. (2011). *Interactions and Constraints*, pages 175–232. John Wiley & Sons (Asia) Pte Ltd.

Anderson, R. J. and Spong, M. W. (1988). Hybrid Impedance Control of Robotic Manipulators. *Journal of Robotics and Automation*, 4(5):549–556.

Eik, K. J. (2010). *Ice Management in Arctic Offshore Operations and Field Developments.* PhD thesis, PhD thesis, Norwegian University of Science and Technology, Trondheim, Norway.

Eisenman, I., Schneider, T., Battisti, D. S., and Bitz, C. M. (2011). Consistent Changes in the Sea Ice Ieasonal Cycle in Response to Global Warming. *Journal of Climate*, 24(20):5325–5335.

Euler, L. (1776). Formulae Generals, Pro Translatione Quacunque Corporum Rigidorum. *Novi Commentarii academiae scientiarum imperialis Petropolitanae*, 20:188.

Fossen, T. I. (2011). *Handbook of Marine Craft Hydrodynamics and Motion Control.* John Wiley & Sons Ltd.

Fossen, T. I. and Perez, T. (2004). www.marinecontrol.org.

Freedman, R. A. and Young, H. D. (2008). *University Physics.* McGraw-Hill.

Hogan, N. (1985). Impedance Control - An Approach to Manipulation, Part I: Theory. *Journal of Dynamic Systems, Measurement and Control*, Vol. 107(17).

Hsu, L., Battistel, A., and Nunes, E. V. (2013). Multivariable MRAC Design Without Gain Symmetry Conditions Using a Stabilizing Multiplier.

IMO (1994). Guidelines for Vessels with Dynamic Positioning Systems.

Imsland, L. (2013). personal communication.

Ioannou, P. A. and Sun, J. (1996). *Robust Adaptive Control.* Prentice Hall.

Jenssen, N. A., Hals, T., Jochmann, P., Haase, A., Dal Santo, X., Kerkeni, S., Doucy, O., Gürter, A., Hetschel, S. S., Moslet, P. O., Metrikin, I., and Løset, S. (2012). DYPIC - a Multinational R&D Project on DP Technology in Ice.

Jenssen, N. A., Muddesitti, S., Phillips, D., and Backström, K. (2009). DP in Ice Conditions. In Society, M. T., editor, *Dynamic Positioning Conference*. Dynamic Positioning Comittee.

Juva, M. and Riska, K. (2002). On The Power Requirement in the Finnish-Swedish Ice Class Rules. *Winter Navigation Research Board*, 53.

Kaufman, H., Barkana, I., and Sobel, K. (1998). *Direct Adaptive Control Algorithms: Theory and Applications*. Springer.

Kerkeni, S., Dal Santo, X., and Metrikin, I. (2013). Dynamic Positioning in Ice - Comparision of Control Laws in Open Water and Ice. In *International Conference on Ocean, Offshore and Arctic Engineering*.

Khalil, H. K. and Grizzle, J. (2002). *Nonlinear Systems*, volume 3. Prentice hall Upper Saddle River.

Kjerstad, Ø. K., Metrikin, I., Løset, S., and Skjetne, R. (in review 2014). Experimental and Phenomenological Investigation of Dynamic Positioning in Managed Ice.

Kjerstad, Ø. K. and Skjetne, R. (2012). Observer Design with Disturbance Rejection by Acceleration Feedforward. In *7th IFAC Symposium on Robust Control Design (ROCOND)*.

Kjerstad, Ø. K., Skjetne, R., and Jenssen, N. A. (2011). Disturbance Rejection by Acceleration Feedforward: Application for Dynamic Positioning. In *18th World Congress of the International Federation of Automatic Control*.

Li, S. and Tao, G. (2010). Output Feedback MIMO MRAC Schemes with Sensor Uncertainty Compensation. In *American Control Conference (ACC), 2010*, pages 3229–3234. IEEE.

Liu, G. and Goldenberg, A. (1991). Robust Hybrid Impedance Control of Robot Manipulators. In *Robotics and Automation, 1991. Proceedings., 1991 IEEE International Conference on*, pages 287–292. IEEE.

Ljung, L. (1999). *System Identification (2nd ed.): Theory for the User*. Prentice Hall PTR.

Love, L. J. and Book, W. J. (1995). Environment Estimation for Enhanced Impedance Control. In *1995 IEEE International Conference on Robotics and Automation,*, volume 2, pages 1854–1859. IEEE.

Metrikin, I., Løset, S., Jenssen, N. A., and Kerkeni, S. (2013). Numerical Simulation of Dynamic Positioning in Ice. *Marine Technology Society Journal*, 47(2):14–30.

Nocedal, J. and Wright, S. (2006). Numerical Optimization, Series in Operations Research and Financial Engineering. *Springer, New York*.

Riska, K. (2011). Design of Ice Breaking Ships. *Course material, NTNU*.

Robertson, J. and Pierce, B. (2008). 90 billion barrels of oil and 1,670 trillion cubic feet of natural gas assessed in the arctic.

Scibilia, F., Metrikin, I., Gürtner, A., Teigen, S. H., et al. (2014). Full-scale trials and numerical modeling of sea ice management in the greenland sea. In *OTC Arctic Technology Conference*. Offshore Technology Conference.

Singh, S. K. and Popa, D. O. (1995). An Analysis of Some Fundamental Problems in Adaptive Control of Force and Impedance Behavior: Theory and Experiments. *Robotics and Automation, IEEE Transactions on*, 11(6):912–921.

SNAME (1950). Nomenclature for Treating the Motion of a Submerged Body Through a Fluid. *The Society of Naval Architects and Marine Engineers, Technical and Reserach Bulletin No. 1-5*, pages 1–15.

Spong, M. W., Hutchinson, S., and Vidyasagar, M. (2006). *Robot Modeling and Control*. John Wiley & Sons New York.

Østhus, V. (project work 2013). Hybrid Impedance Control of a Surface Vessel in Managed Ice.

Stroeve, J., Holland, M. M., Meier, W., Scambos, T., and Serreze, M. (2007). Arctic Sea Ice Decline: Faster Than Forecast. *Geophysical research letters*, 34(9).

Van Manen, J. and Van Oossanen, P. (1988). Principles of Naval Architecture, Second Revision, Volume II: Resistance, Propulsion, and Vibration. *Society of Naval Architects and Marine Engineers, Jersey City, New Jersey USA*.

White, F. M. (2007). *Fluid Mechanics (6th International Edition)*. McGraw-Hill.

Wold, H. E. (2013). *Thrust Allocation for DP in Ice*. Thesis.